6. Convection: Why can't we predict rainfall?

6.0. Two categories of convection

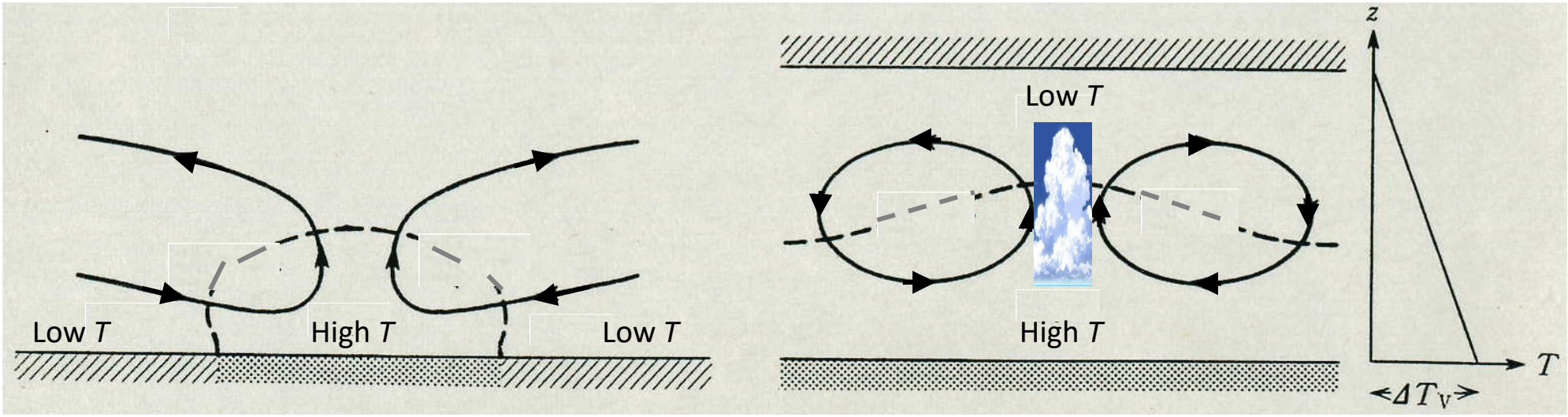

Horizontal Convection

- Vertically *stably*-stratified atmosphere
- Horizontal temperature gradient at ground

- Scales: $\geq 10^2$ km, ≥ 1 day

- Meridional (Hadley/monsoon) circulations
- Local (sea-land/mountain-valley) breezes

Vertical Convection

- Vertically *unstably*-stratified atmosphere
- *Conditional* instability by latent heat release with cloud condensation

- Scales: < 10 km, < 1 h

- Individual convective clouds (cumulus, cumulonimbus)
- *Clustering* mechanisms needed

Rainfall “not so easy” even in tropics (Conditional instability paradox)

- Dry adiabatic ＜ actual lapse rate ＜ Moist adiabatic
  (－10ºC/km)　(－6.5ºC/km)　(－5ºC/km)
- Convection generated if condensation (cloud) started
- Condensation (cloud) if convection (lifted / moistened)
- Therefore “initial upward motion” must be forced

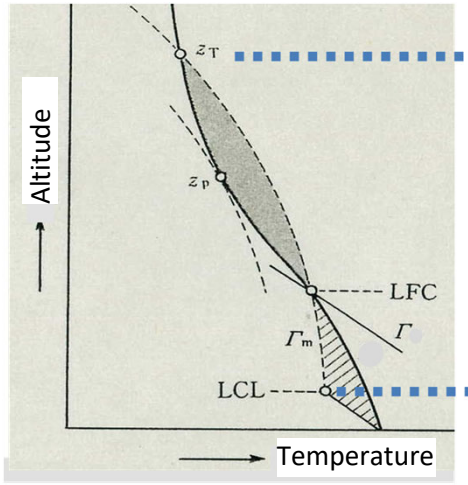

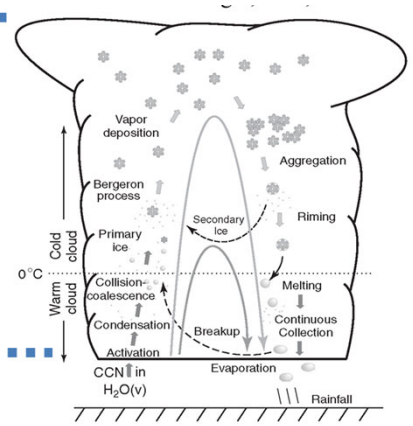

(i) Cold /warm air boundary (*extratropical* cyclone “front”)

(ii) *Subtropical* vortex organization (Typhoon)

(iii) Equatorial *oceanic* wave organization (*Intraseasonal* Madden-Julian oscillation)

(iv) **Diurnal-cycle sea-land breeze circulation**

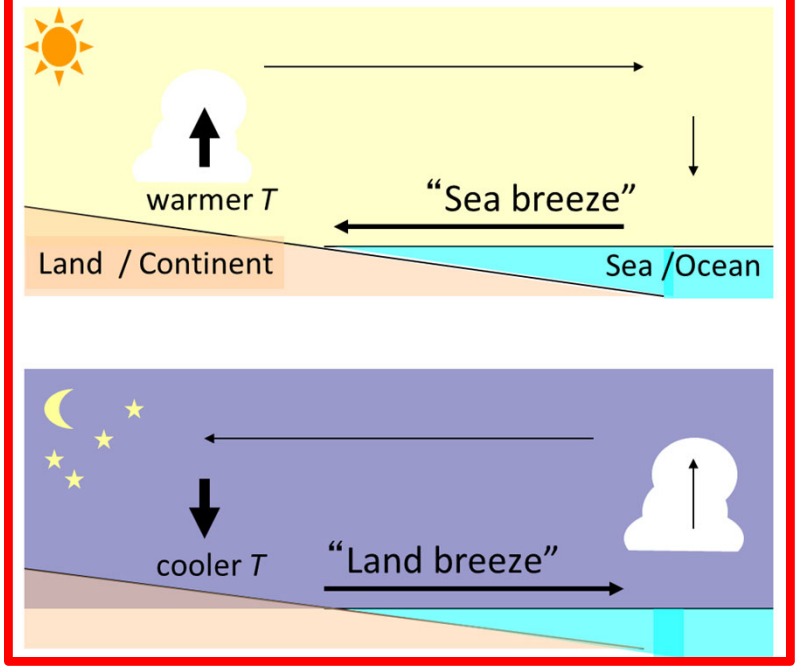

(v) Windward side of *mountain*
(leeside: dry and hot, so-called Föhn)

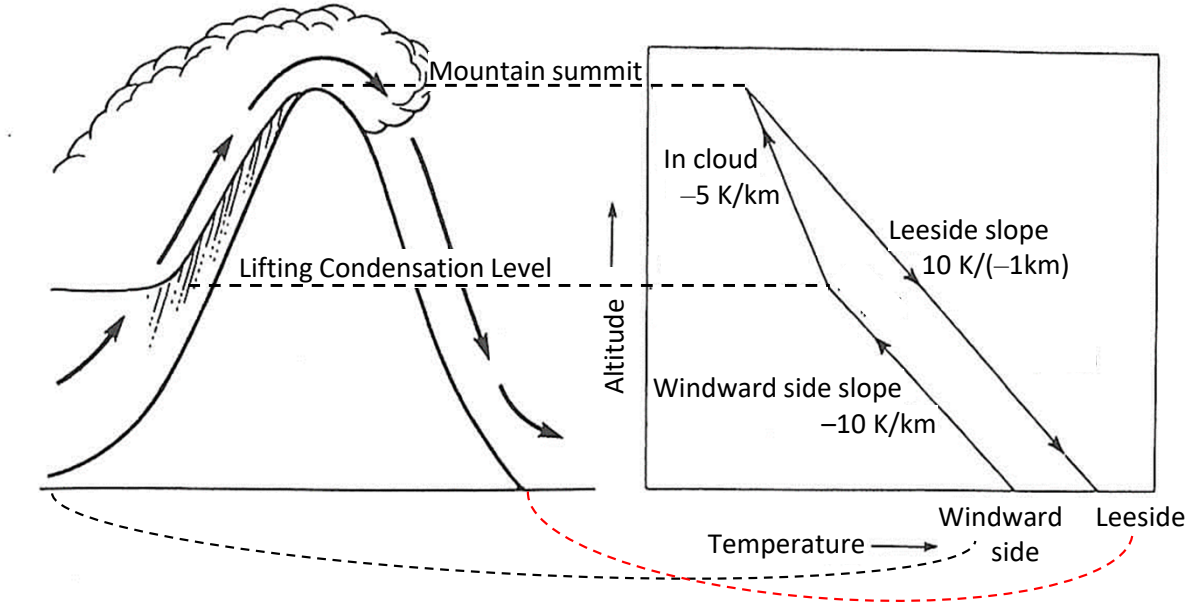

Boundary layer (surface + atmosphere) heat balance

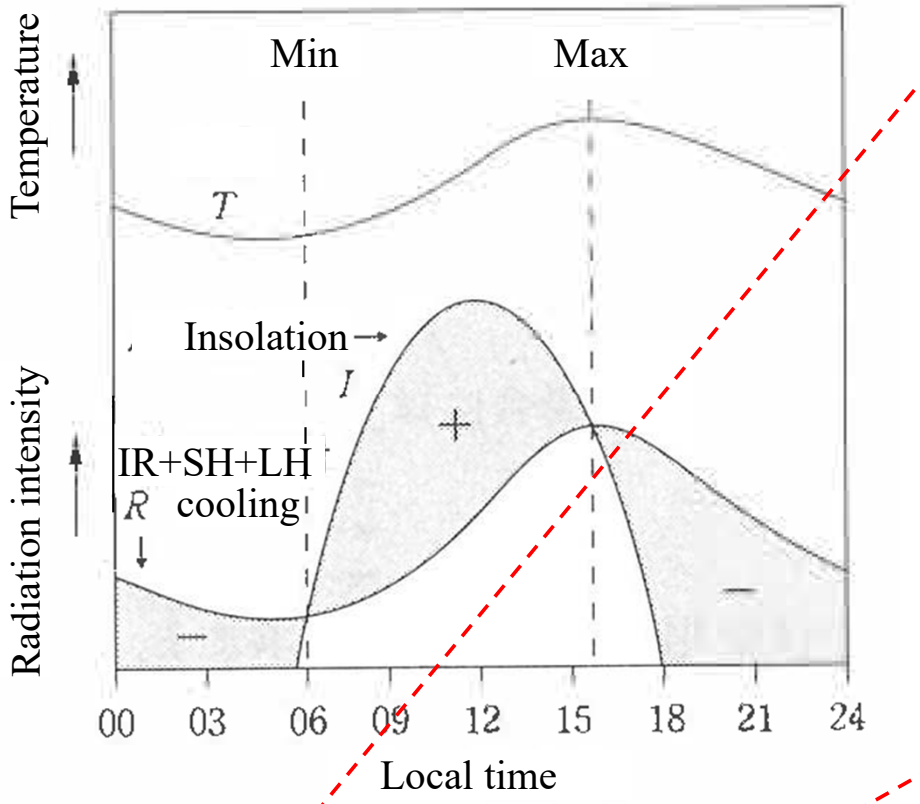

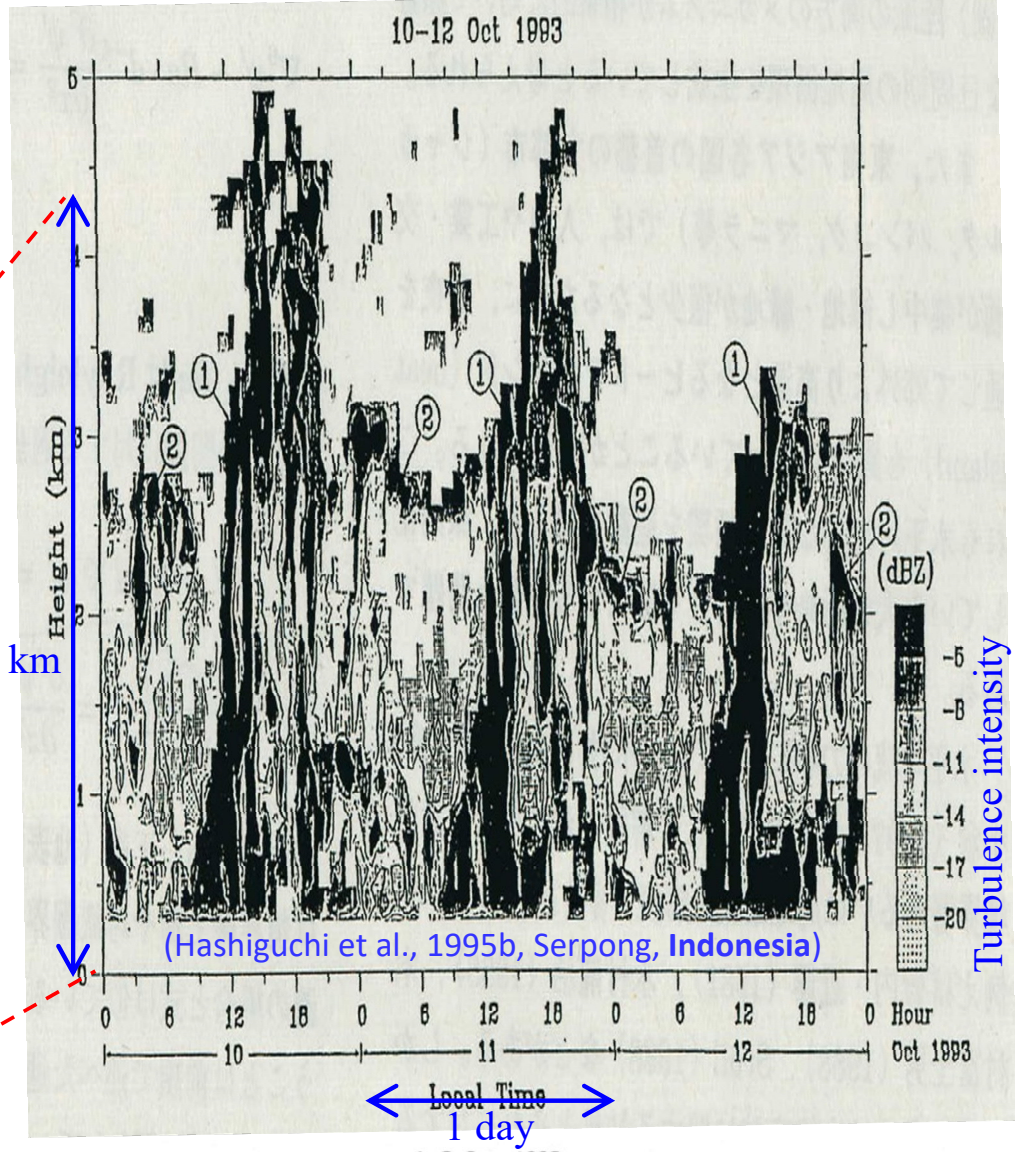

3–5 km

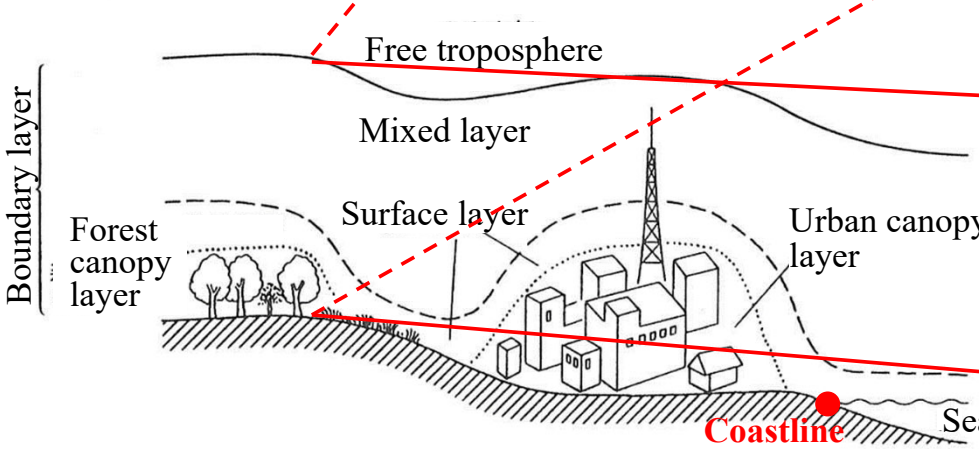

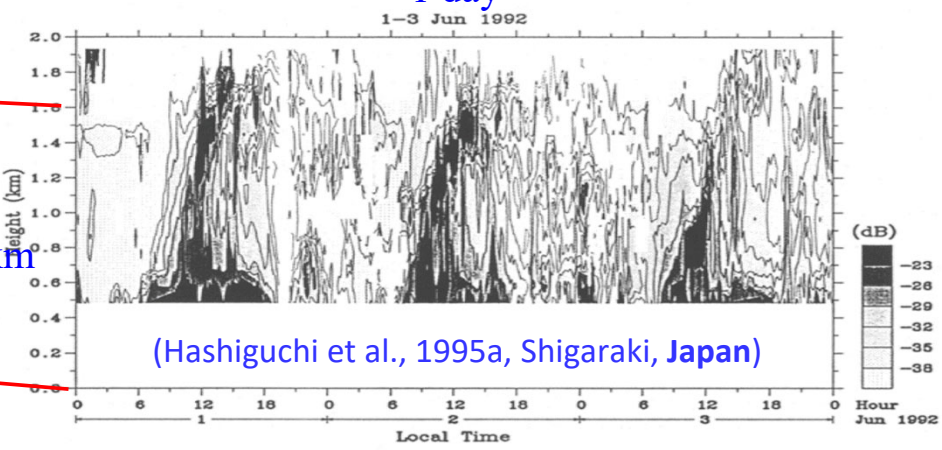

1–2 km

No “tropical night” in the tropics

- In the mid latitudes wind and rain are mainly by cyclones without depending upon the local time, and the diurnal-cycle sea-land breezes are by daytime solar heating and nighttime infrared cooling in the anti-cyclonic fine weather.
- In the equatorial tropics precipitating clouds themselves generate the diurnal cycle and temperature < 25℃ (not satisfying “tropical night”) before sunrise.

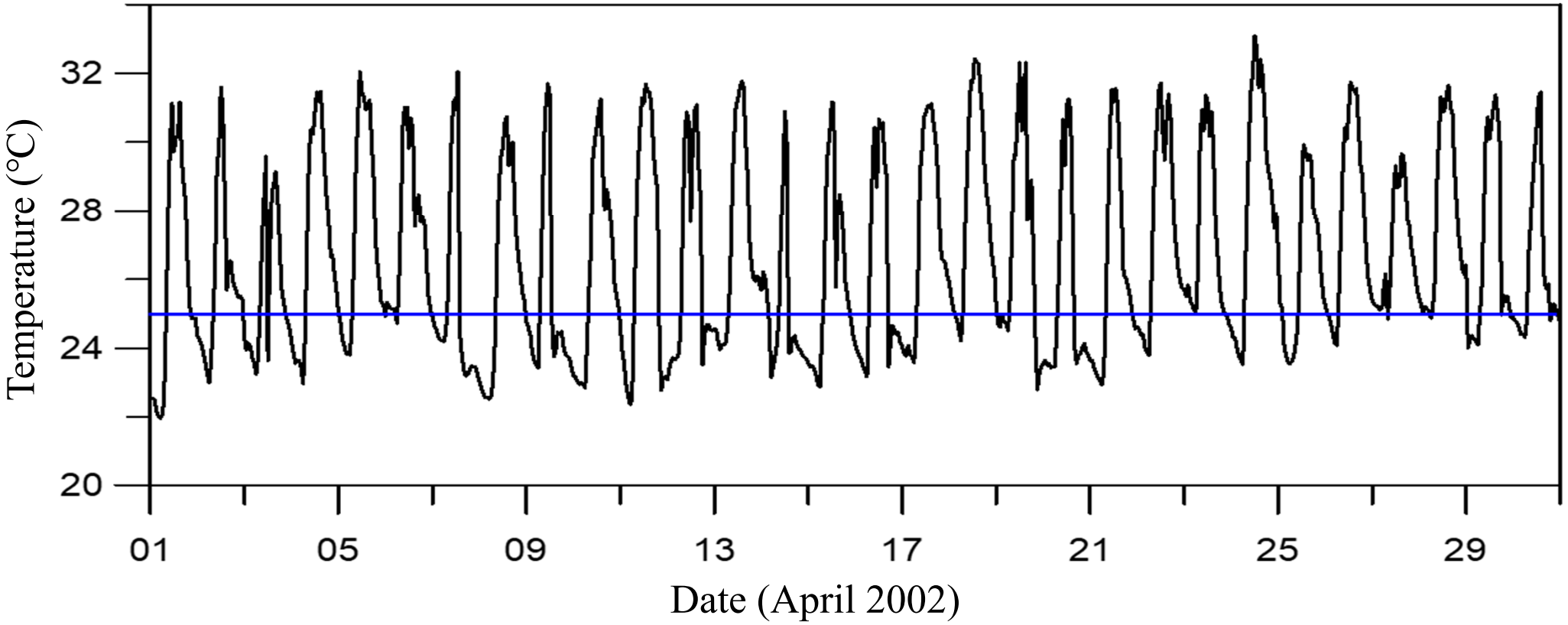

Hourly observation data of temperature at Pontianak during April 2002 (Wu et al., 2008).
A blue line indicates the lowest temperature limit 25℃ defined as “tropical night” by JMA.

Aspects determining land-sea temperature difference

- Heat capacity: solid land smaller than liquid sea/lake water

  Heating/cooling = heat capacity × temperature change → Land is heated/cooled more quickly than water.

- A part of heat given to sea/lake water is used for evaporation and does not contribute to temperature increase.

  Swamp and plants on land also may cause evaporation/evapotranspiration.

  Evening rainfall has a role of sprinkler and makes land cooling

- A part of heat on sea/lake surface may be transported to deeper layers by water motions.
- Mountain slope is heated/cooled more easily than the bottom basin/plain.
- Dry dessert, rocks and concrete surface (with a large albedo decreasing solar heating) have smallest heat capacity.

Observational difficulties

- Horizontal/temporal resolution/inhomogeneity/representability
- Vertical resolution: Stability indeterminacy
- Observations on the sea side (although more homogeneous/steady than land)
- Non-meteorological parameters on the land side

First Dutch arrival (bypassing Melaka)

Cornelis de Houtman
(1565–1599)

Frederick de Houtman
(1571–1627)

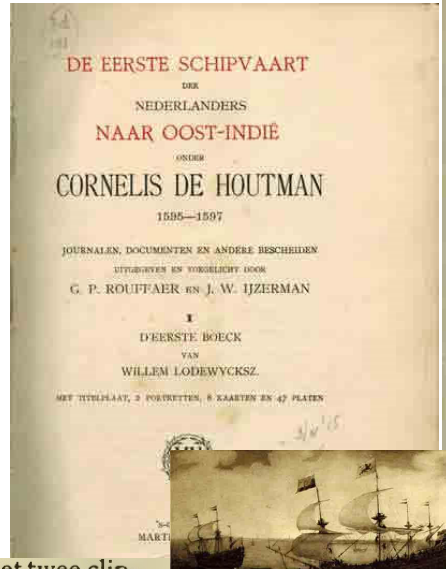

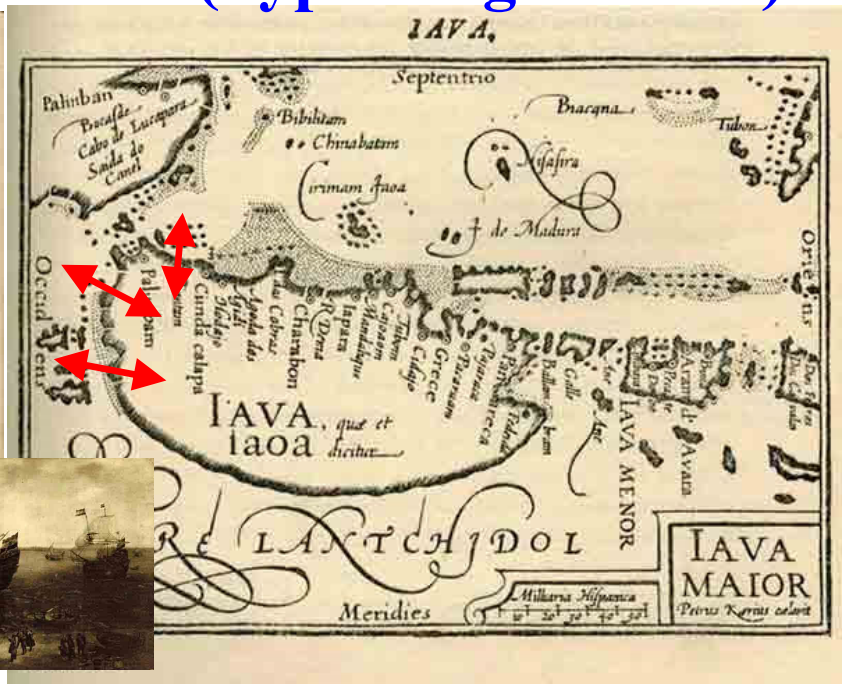

1596/6/15 hadden, laghen noch vier passelijcke Eylandekens [8]), met twee clippen, ende hadden desen nacht eenen harden wint uyten noordtwesten.

6/16 Den 16. Junij lichten wy ons ancker ende gingen tseijl met eenen n.w. wint, n.o. ten n. aen, wierpen twee mael tloot in 22. vademen suyversandt grondt, ende overmidts stillekens worde, moesten d'ancker laten vallen, want wy anders te rugghe dreven, overmidts de [26r°] stroomen van 't oosten nae 't westen liepen tot nae de middagh datter stercke coelte quam, gingen alsdoen n. ten o. aen, ende de Strate streckte haer tusschen tlanck hooghe Eylandt, ende tlanckwerpich oost [9]), den wint quam recht uyt de Straet, derhalven na ons lootsmans begeiren weder setten in 19. vademen. Saghen noch diversche *Paraos* die van *Bantam* quamen, ende wy moestent onder d'Eylanden setten, overmidts wy recht inde wint creghen om den morghen

6/17 stont te verwachten, dat de wint uyt thooghe landt van *Dampin* valt, welck de plaetse was daer wy met de Pinas ende Sloep gheweest waren int Eylandt van *Sumatra*, ende ginghen int dagh quartier tseijl [10]), waerschouwende de andere schepen van ghelijcken te doen, doende onsen cours o.n.o. aen [11]), den wint noordt west. Sagen noch

Saghen di-

Krakatau

is noch een ander seer hooghe Eylandt, hebbende in top vanden bergh een cloue, twelck twee toppen maect [16]), is niet seer groot, ende also de wint altoos nae de middag uyten oosten comt, hebbent wy wedergheset in 15. vademen goet ancker gront tot des anderen daeghs.

Strong rain before sunrise

met hare handen haer aensicht tot over haer hooft *: het was desen wesen. nacht seer reghenachtich weder. Ende des anderen daeghs zijnde

6/18 den 18. dito, saghen wy 7. seylen in diversche plaetsen, waer van ons de twee aen boort quamen, zijnde d'eene des lootsmans *Parao*,

6/19 Den 19. also wy voorby een stedeken [19]) passeerden, quamen ons veel *Paraos* aen boort, van 't Eylandt *Sumatra*, eenighe met seylen, ende brachten Cocos, wat Peper, Naghelen, Muscaten, Vannanas, [26v°] ende wat Hoenderen, Oraengien, vraghende oft wy van *Goa* oft *Cochin* quamen, ende nae *Bantam* voeren [20]), ende luttel ghevoordert hebbende, lieten onse anckers weder in 27. vademen. De stroom was ons contrary ende luttel coelte, ende hadden z. o. aen ontrent 3. my-

6/20 len geseylt. Ende also des anderen daeghs stil was, bleven wy liggen: maer des anderen daeghs, also de wint w.z.w. was, lichten wy

6/21 ons ancker, ende ginghen cours o. ten z. dan overmidts de stilte, lieten d'ancker vallen in 22. vademen, ende andere in 30. ende ginghen nae de middagh weder tseijl, ende saghen diversche seylen.

DAT 16. CAPITTEL.

Hoe wy voor de Haven van Sunda quamen, ende wat aldaer gheschiet is inde aencomste.

Night–10 AM: land wind; noon–evening: sea wind

6/22 Seylende dan dus lancksamich (overmidts de contrary stroomen, als oock de veranderinghe vanden wint: want nae middernacht is den wint oost tot den 10. uren voor middagh, ende voort tot den avont west, waer deur so moeyelijken is om de Straet te passeren) [27v°] zijn wy den 22. Junij voor de haven van *Bantam* [1]), ende de Custe van *Sunda* gecomen, siende voor ons een leegh, groen, schoon Eylandt, twelck de Javanen *Pulo Pajan* noemen [2]), dwelck een lanckwerpigh

Anno 1596. den 22. Junij.

van Bemmelen (1913, 1922)

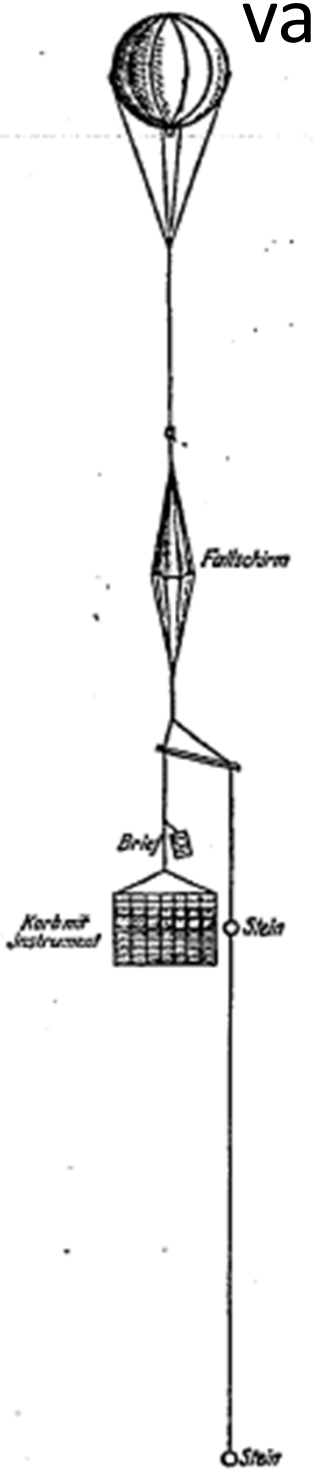

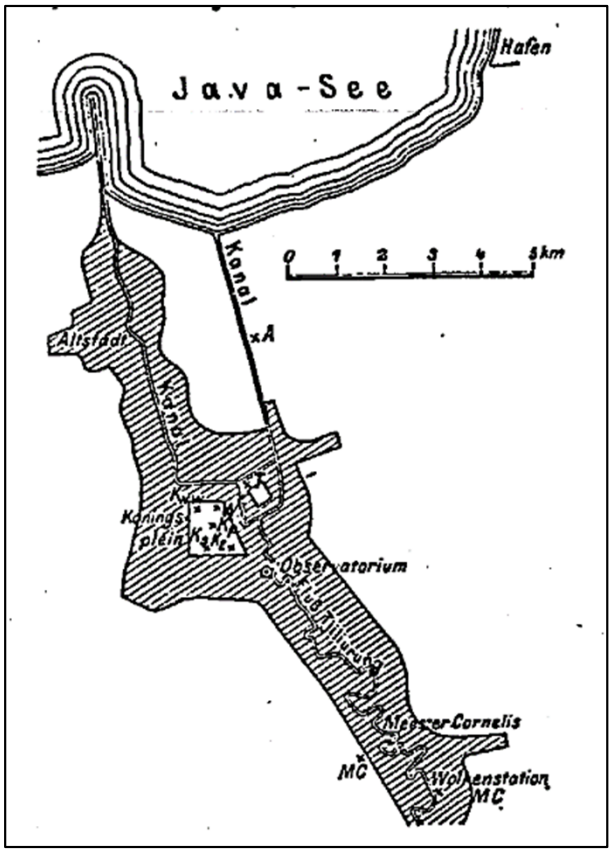

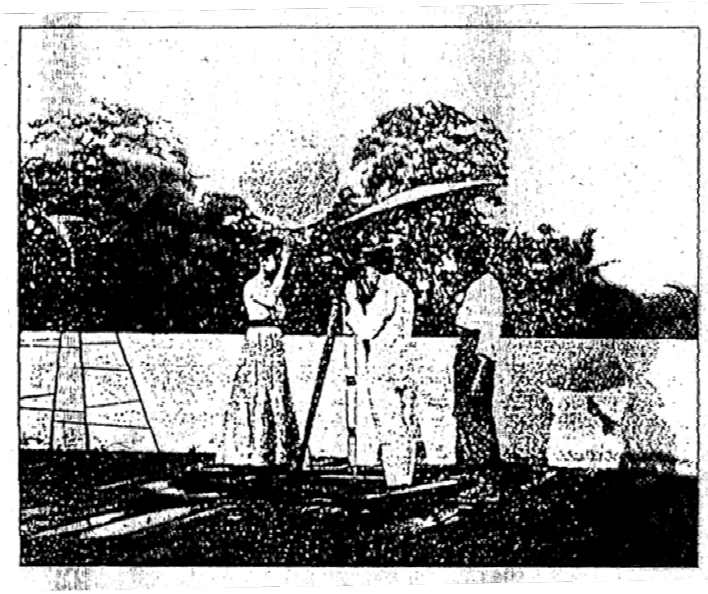

Rainy (Dec-Feb) Dry (Jul-Sep)

N E S W N N E S W N

QBO

Monsoon

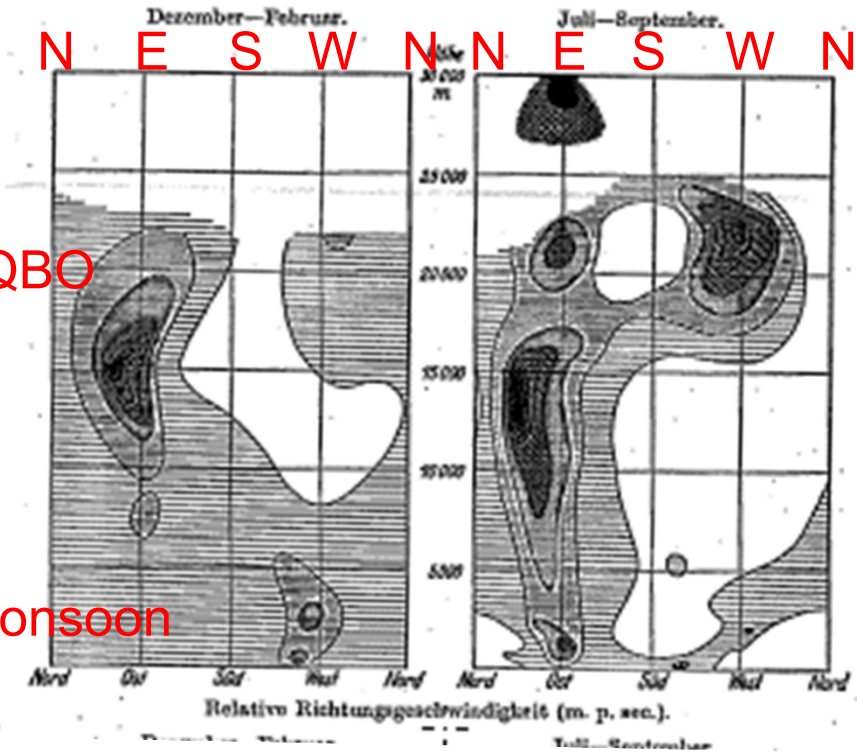

06-24 LT hourly for May-Nov;
08, 14, 19 LT for Dec-Apr
during 1905-15

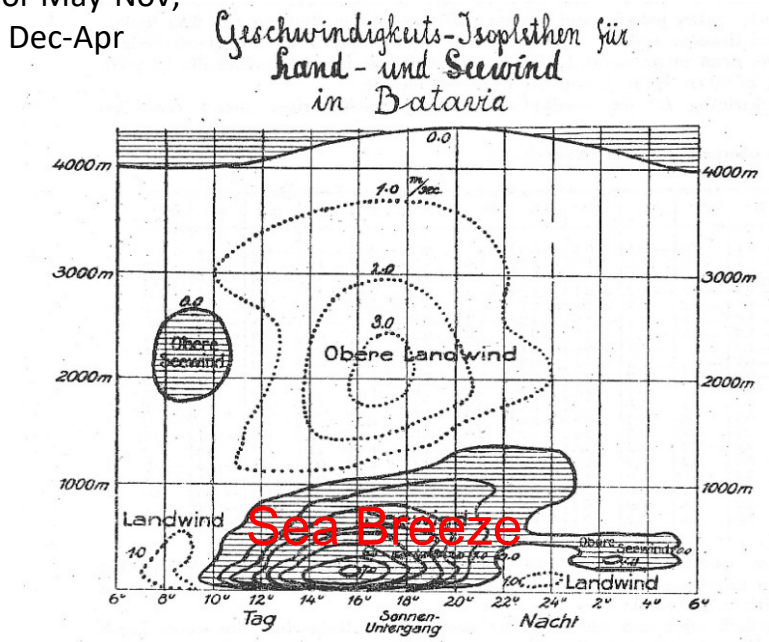

06 12 18 00 LT

Pre-YMC observations in Nov-Dec 2015

YMC obs in Nov 2017-Jan 2018

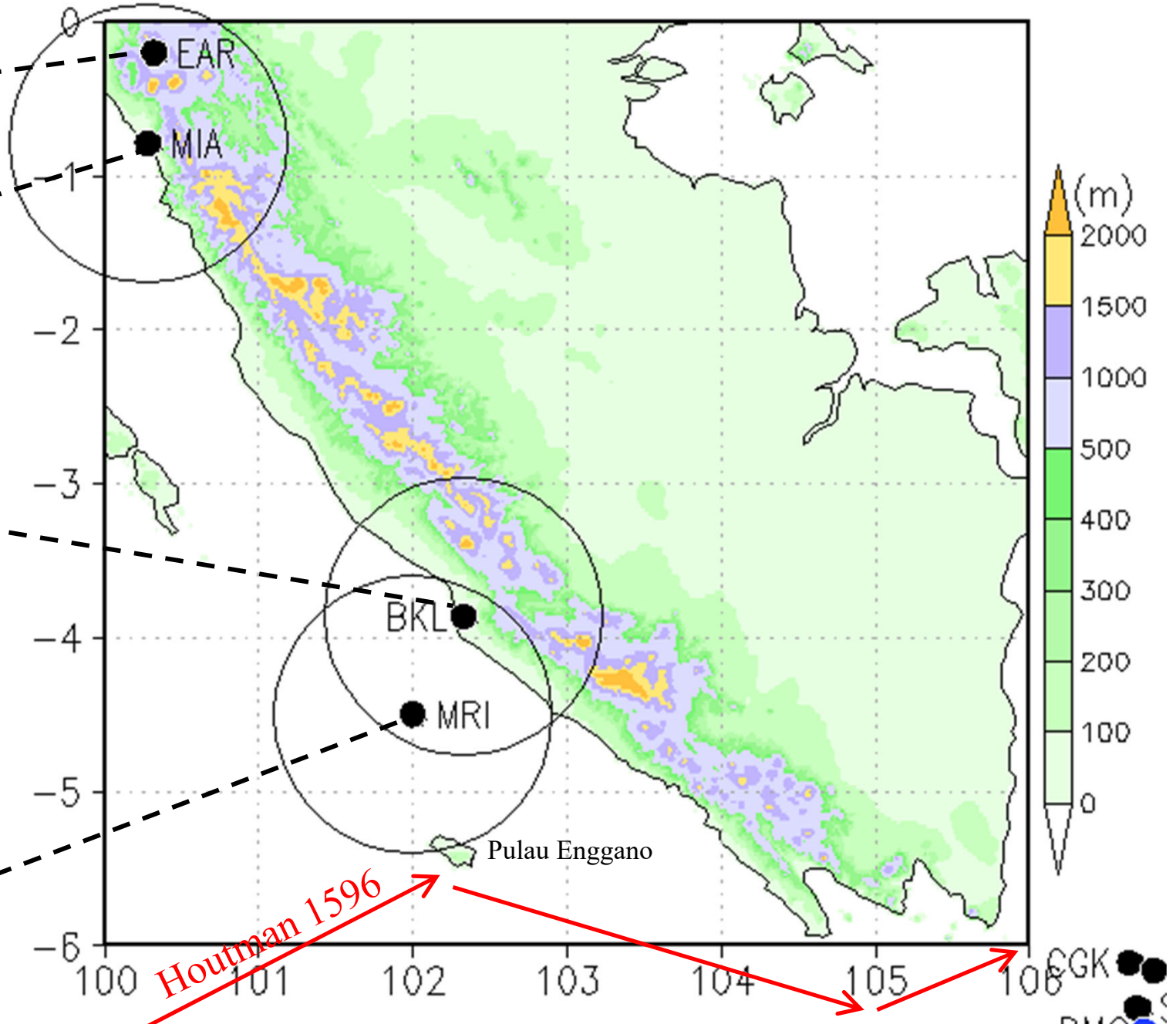

Lower-tropospheric temperature at/off Bengkulu (8-18 Dec 2016)

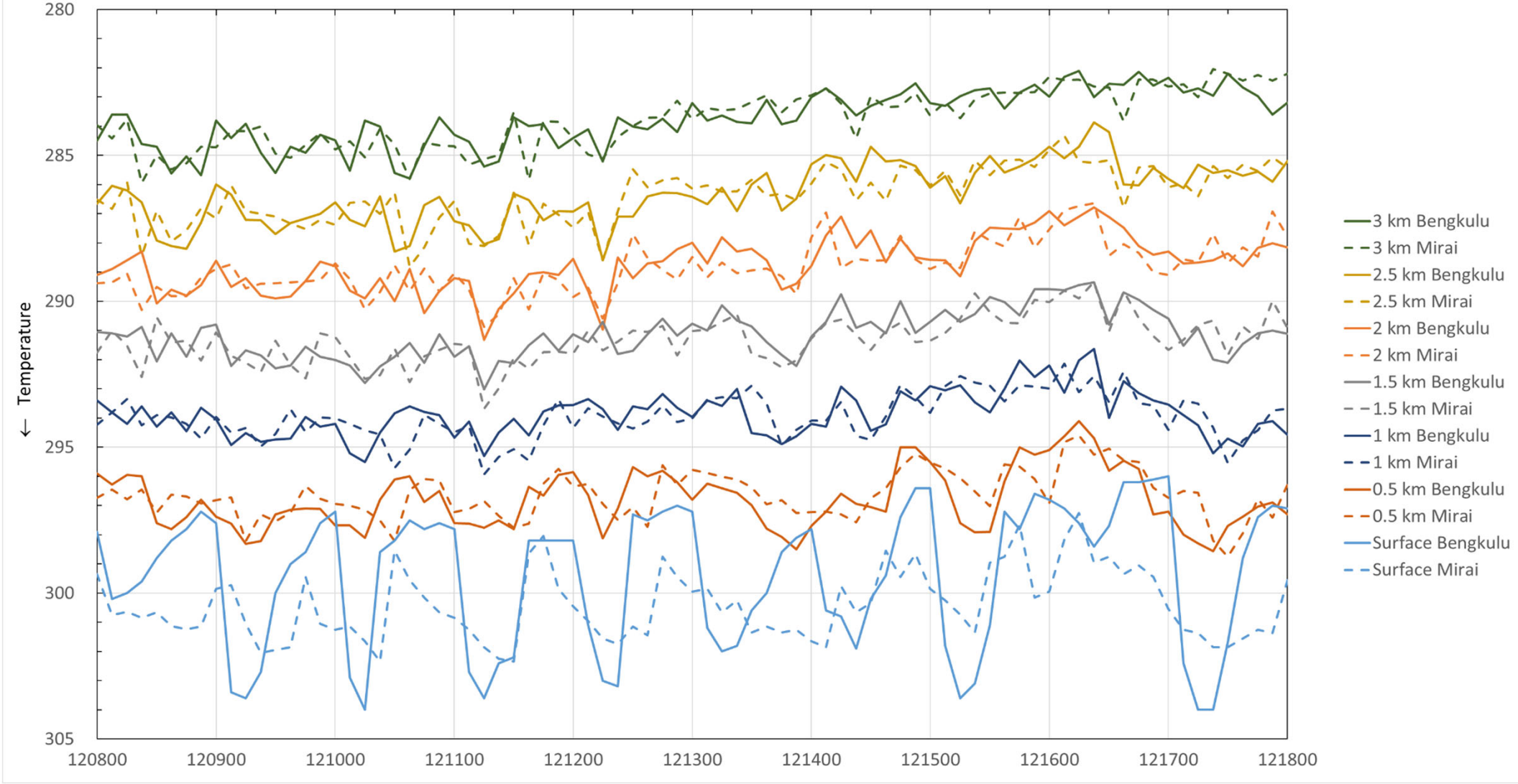

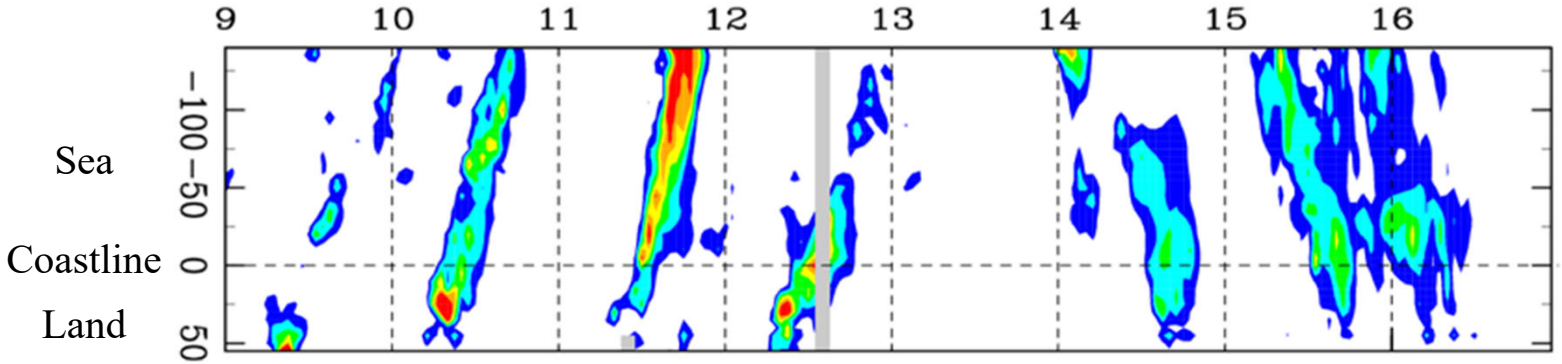

00Z = 07 LT (≒sunrise)

Radar echo Hovmöller
(analyzed byYokoi)

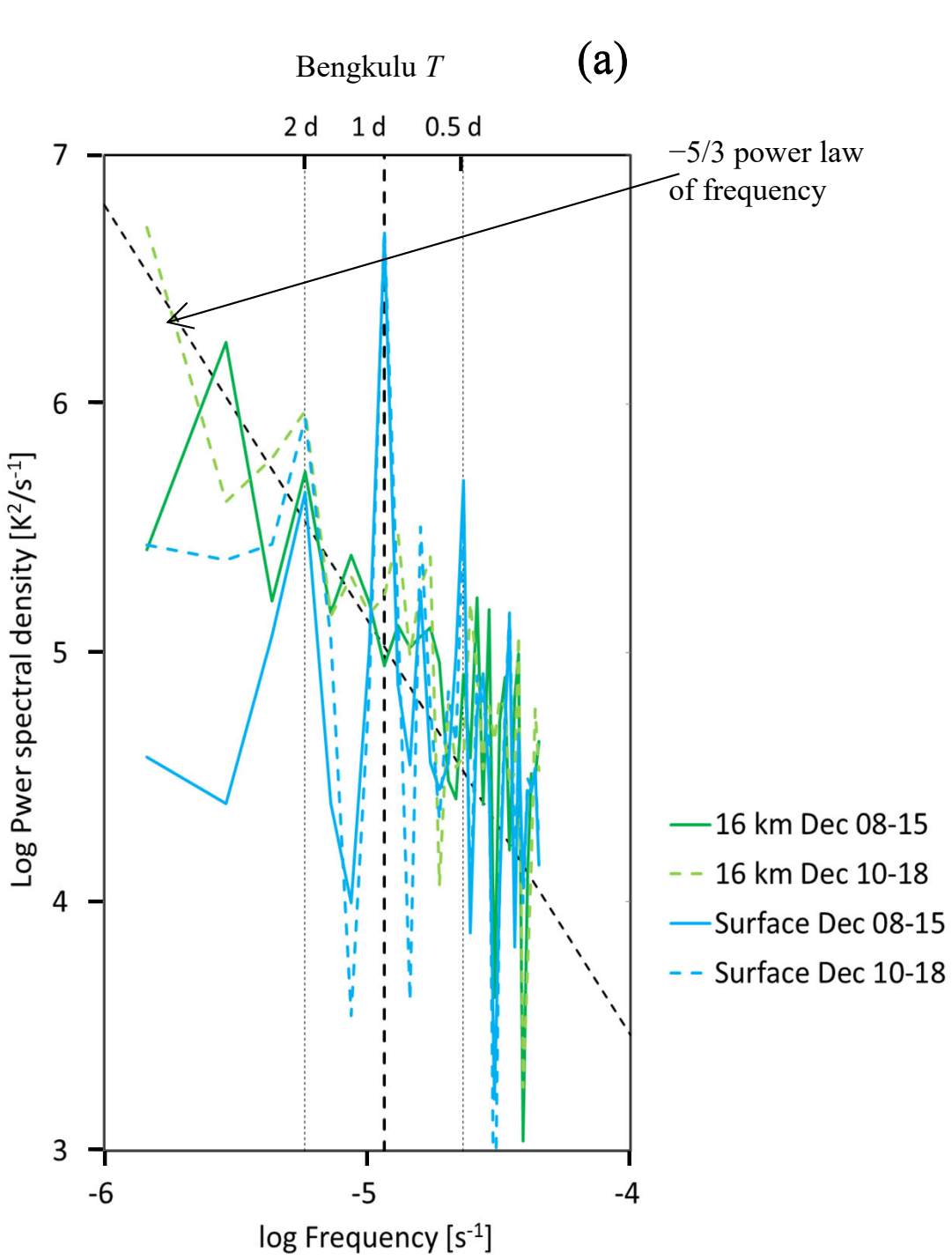
Bengkulu T
(a)
2 d
1 d
0.5 d
−5/3 power law of frequency
Log Pwer spectral density [K²/s⁻¹]
log Frequency [s⁻¹]
16 km Dec 08-15
16 km Dec 10-18
Surface Dec 08-15
Surface Dec 10-18

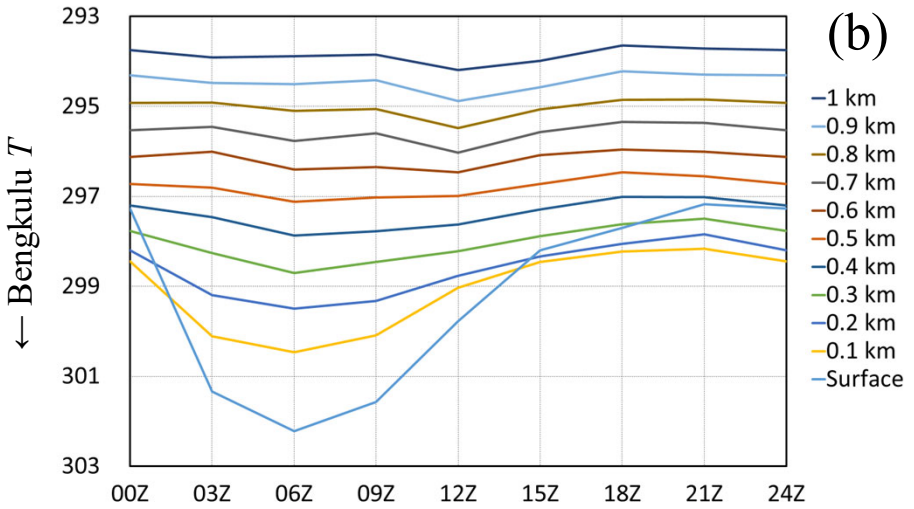
(b)
← Bengkulu T
−1 km
0.9 km
0.8 km
0.7 km
0.6 km
0.5 km
0.4 km
0.3 km
0.2 km
0.1 km
Surface

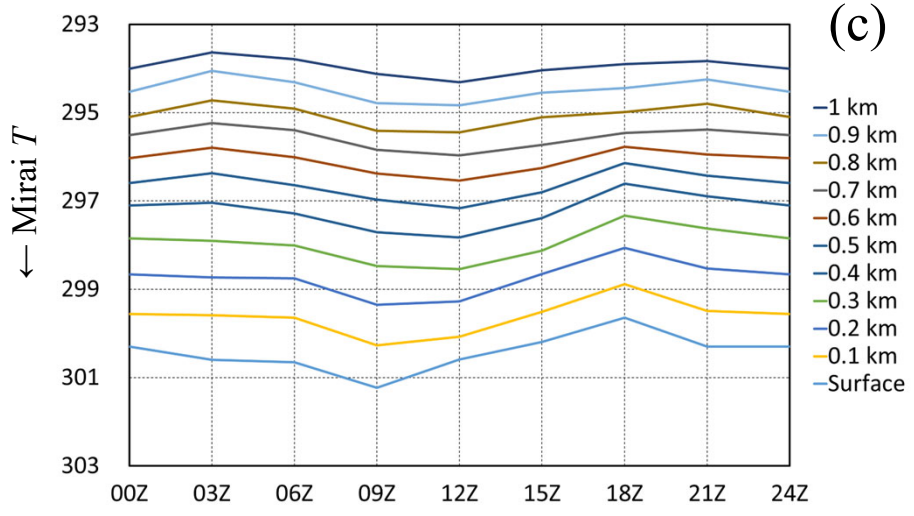
(c)
← Mirai T
−1 km
0.9 km
0.8 km
0.7 km
0.6 km
0.5 km
0.4 km
0.3 km
0.2 km
0.1 km
Surface

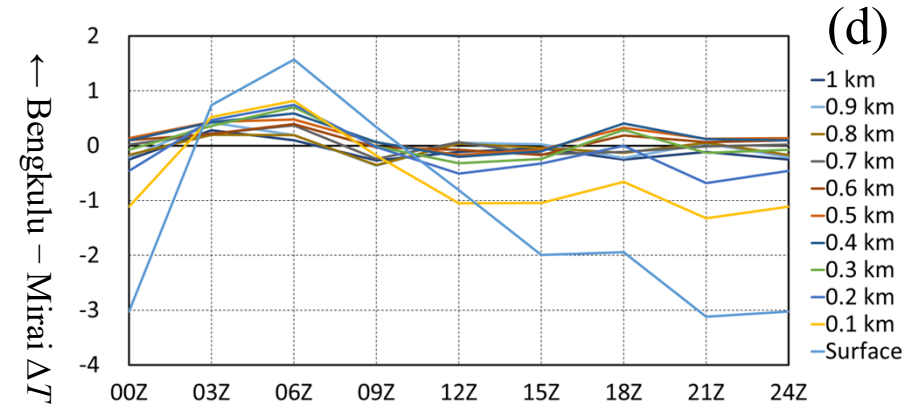
(d)
← Bengkulu − Mirai ΔT
−1 km
0.9 km
0.8 km
0.7 km
0.6 km
0.5 km
0.4 km
0.3 km
0.2 km
0.1 km
Surface

Sea-land breeze circulation over ASEAN

00 UT (07 LT)
Land breeze in midnight - morning

12 UT (19 LT)
Sea breeze in afternoon - evening

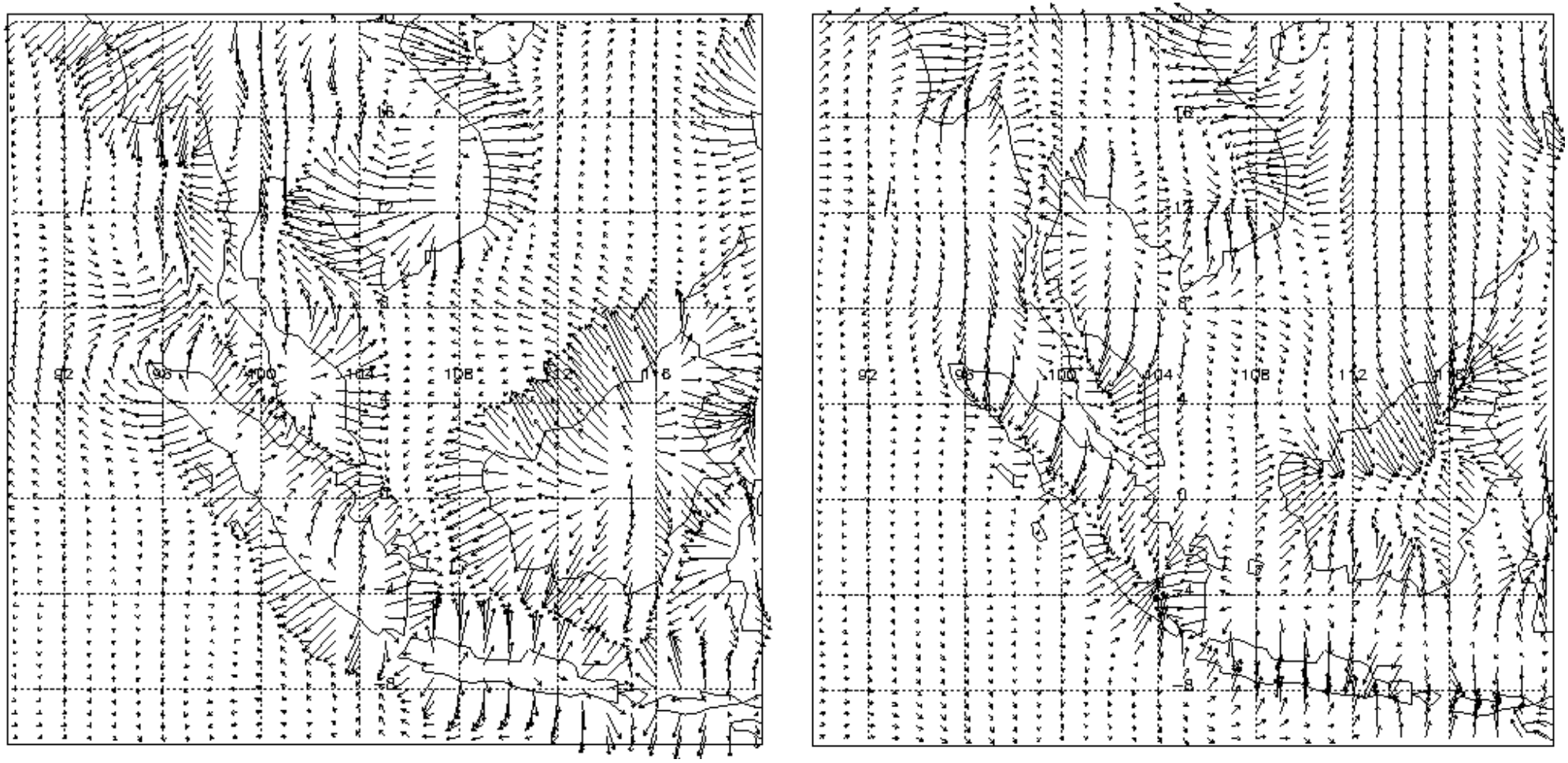

→ 2 m/s

JMA reanalysis (April – October 1998)

(Uchida, Yamanaka, et al., 2003)

Modeling of the sea-land breeze circulation

- A pioneering study (Estoque, 1962; Bay of Manila)

  Land surface temperature: Diurnal cycle of 10℃

  Sea surface temperature: constant

  Results are shown for maximum sea breeze in the afternoon

- (a) No back ground wind :

  Maximum sea wind 10 ms^{-1} at 250 m height

  Sea-breeze front: 32 km from the coastline

  U, T' : large gradient, $W \sim 0.1$ ms^{-1}

  V (along coastline) due to Coriolis force ($V < 0$ for $U > 0$)

- (b) Landward background wind:

  Larger intrusion of the sea breeze (unclear front)

- (c) Seaward background wind:

  Stronger front and upstream near the coastline

- Land breeze weaker than sea breeze

  (However, the mountain and "sprinkler" effects may enhance the land wind in case of Indonesian Maritime Continent)

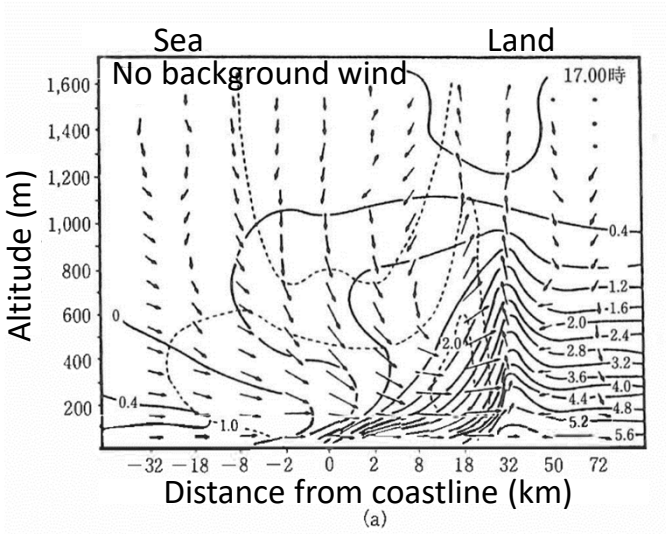

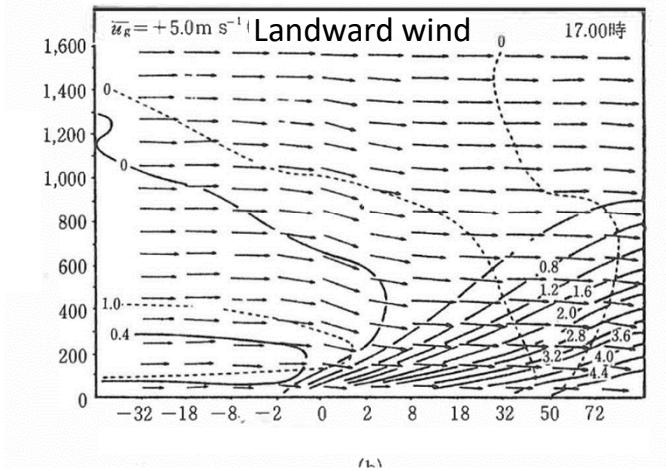

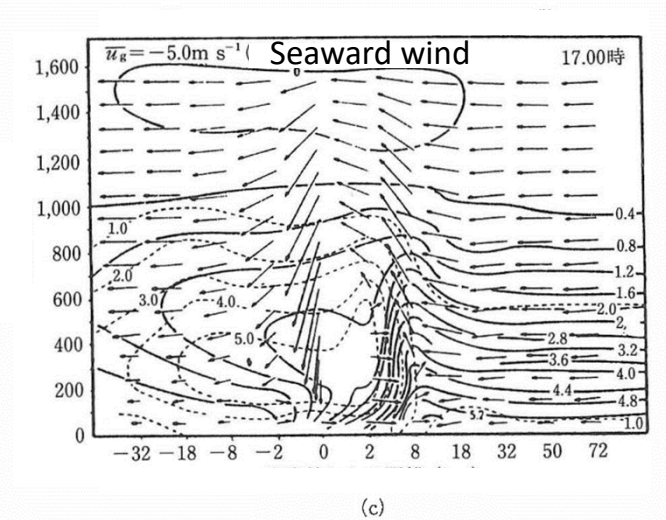

Pair of internal (up-/down-ward propagating) waves = Convection

Plain monochromatic wave far/free from boundary

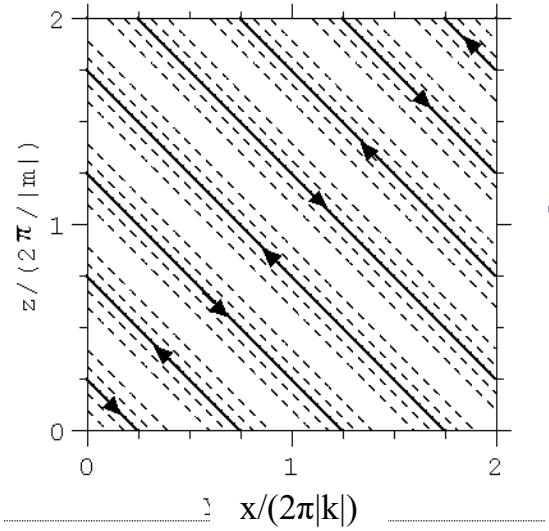

$\psi = \cos(kx + mz)$

+

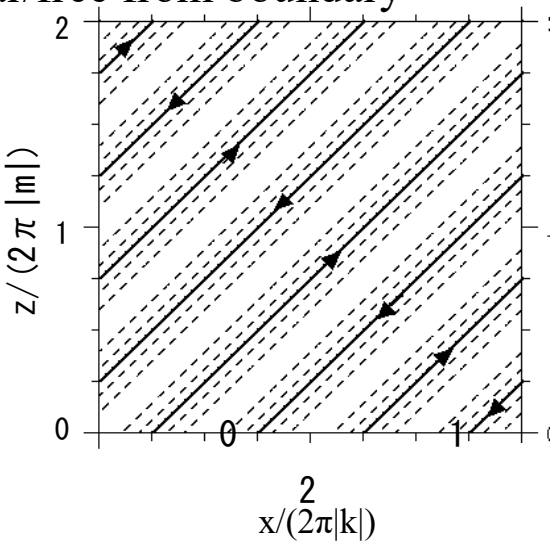

$\psi = \cos(kx - mz)$

=

On solid boundary ($w = 0$ at $z = 0$)

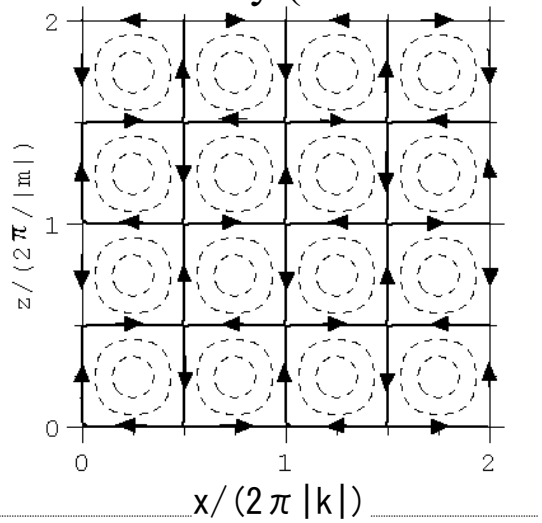

$\Psi = \cos(kx + mz) - \cos(kx - mz)$
$= -2\sin kx \sin mz$

Westward traveling convection

(|Wetward| > |Eastward|)

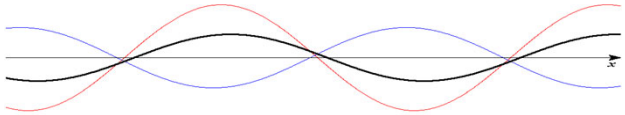

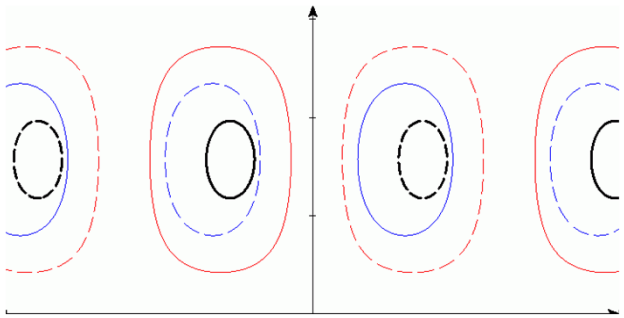

Stationary convection

(|Westward| = |Eastward|)

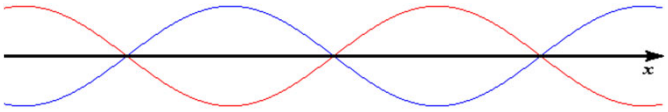

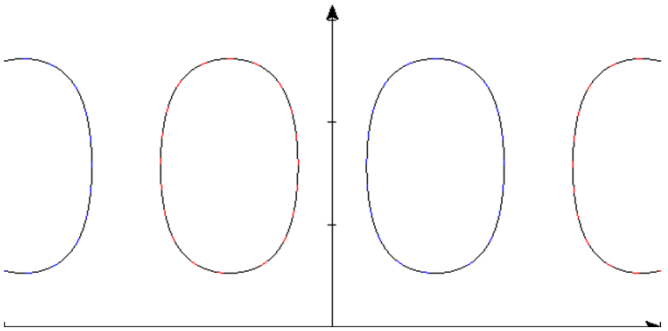

Eastward traveling convection

(|Westward| < |Eastward|)

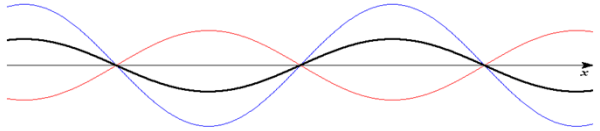

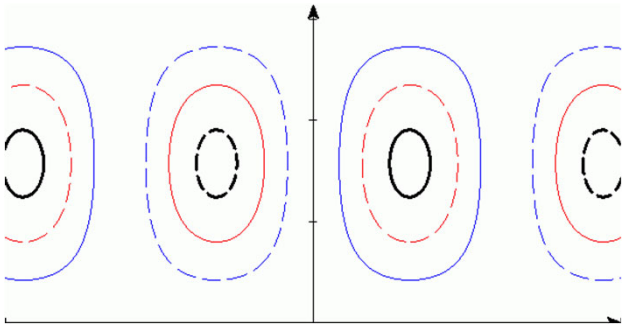

Noontime clear sky over land permits solar heating dependent on season & latitude
→ "rainy season" as southern hemisphere

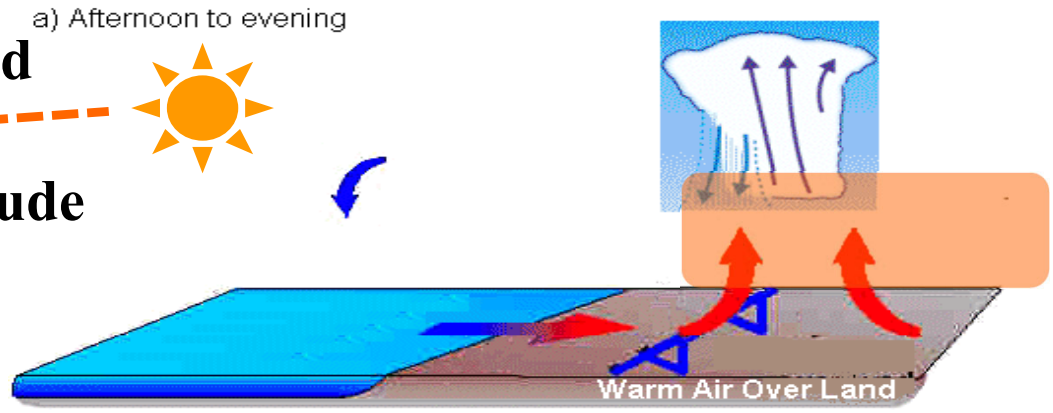

Rainfall cools land
→ Dominant diurnal cycle even in rainy day/season

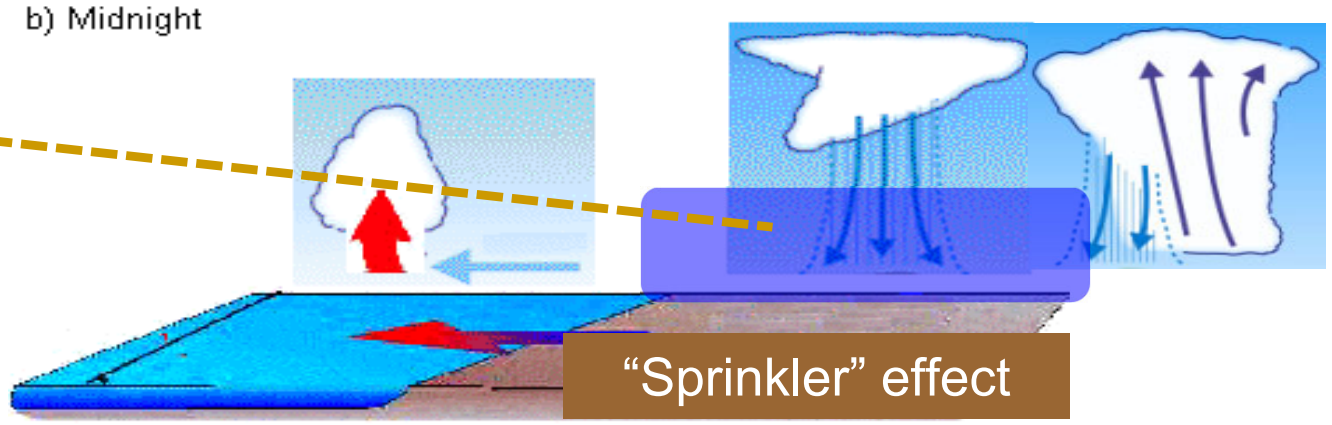

Sea water temperature determines intensity of morning maritime convection
→ Less rainfall in El Nino and More rainfall in La Nina

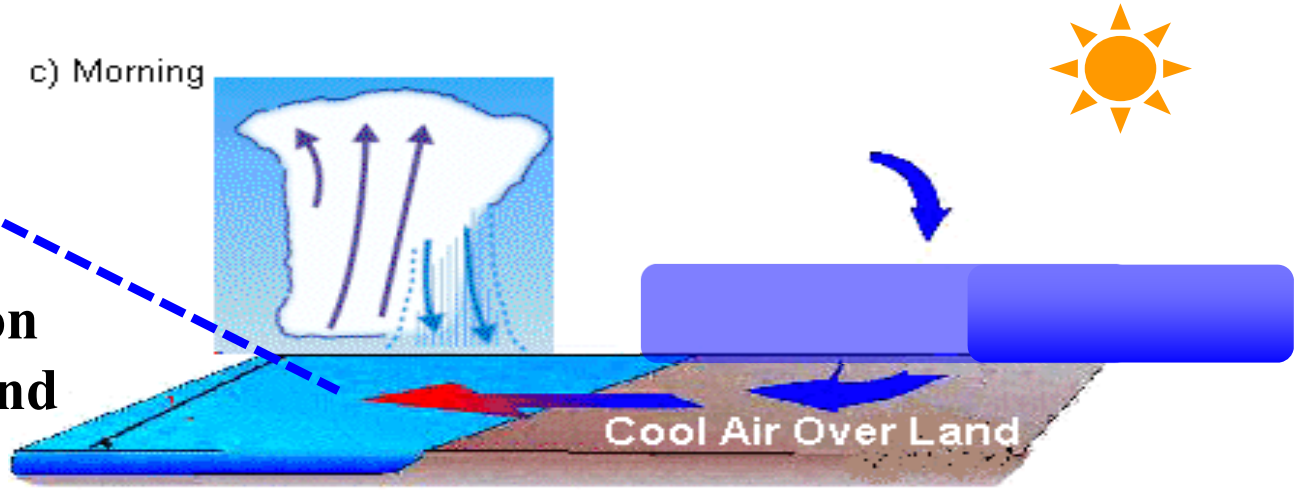

(Wu, Yamanaka & Matsumoto., 2008)

Satellite tracking of rain cloud migration

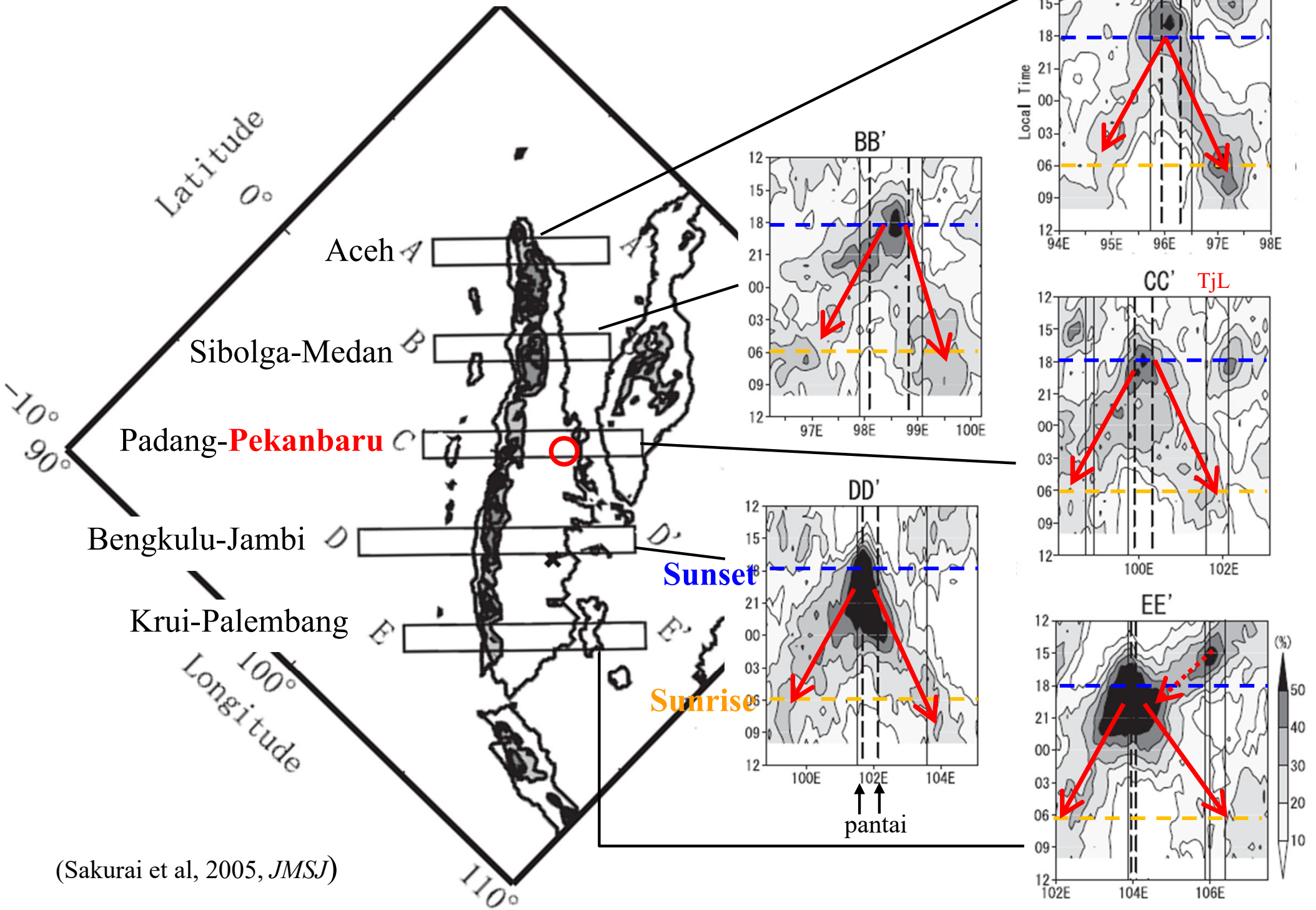

(Sakurai et al, 2005, *JMSJ*)

Sumatran diurnal cycle and Riau peatland rainfall

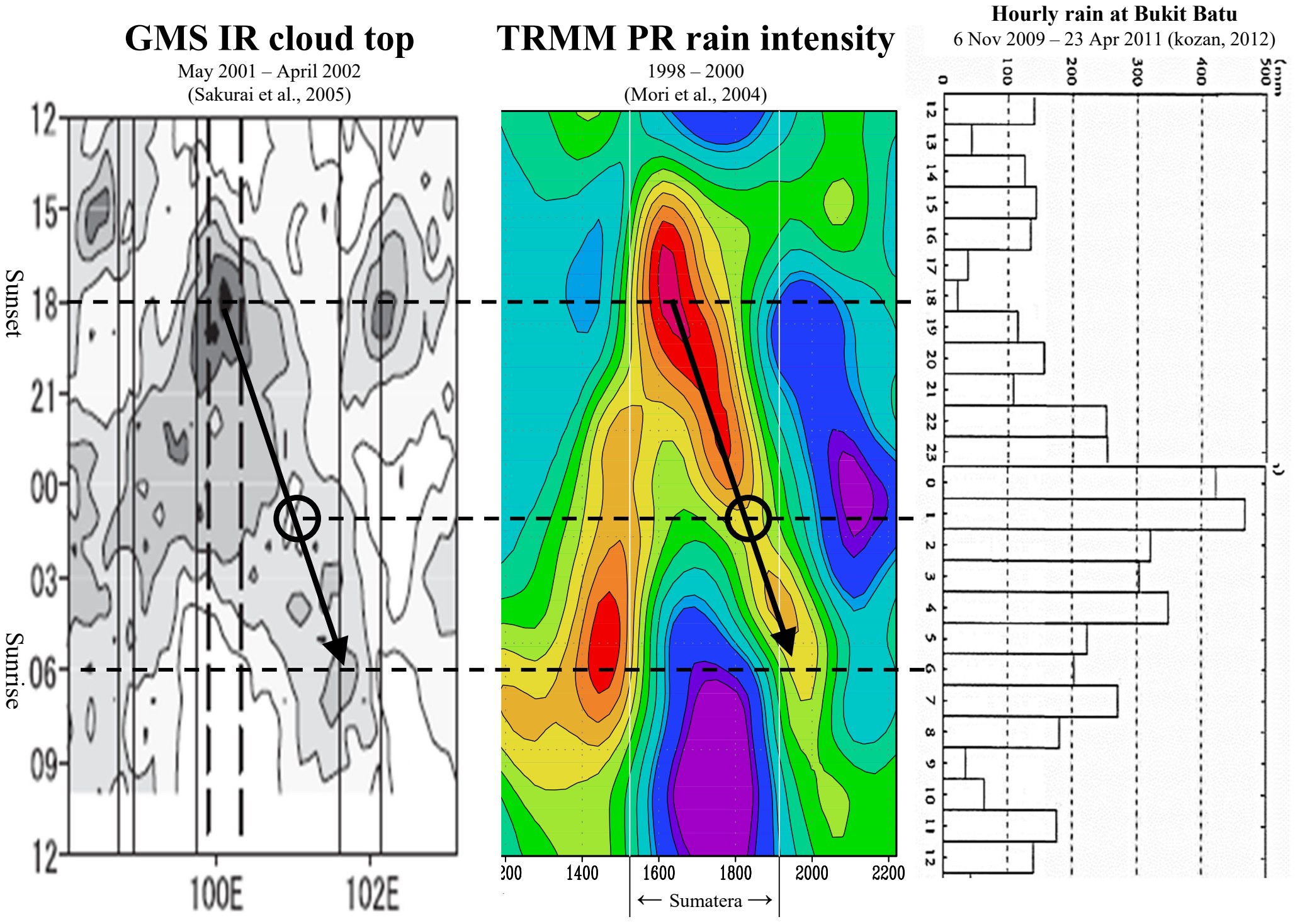

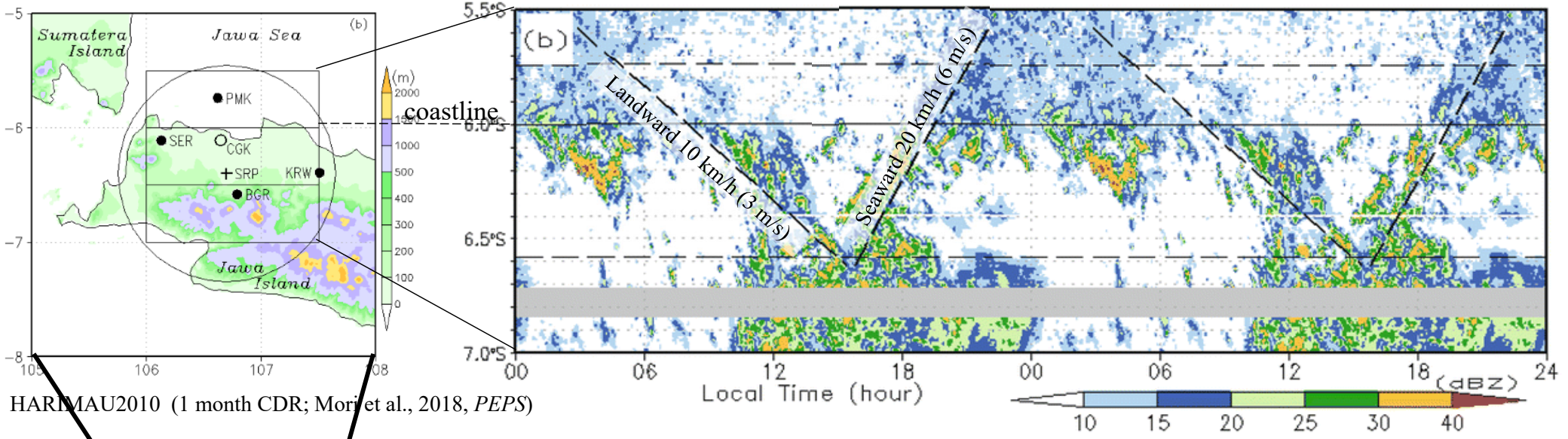

HARIMAU2010 (1 month CDR; Mori et al., 2018, *PEPS*)

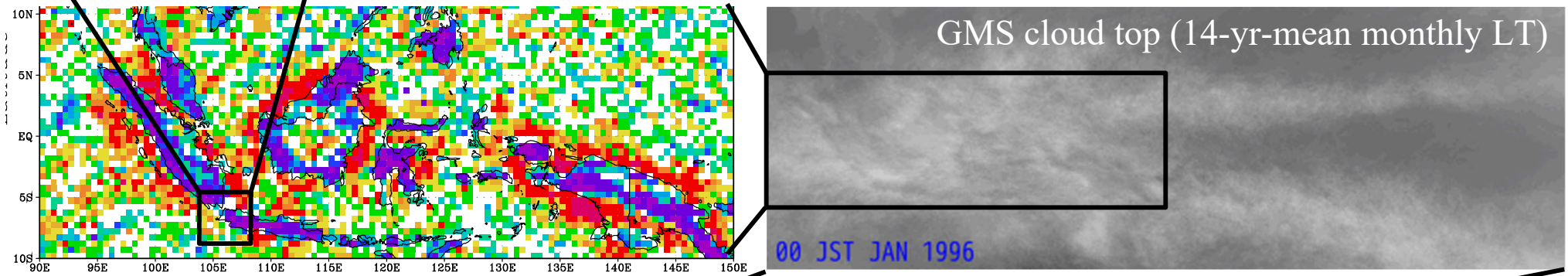

TRMM rainfall (3-year mean LT; Mori et al., 2004)

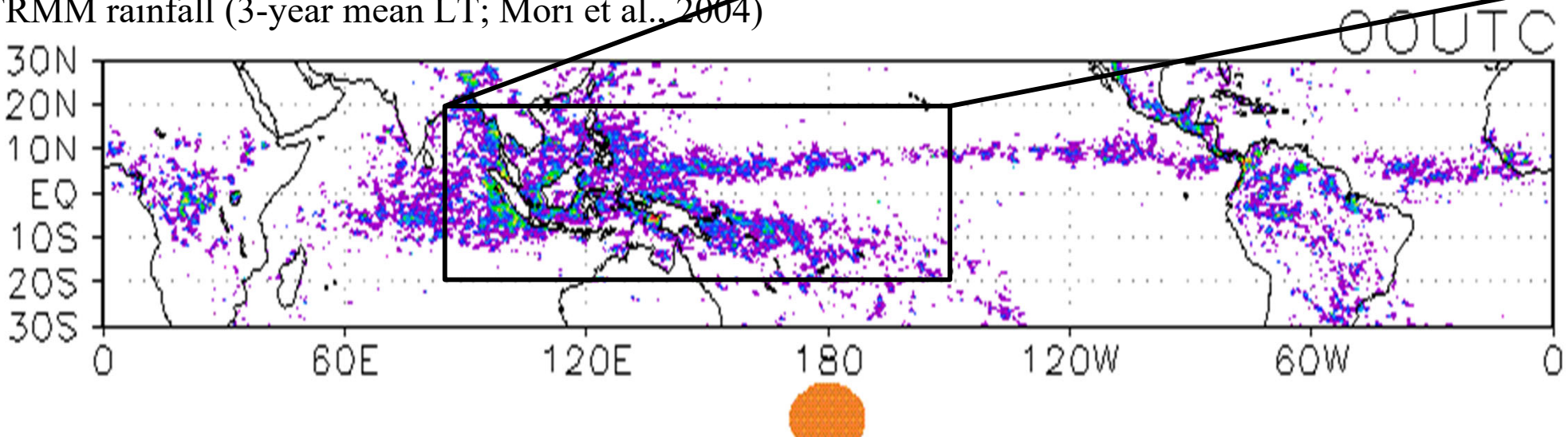

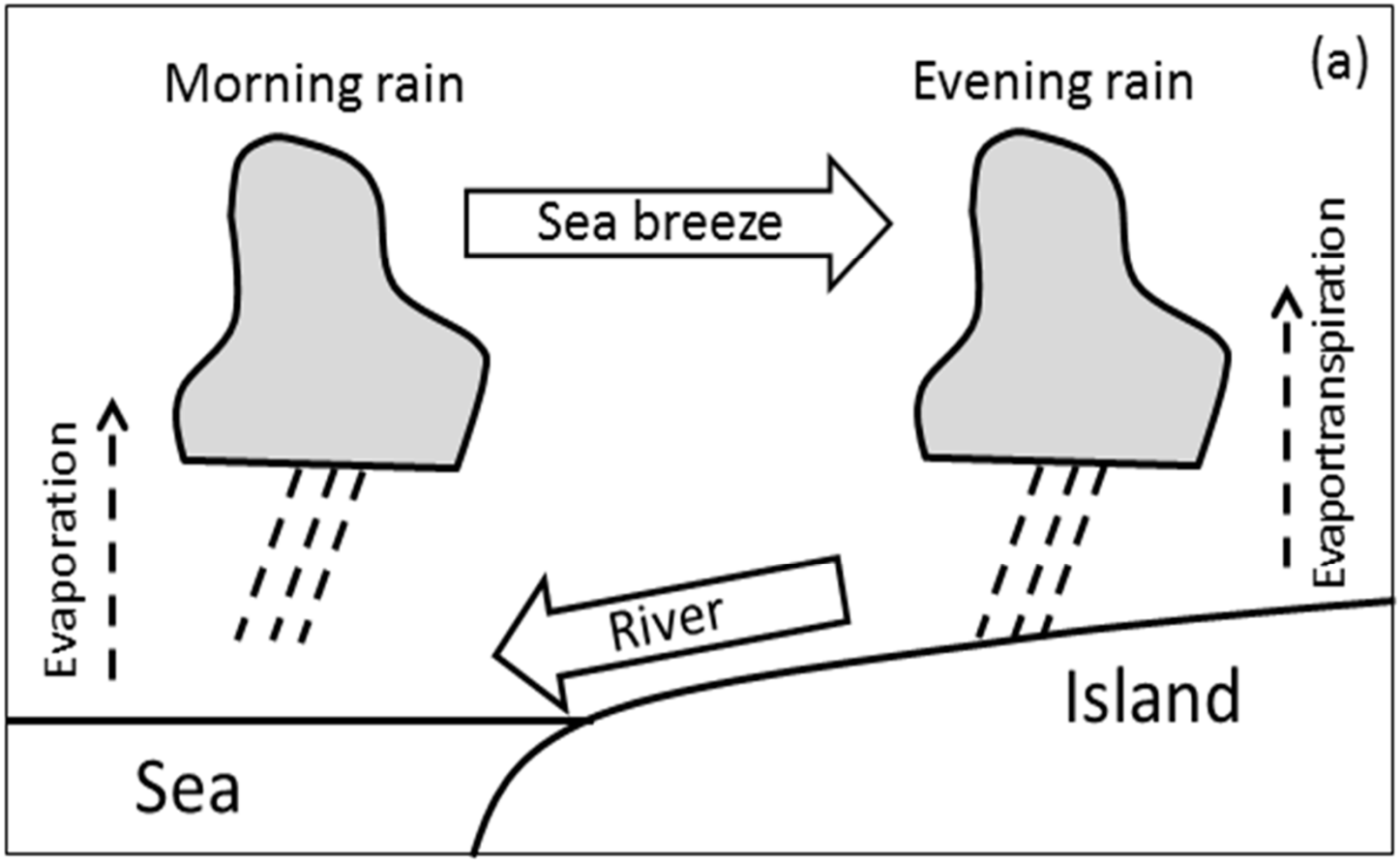
(a)
Morning rain
Evening rain
Sea breeze
Evaporation
Evaportranspiration
River
Island
Sea

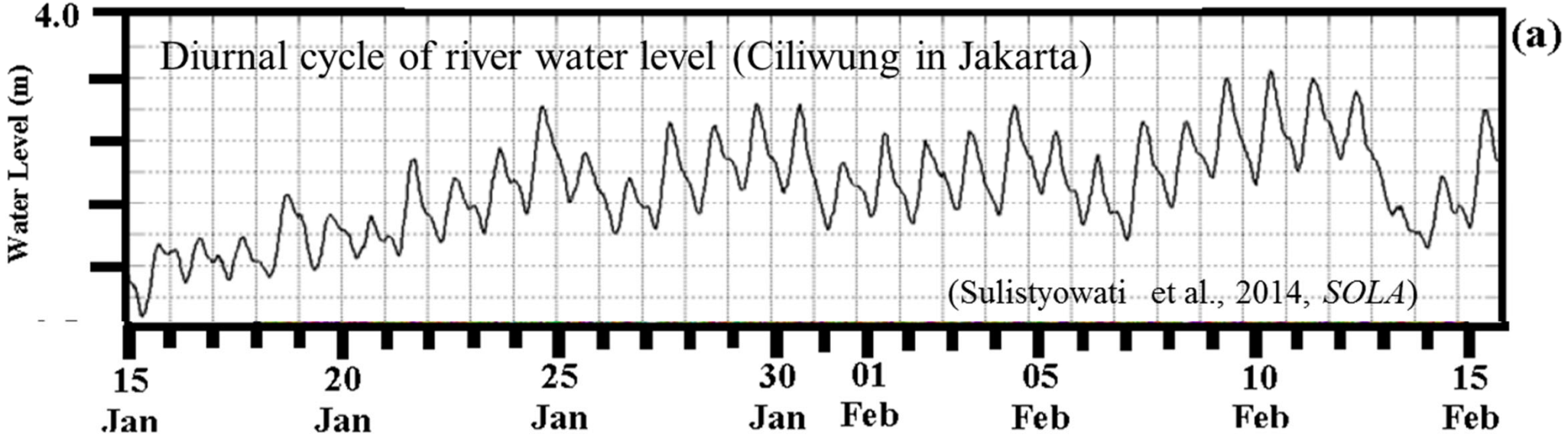
(a)
Diurnal cycle of river water level (Ciliwung in Jakarta)
(Sulistyowati et al., 2014, SOLA)
Water Level (m)
4.0
15 Jan
20 Jan
25 Jan
30 Jan
01 Feb
05 Feb
10 Feb
15 Feb

Diurnal cycle enhancing seasonal cycles

- Noon insolation before could parasol effect → seasonal cycle
  - **Rainy in each hemispheric summer** (Semiannual near equator)
    (Hamada et al., 2002; Aldrian & Susanto, 2003)
  - Cloud parasol effect: after could generation mainly afternoon
- Monsoon in the western IMC (Matsumoto & Murakami, 2000)
  - Eurasia-Indian Ocean location enhancing hemispheric contrast
  - Coriolis force → NE-SW / NW-SE wind in N / S hemispheres
  - N-winter "**cold surge**" → wet on E/S-China & Jawa Seas
    → flooding diurnal rain in Jakarta (Wu et al., 2007, 2013)

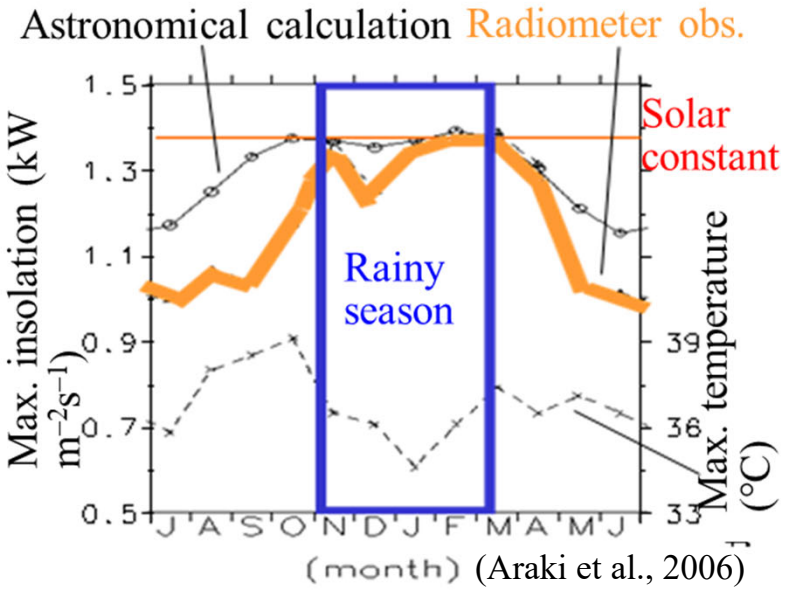

(Araki et al., 2006)

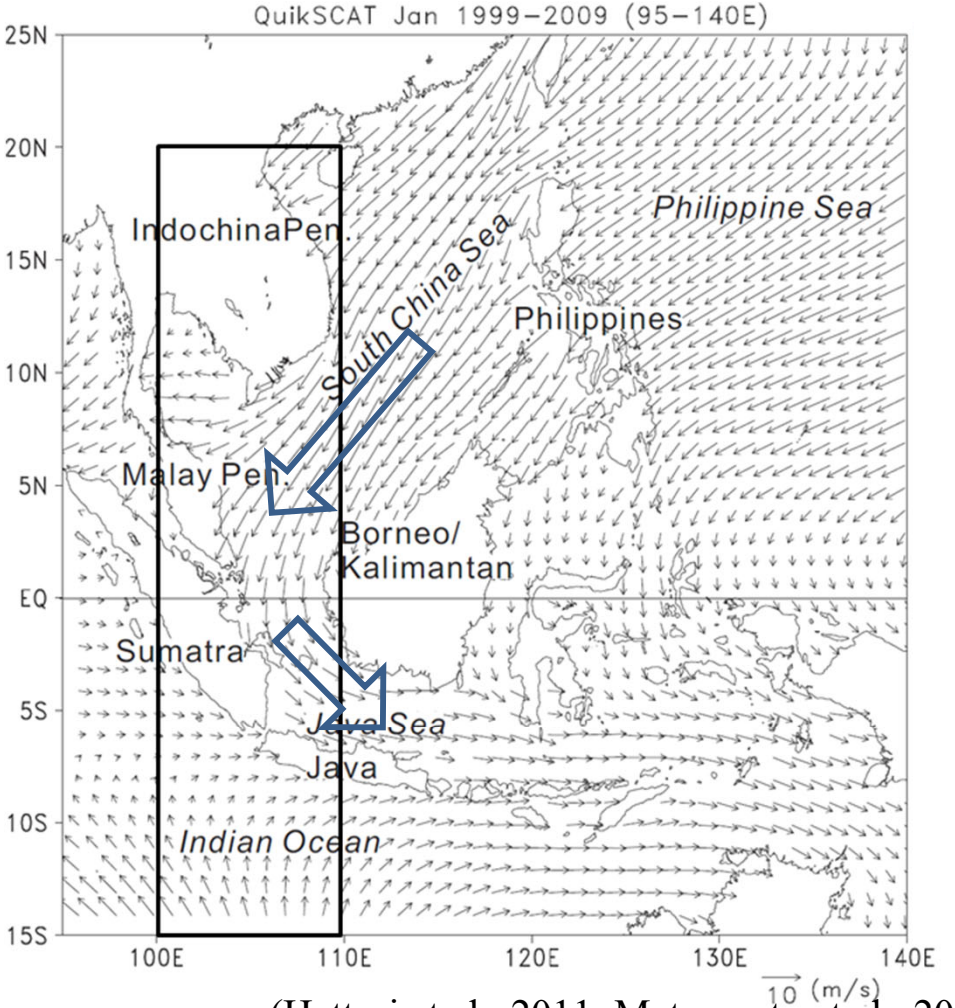

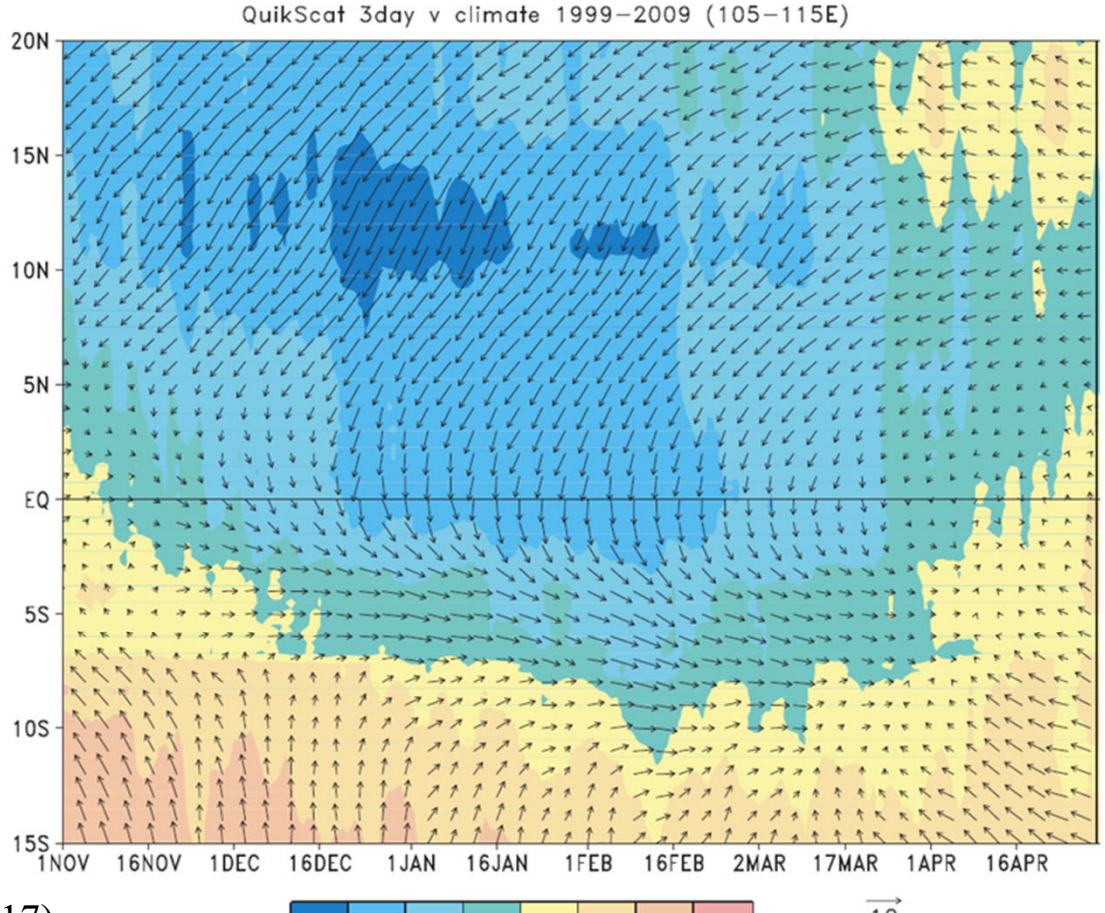

(Hattori et al., 2011; Matsumoto et al., 2017)

Jan-Feb 2007

La Nina
+ Monsoon
+ MJO
(Indian Ocean eastward cloud)
+ Local Diurnal Cycle

Jan 2013

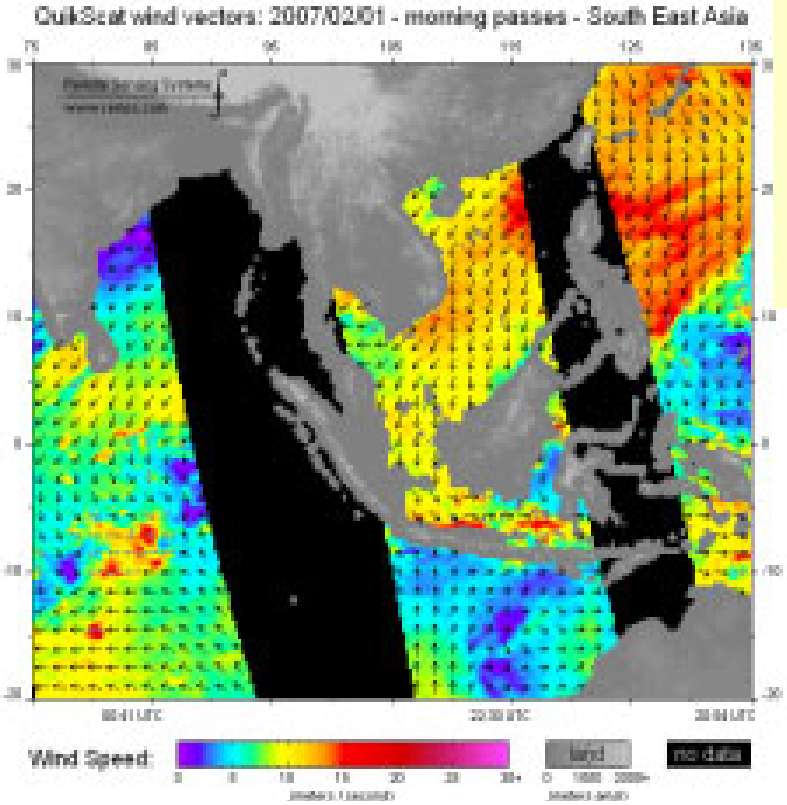

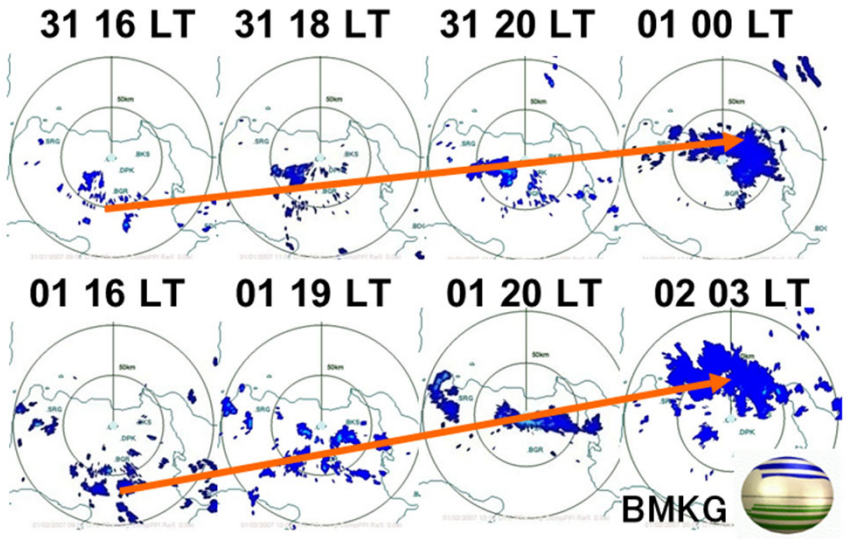

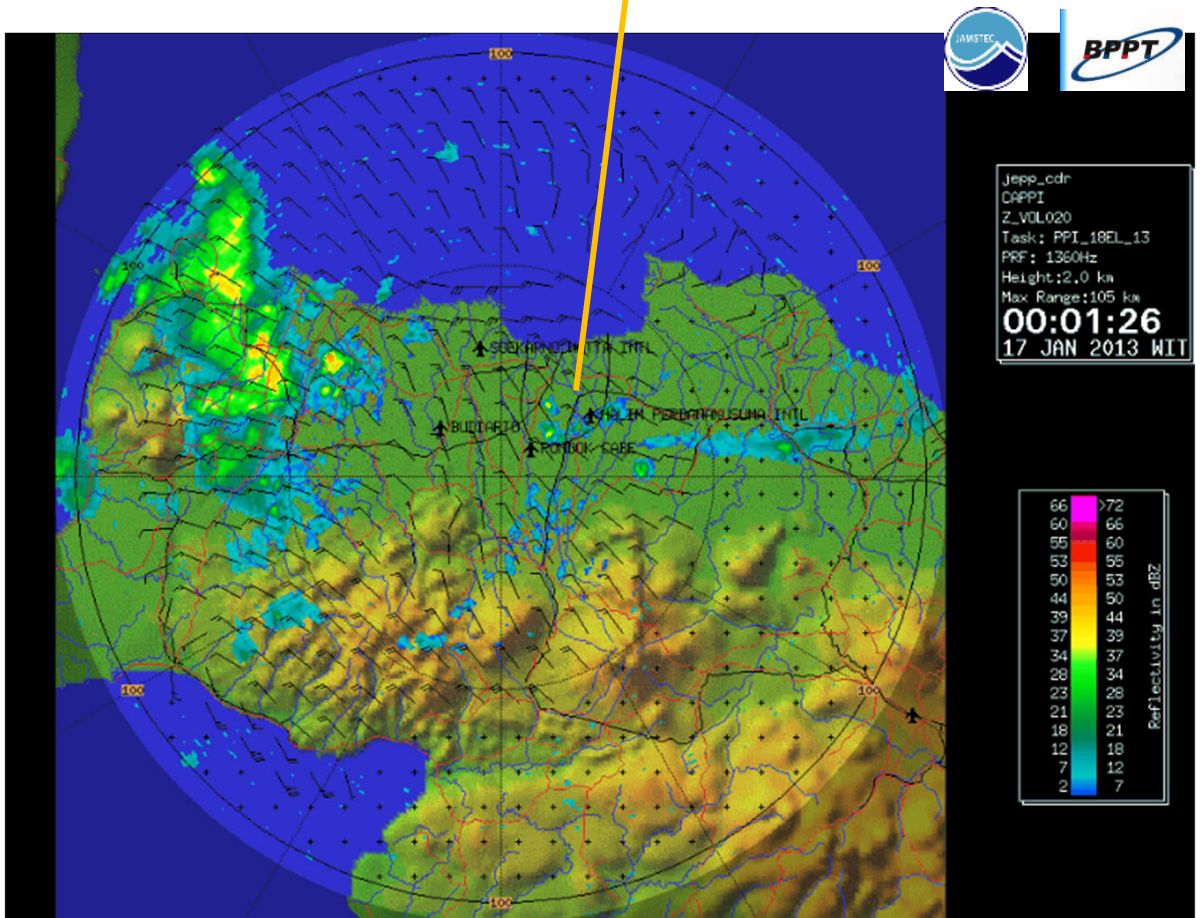

Diurnal cycle interactions at small/large islands

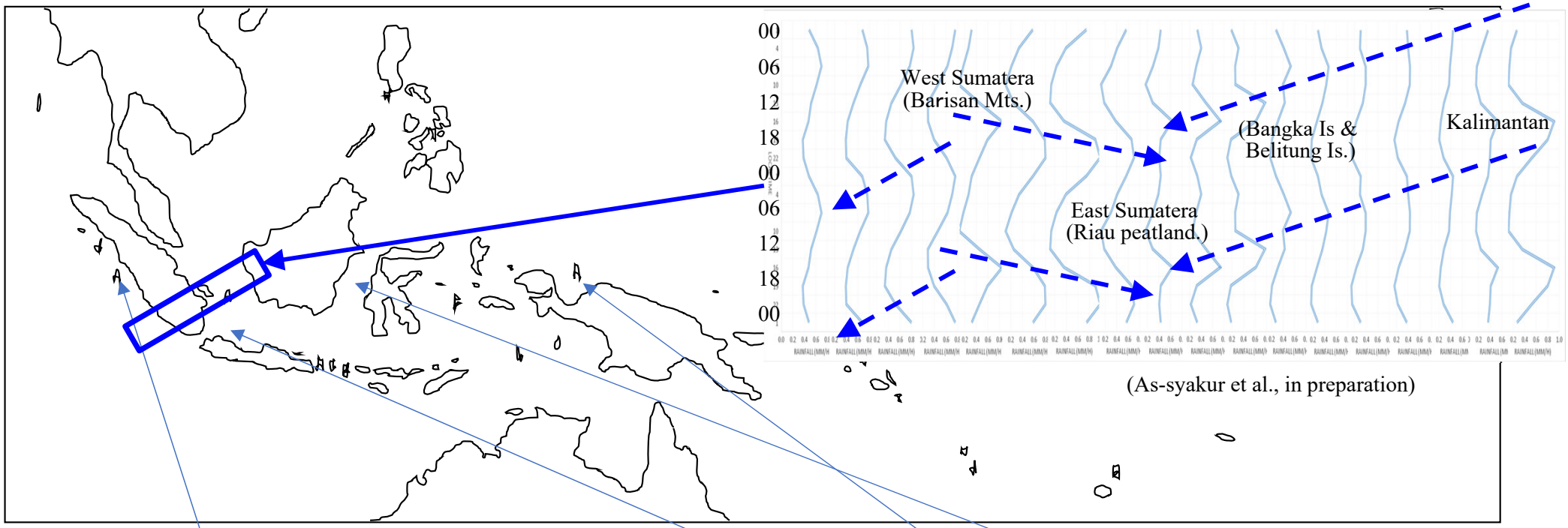

(As-syakur et al., in preparation)

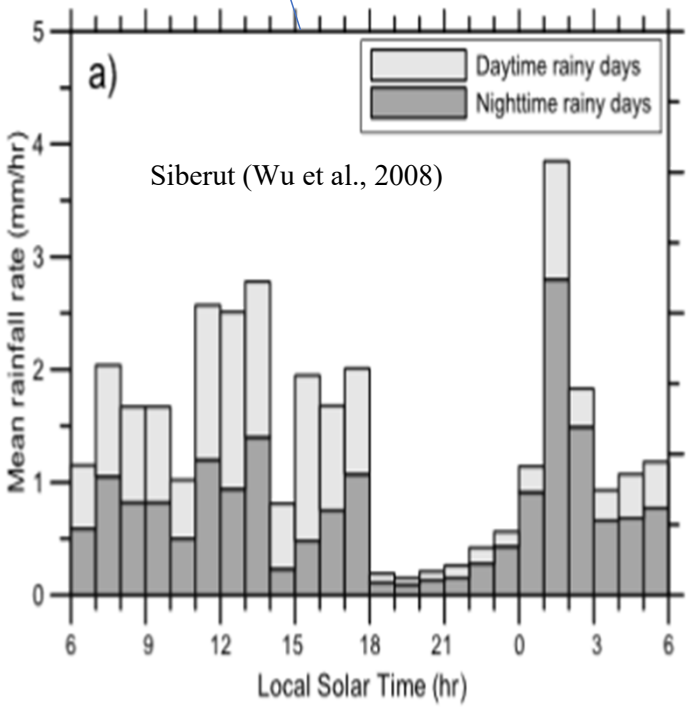

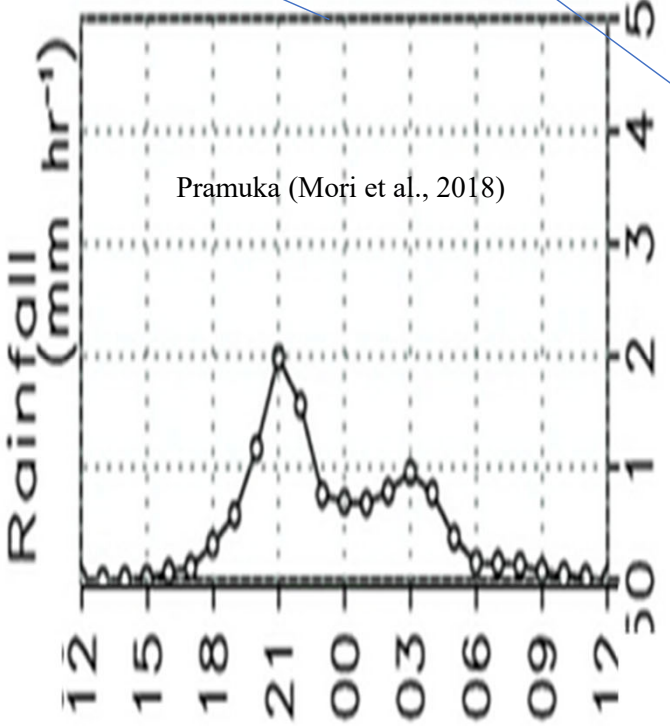

Kalimantan-Sulawesi case
(Ichikawa and Yasunari, 2006)

Biak (Tabata et al., 2011)

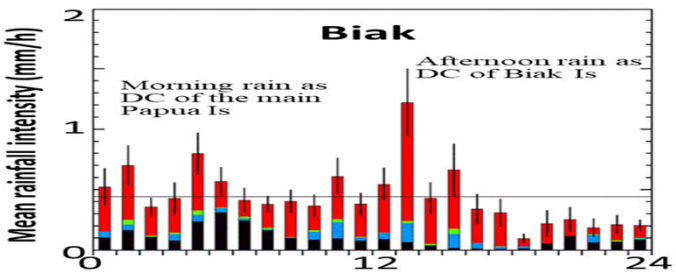

Tropical convection/rainfall as functions of coastline distance/length

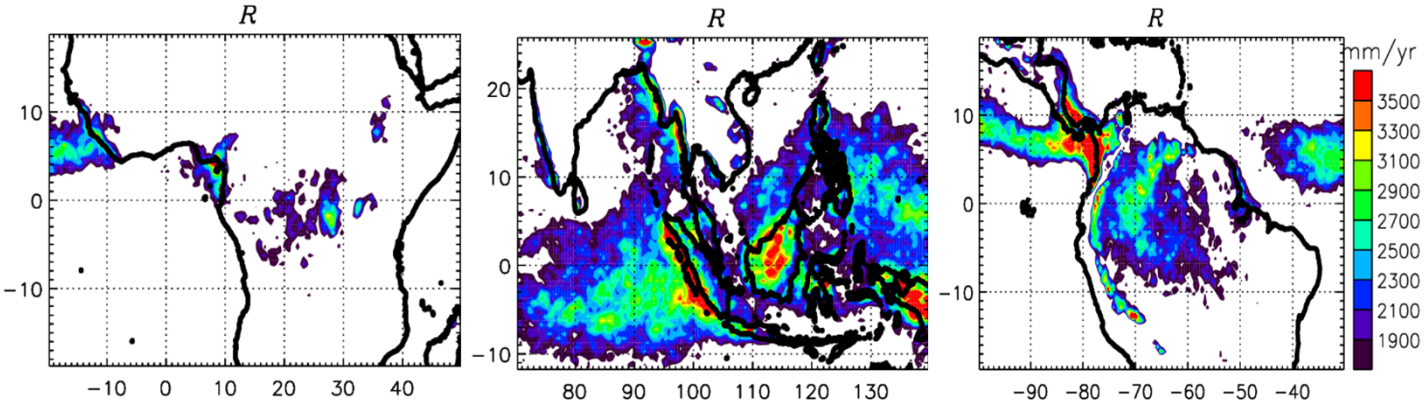

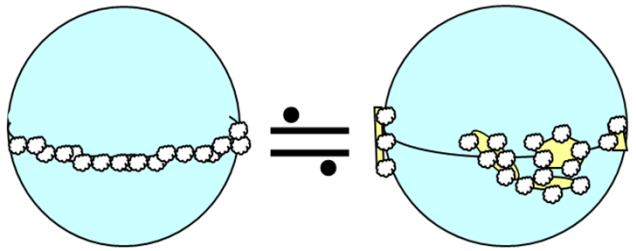

(TRMM, Dec 1997-Jan 2011, 37S-37N; Ogino et al., 2016, *JC*)

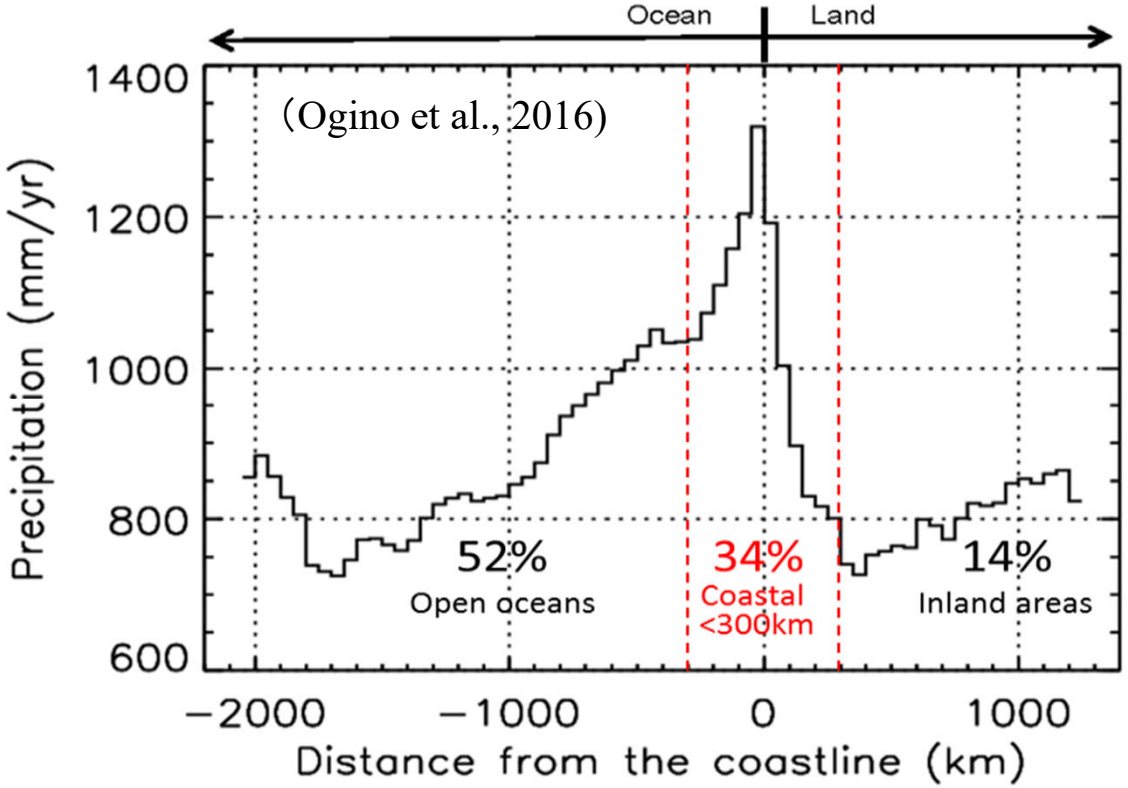

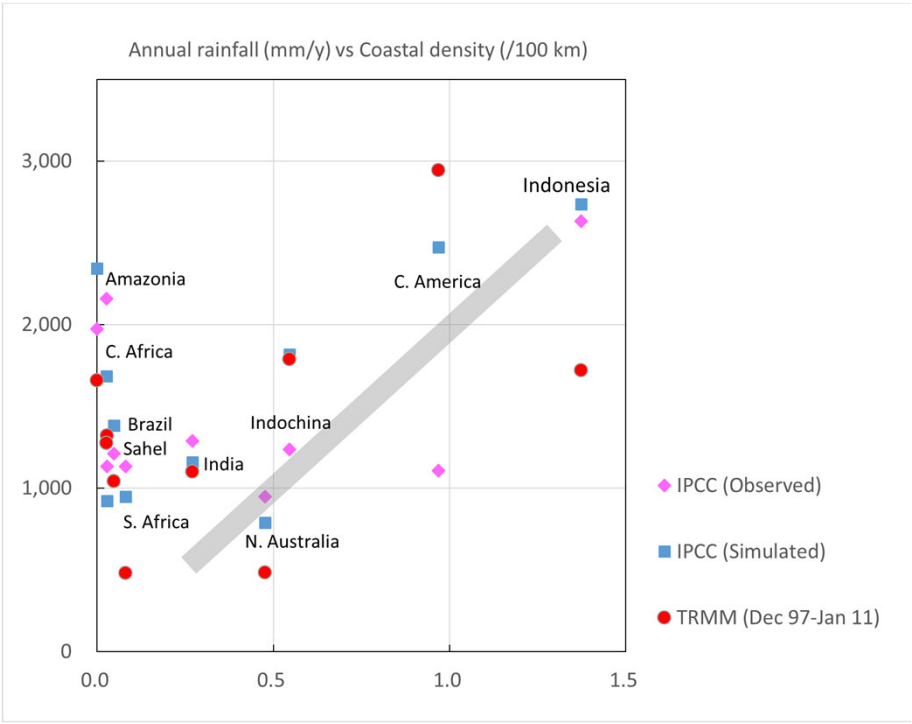

(Yamanaka, 2016, *AR*, invited overview)

Rainfall concentrated along the coastlines.
→ Regional rainfall dependent on the coastline length

Regional rainfall (mm/yr)＝2000 (mm/y10^2 km)
×[coastline length (10^2 km)/land area (10^4km^2)]

Costal regions in the global energy/water cycle

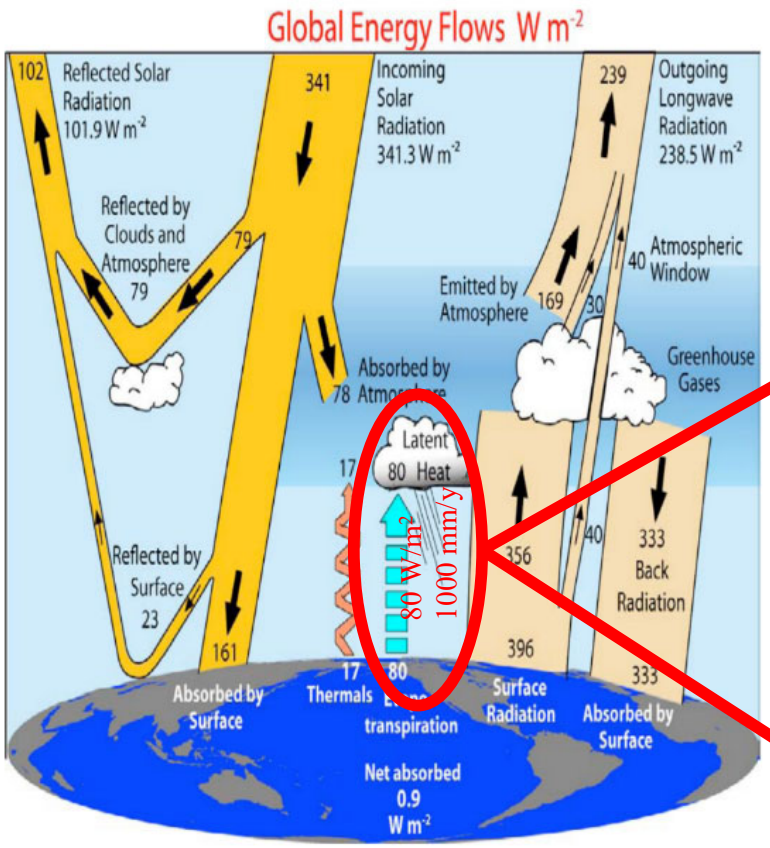

(Trenberth et al., 2009)

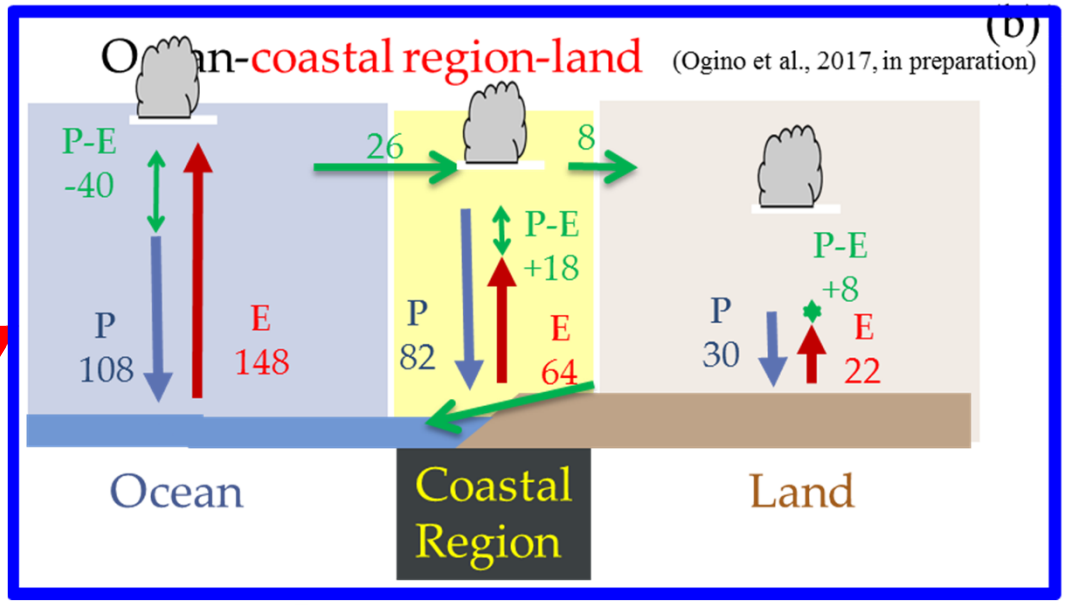

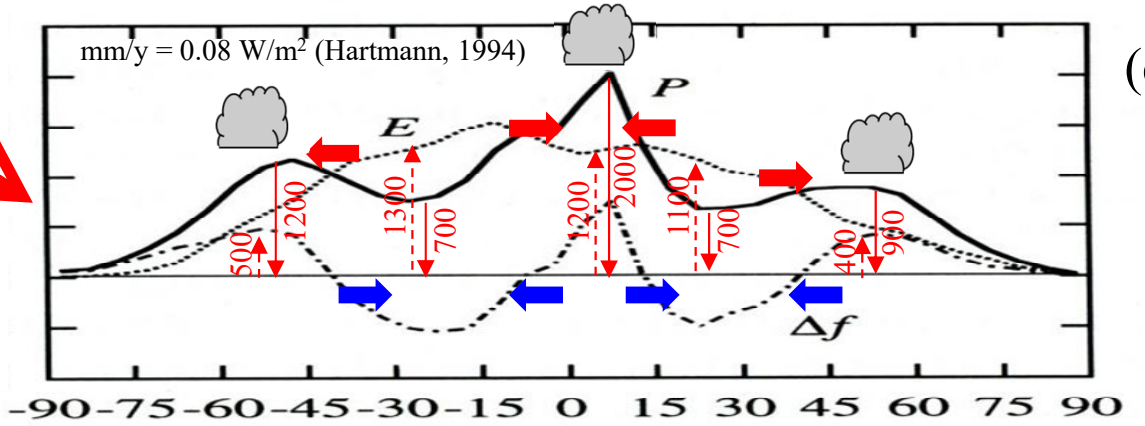

IMC coastal regions in the global water/energy budget

Annual rainfall: 2,500 mm

≒ 2.5 × global mean latent heat release 1,000 mm or 80 W/m^2 (1/3 of GH effect)

Annual rainwater amount: 1 × 10^{14} m^3

. ≒ 1/3 × tropical total amount . ≒ 1/6 × global total amount

6.2. Vertical (cloud) convection:
Conditional instability and cumulus clouds

- Vertical heat transport:
  - Radiation: electromagnetic (without any media)
  - Conduction: molecule motions
  - Convection: hydrodynamic motions
- Classical hydrodynamics of convection
  - Rayleigh-Taylor, Benard-Rayleigh, …
  - viscosity, gravity
- (Conditionally) Unstable stratification
  - Latent heating ⇒ "Pseudo"-adiabatic process
  - Equivalent potential temperature
- Coupling with cloud microphysics
  - Condensation/evaporation, freezing/melting, sublimation
  - Heterogeneous growing, aerosol nuclei, chemistry, electricity
  - Warm rain: stochastic coalescence, droplet/drizzle/raindrop
  - Cold rain: ice crystal/snow/graupel /hail

Rainfall “not so easy” even in tropics (Conditional instability paradox)

- Dry adiabatic ＜ actual lapse rate ＜ Moist adiabatic
  （−10ºC/km） （−6.5ºC/km） （−5ºC/km）
- Convection generated if condensation (cloud) started
- Condensation (cloud) if convection (lifted / moistened)
- Therefore “initial upward motion” must be forced

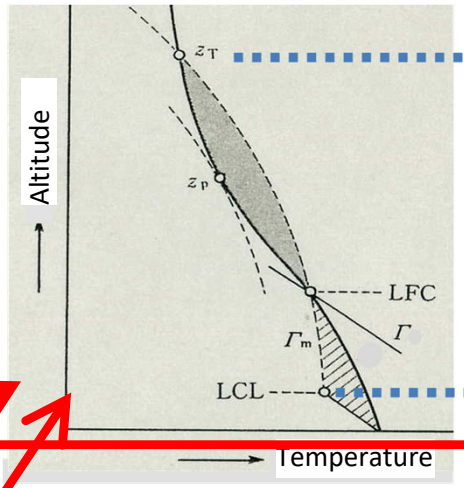

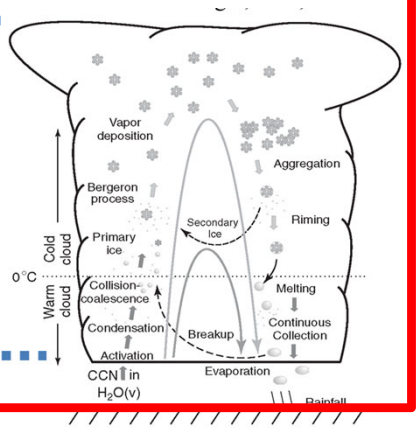

(i) Cold /warm air boundary (*extratropical* cyclone “front”)

(ii) *Subtropical* vortex organization (Typhoon)

(iii) Equatorial *oceanic* wave organization (*Intraseasonal* Madden-Julian oscillation)

(iv) **Diurnal-cycle sea-land breeze circulation**

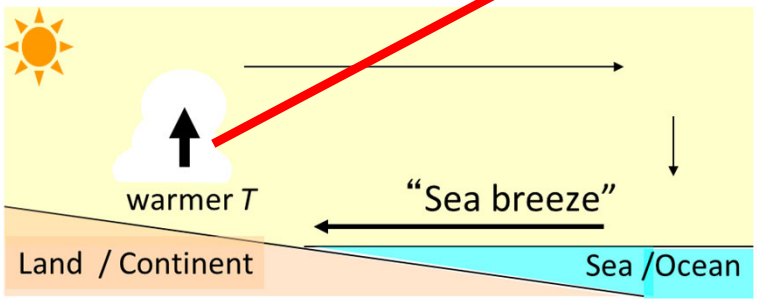

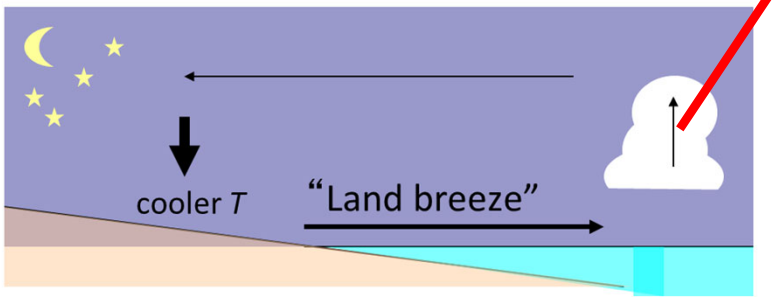

(v) Windward side of *mountain*
(leeside: dry and hot, so-called Föhn)

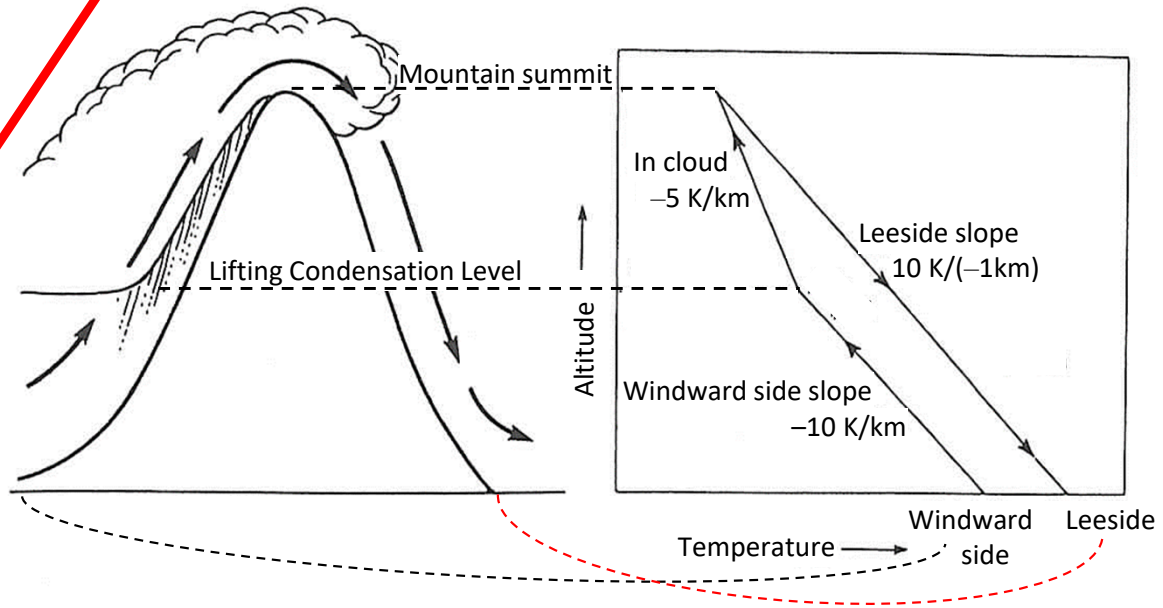

Cumulonimbus

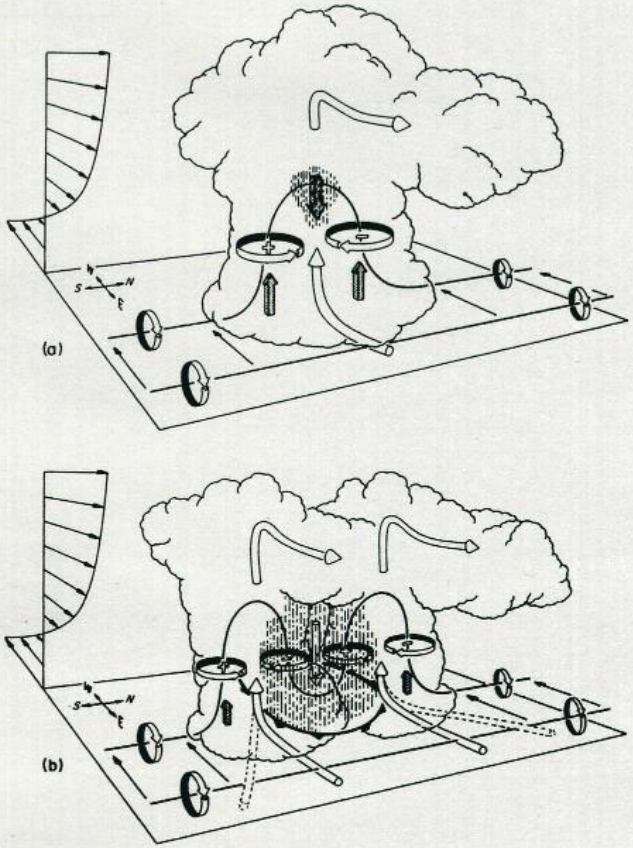

Fig. 9.12 Development of rotation and splitting in a supercell storm with westerly mean wind shear (shown by storm relative wind arrows in the upper left corner of each panel). Cylindrical arrows show the direction of cloud relative air flow. Heavy solid lines show vortex lines with a sense of rotation shown by circular arrows. Plus and minus signs indicate cyclonic and anticyclonic rotation caused by vortex tube tilting. Shaded arrows represent updraft and downdraft growth. Vertical dashed lines denote regions of precipitation. (a) In the initial stage, the environmental shear vorticity is tilted and stretched into the vertical as it is swept into the updraft. (b) In the splitting stage, downdraft forms between the new updraft cells. Barbed line at surface indicates downdraft outflow at surface. (After Klemp, 1987.)

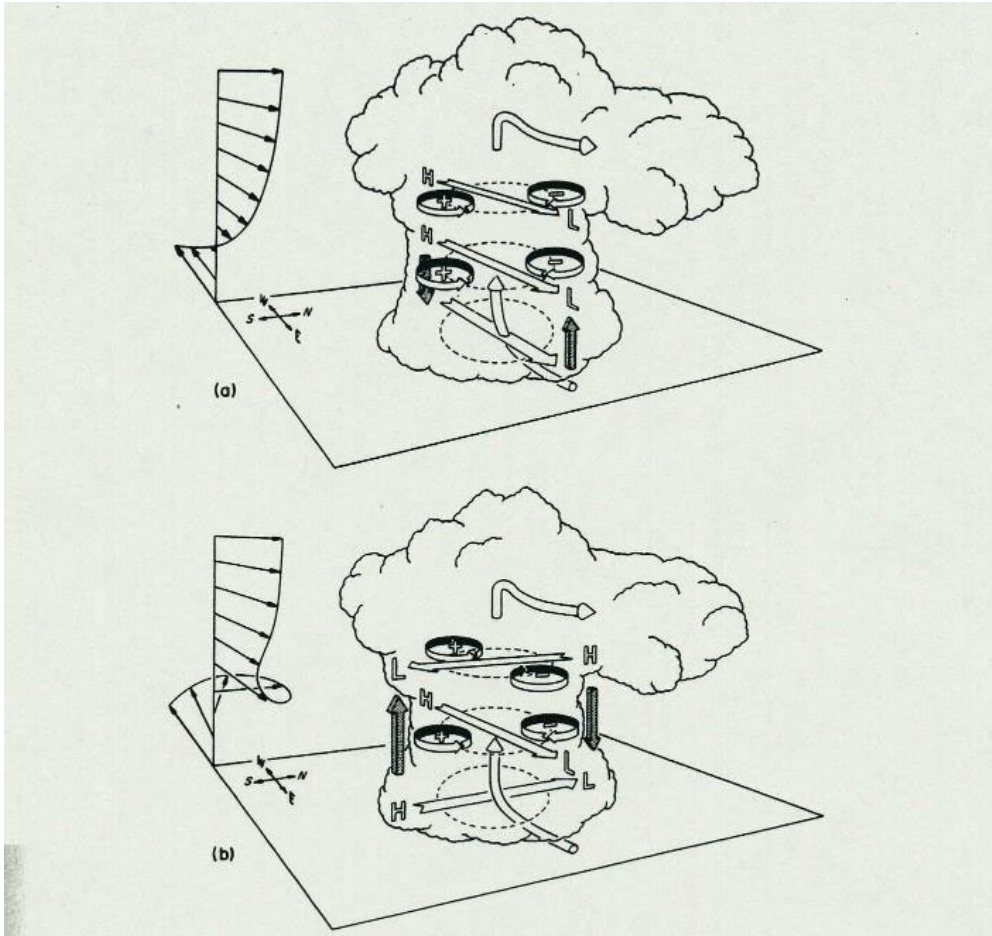

Fig. 9.13 Pressure and vertical vorticity perturbations produced by interaction of the updraft with environmental wind shear in a supercell storm. (a) Wind shear does not change direction with height. (b) Wind shear turns clockwise with height. Broad open arrows designate the shear vectors. *H* and *L* designate high and low dynamical pressure perturbations, respectively. Shaded arrows show resulting disturbance vertical pressure gradients. (After Klemp, 1987.)

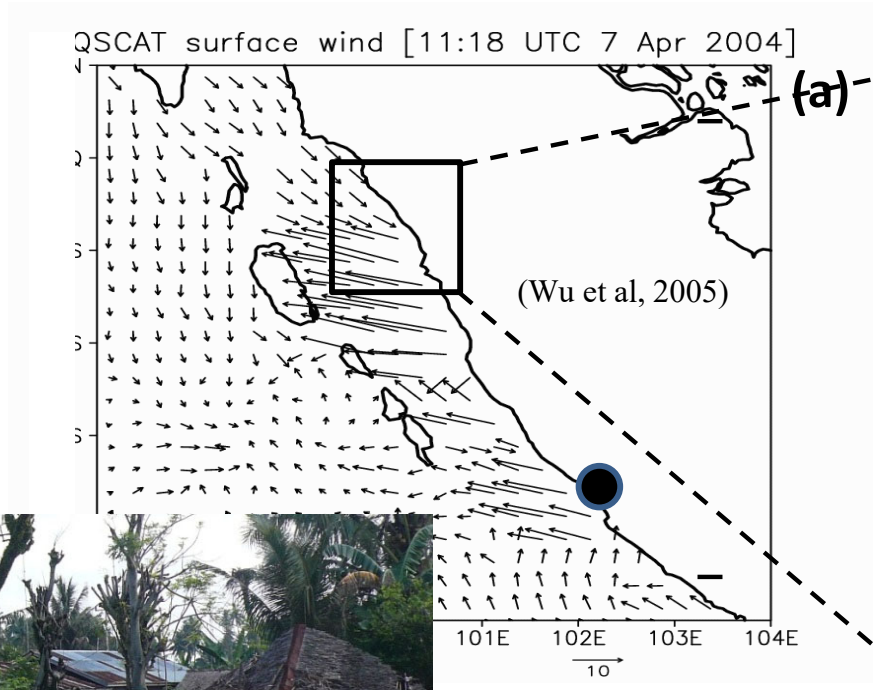

(Sakurai et al, 2011, *JMSJ*;
Kawashima et al, 2011, *JMSJ*)

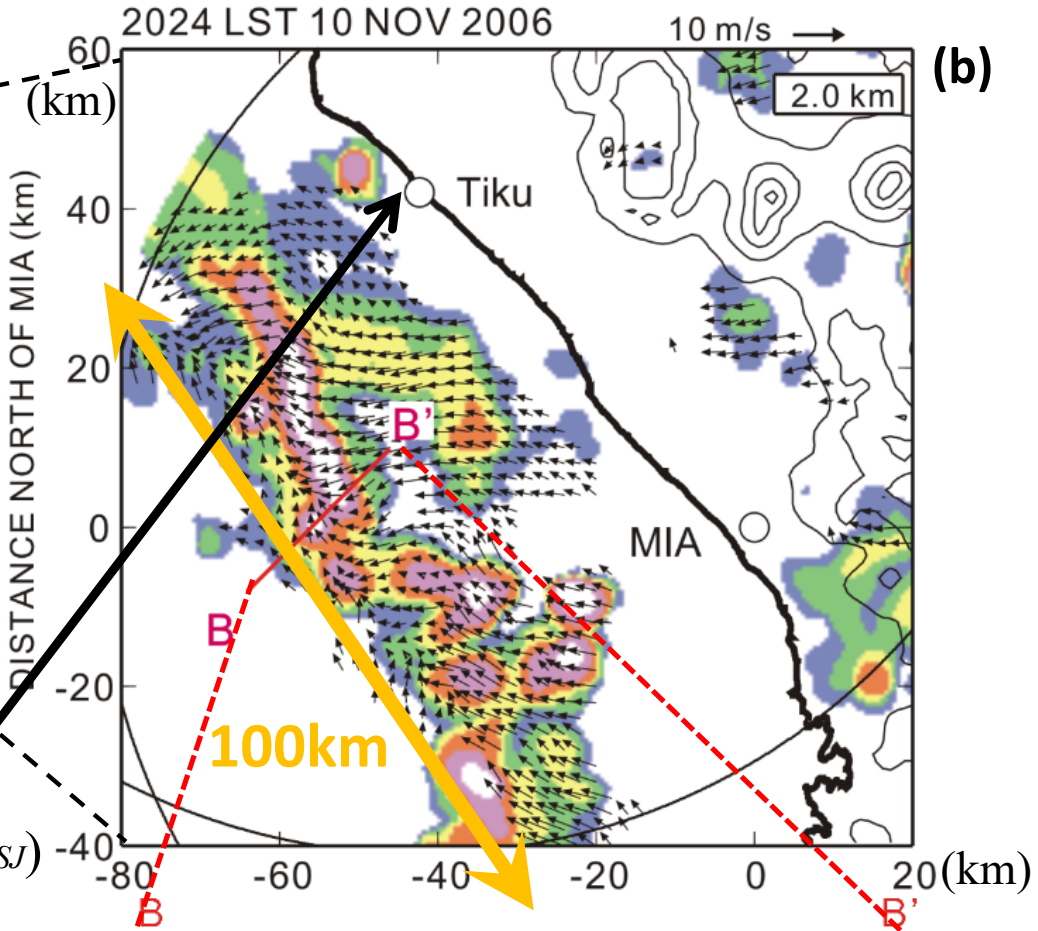

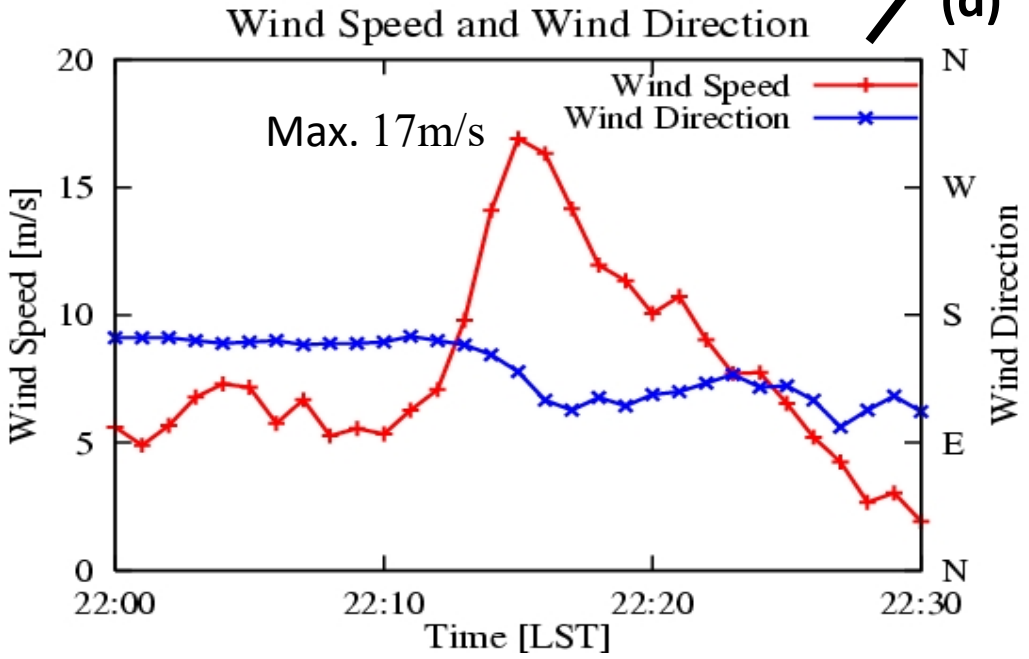

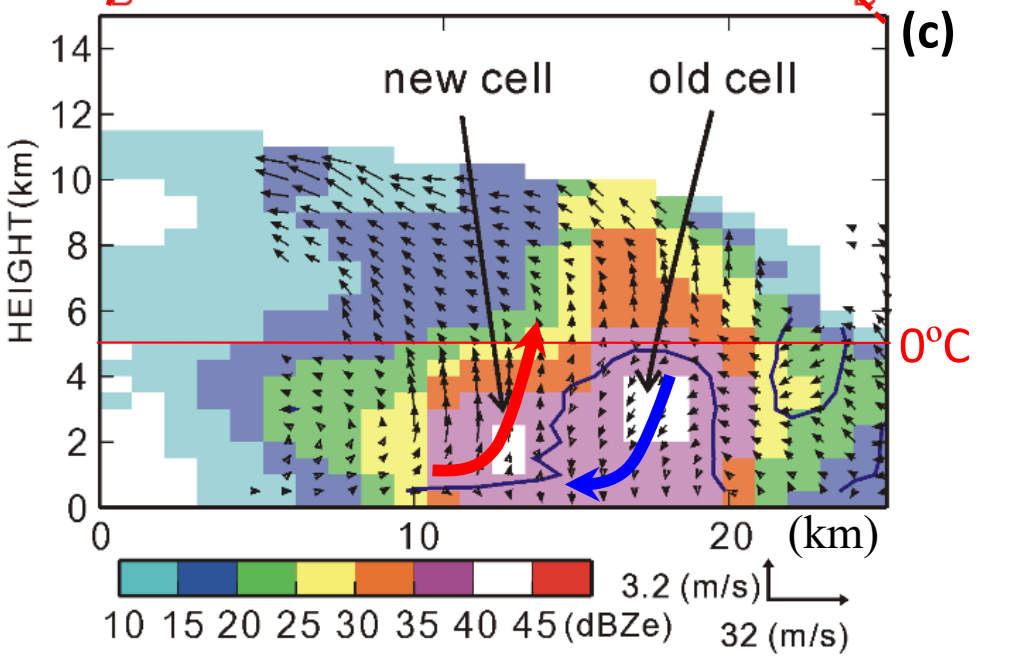

Tornadoes

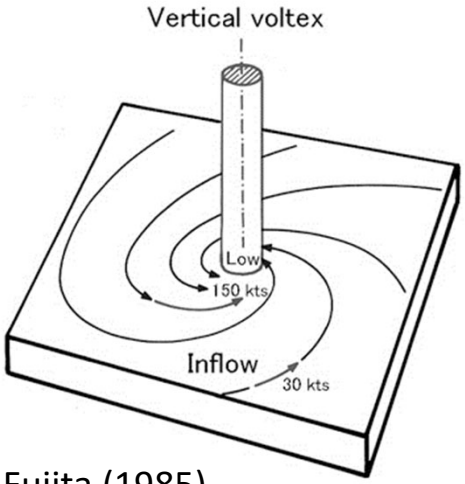

Fujita (1985)

(Jawa Tenggah, May 2012)

(Sumatera Barat, July 2015)

Microbursts

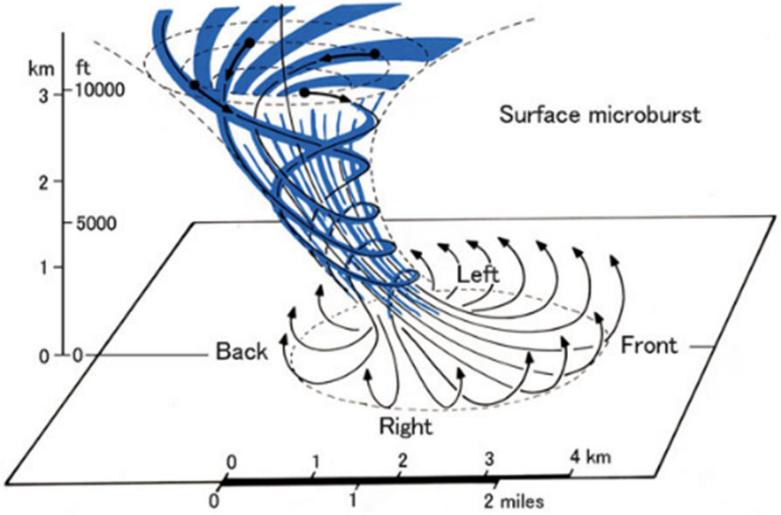

Fig. 11.20 Schematic view of a three-dimensional microburst. Convergence aloft, rotating downdraft, and surface divergence are included [from Fujita 1985, p. 75]

(by Drs. Geng & Katsumata@R/V Mirai, off Bengkulu, 25 Nov 2015)

→ Causes of airplane / ship accidents

Cloud-precipitation microphysics

- Saturation [← a solution of (7)]

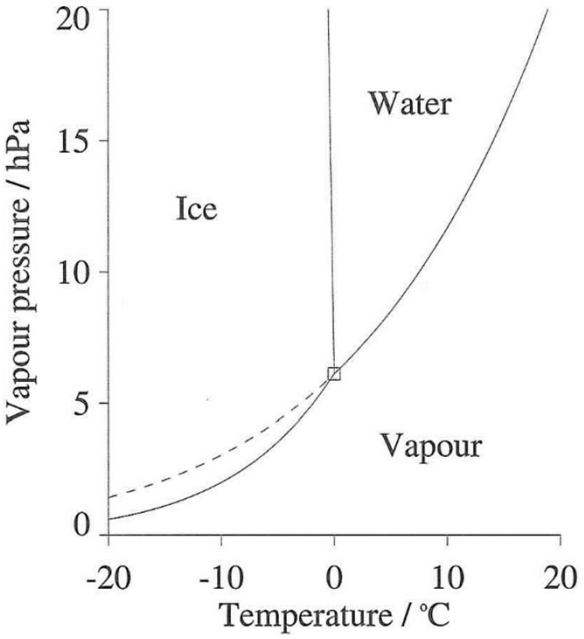

Figure 2.8 Schematic diagram showing the phase transitions between ice, liquid water and water vapour. The difference between the ice-vapour and vapour-water curves below 0 °C (where the vapour-water curve is shown dashed) has been exaggerated. Note that the ice-water curve is not quite vertical, but has a large negative slope. The triple point is indicated by the small square.

(Andrews, 2000)

- Homogeneous nucleation and curvature effect

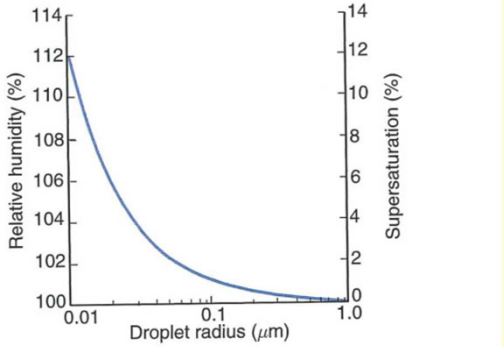

Fig. 6.2 The relative humidity and supersaturation (both with respect to a plane surface of water) at which pure water droplets are in (unstable) equilibrium at 5 °C.

(Wallace & Hobbs, 2006)

- Heterogeneous nucleation and solute effect
- Coagulation and warm rain

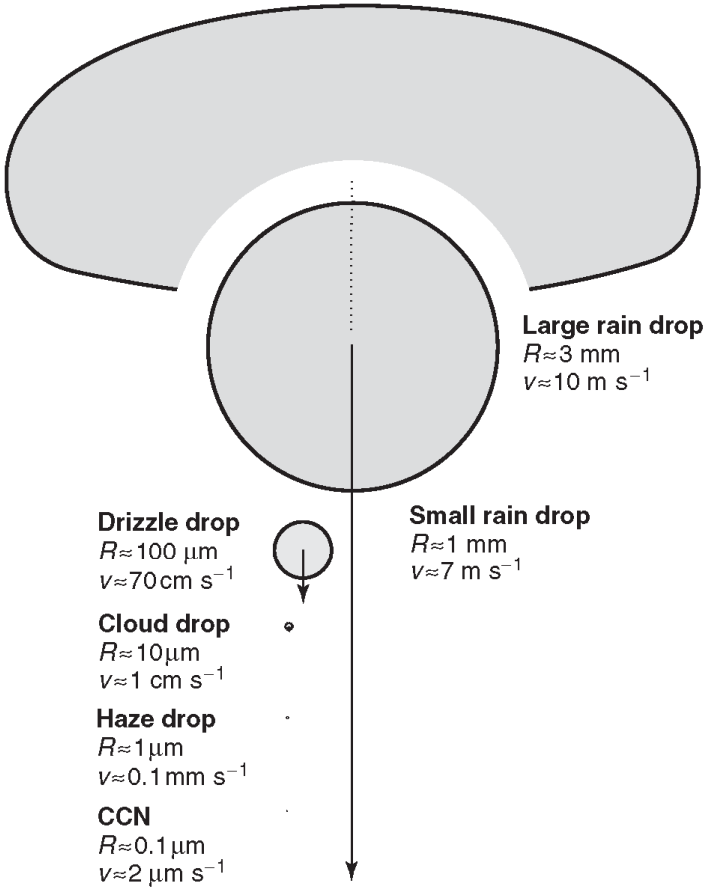

Figure 1 Various categories of liquid drops found in clouds. The indicated drop radii (R) are drawn roughly to scale, as are the arrows representing the terminal fallspeeds (v) of the various drop categories. 'CCN' represents a 'cloud condensation nucleus', a solution droplet that serves as the initial site of condensation. The large raindrop is shown distorted to represent the effect of a large dynamic pressure on its underside.

(Lamb, 2003)

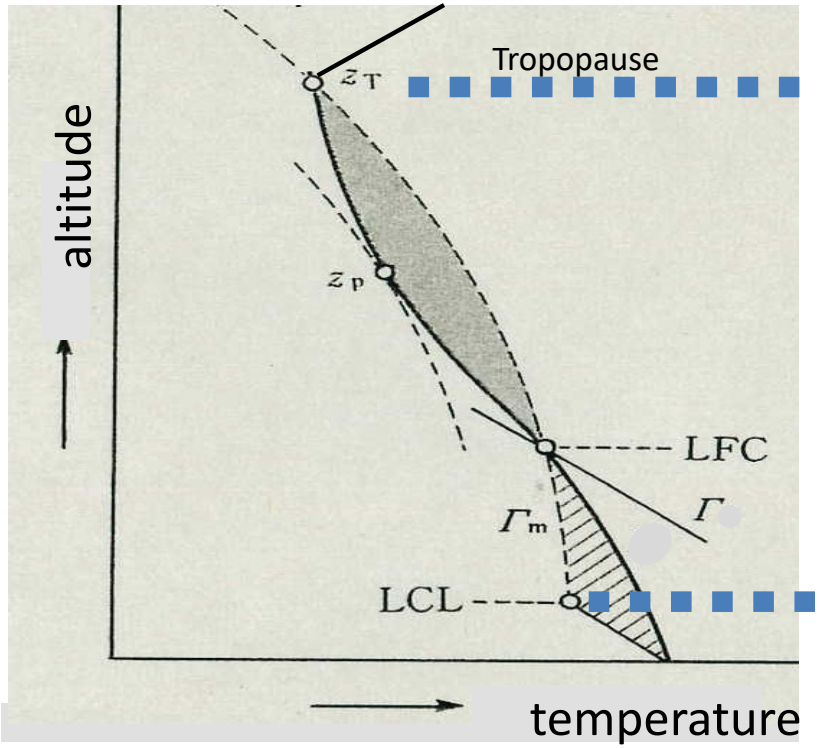
altitude
Tropopause
z_T
z_p
LFC
Γ_m
Γ
LCL
temperature

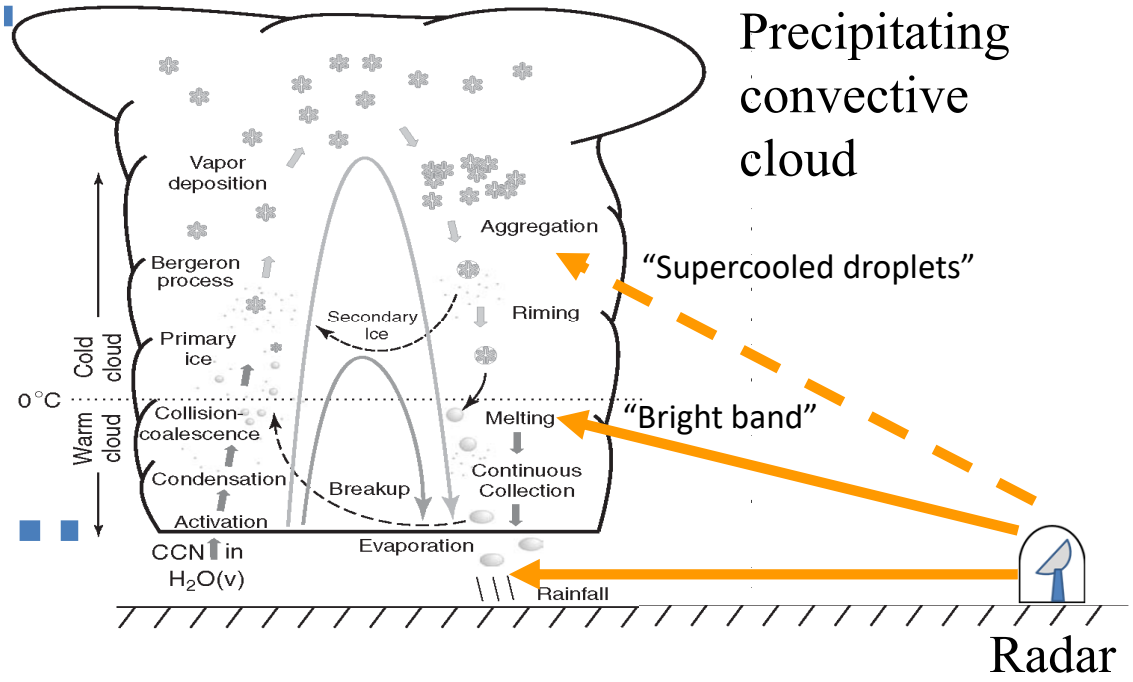
Precipitating convective cloud
Vapor deposition
Aggregation
"Supercooled droplets"
Bergeron process
Secondary Ice
Riming
Primary ice
Cold cloud
0 °C
Warm cloud
Collision-coalescence
Melting
"Bright band"
Condensation
Breakup
Continuous Collection
Activation
CCN ⬆ in $H_2O(v)$
Evaporation
Rainfall
Radar

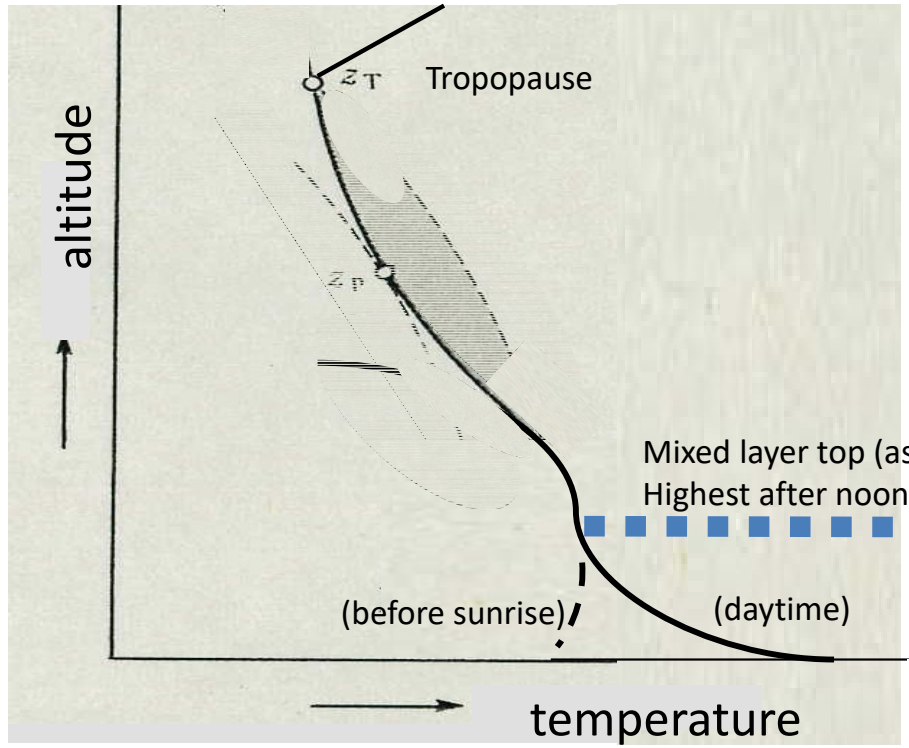
altitude
z_T
Tropopause
z_p
Mixed layer top (ascending after sunrise;
Highest after noon; disappearing before sunset)
(before sunrise)
(daytime)
temperature

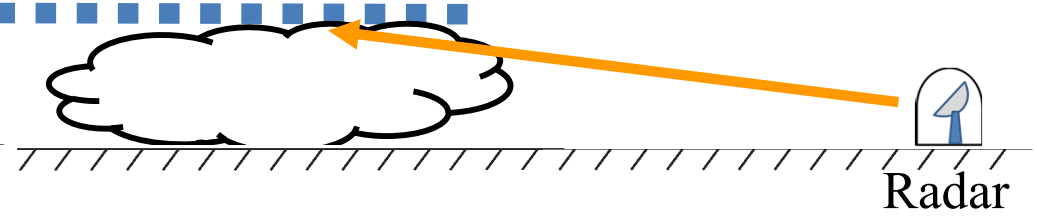
Fog / Smog
Radar

Radar = RAdio Detection And Ranging

(a) Meteorological (or weather) radar

Any hard targets/scatterers
(including aircrafts, ships, …, birds, insects, seeds, …, dusts, ashes, ….)
from factories/volcanos

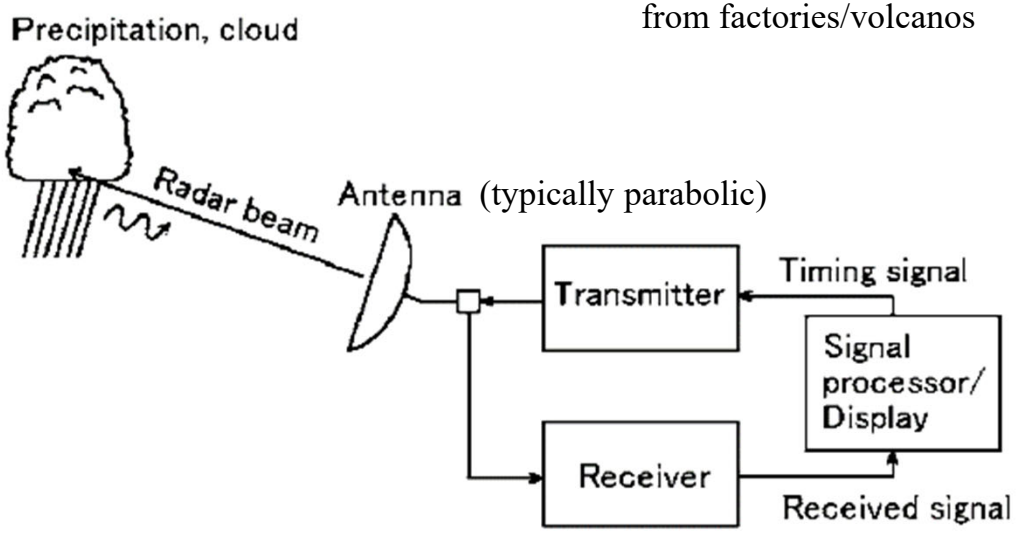

(b) Wind profiler (or atmospheric radar)

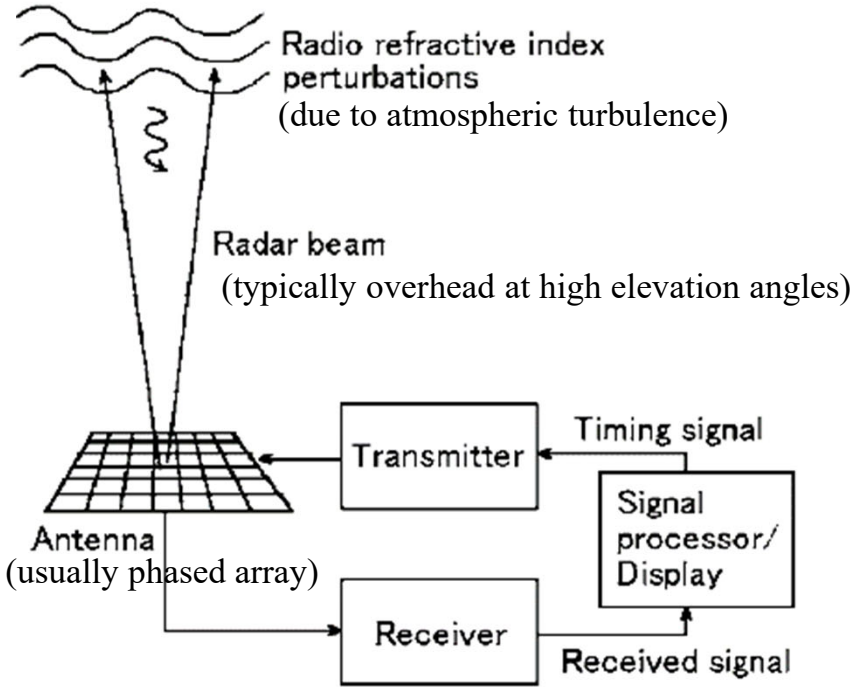

- Direction of the antenna receiving the scattered signal returns to the antenna → **Direction** of the target
- Time of the radio wave round-trip between radar and target (by light speed) → **Distance** of the target

US radars in 1940s-50s

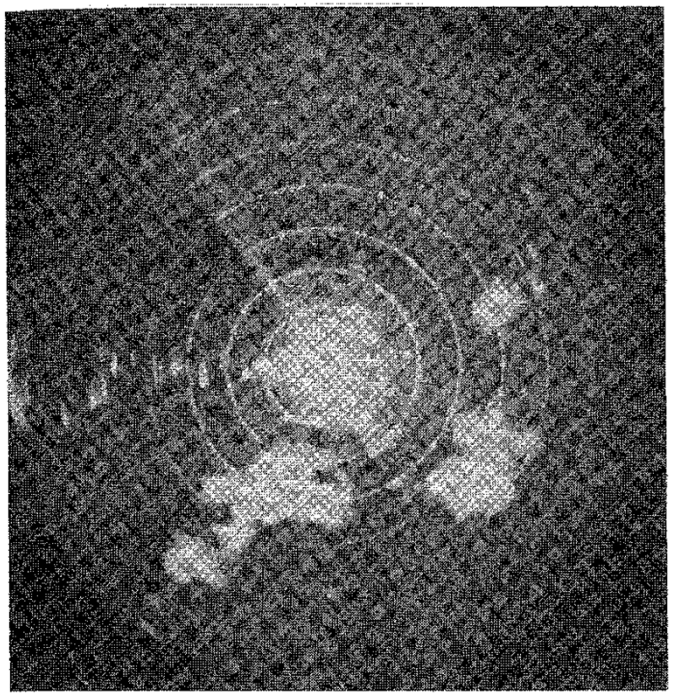

Fig. 1 PPI photograph of thunderstorm conditions in the vicinity of Cambridge, Massachusetts, 14 July 1942 as detected with a 10-cm radar. Range markers are 5 miles apart.

MIT S-band 1942 (Katz & Harney, 1990)

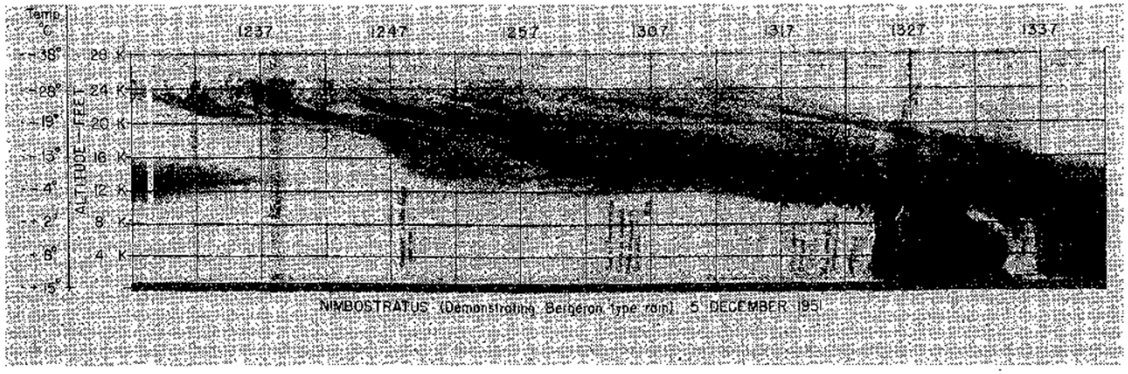

Fig. 1 Precipitation streamers observed by vertically pointing 1.25 cm APS-34 radar in 1951 (after Plank et al. *1955).*

AFGL Ku-band 1951 (Metcalf & Grover, 1990)

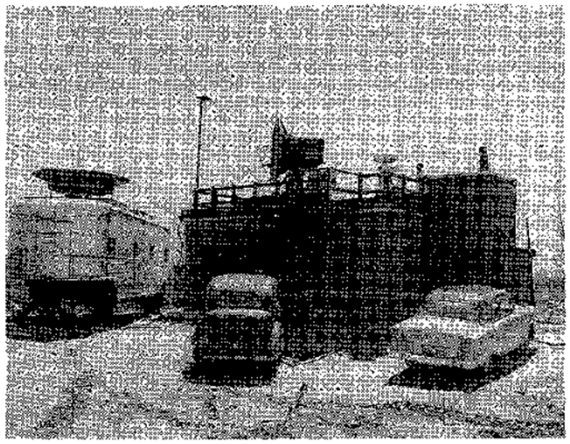

Fig. 2 Facilities of the weather radar program at Hanscom Field about 1954. The APS-34 radar antenna is on the trailer to the left of the building; the TPQ-6 antenna is on the roof.

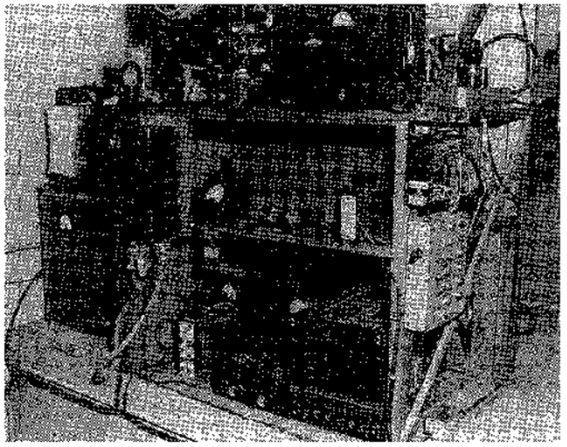

Fig. 3 Controls of the APS-34, inside the trailer. Single oscilloscope display is just visible at the upper left, receiver gain control is on the right, and the signal integrator for a single range gate is at the left.

(にった・じろう)

)12)年長野県生れ。本名
,無線電信講習所(現在電
学)卒業。昭和31(1956)年
にて第34回直木賞受賞。
勤続した気象庁を退職。
田信玄」などの作品によ
吉川英治文学賞受賞。
没。

富士山頂
新田次郎
に1-41
文春文庫
560+税

Mt. Fuji Radar

(S-band, JMA-Mitsubishi, 1964)

Height: 3,776 m; Max. range: 800 km

1959 proposed after “Isewan-Typhoon” killed 5,500 people
1964 started construction (highest), 1965 completed (240 MYen)
1999 stopped (replaced by satellite and advanced radars)

DRAW (C-band, JMA, 2000s-)

Fig. 9.5 The photo of the DRAW installed at Kansai international airport, in Japan [from Hamazu et al. 2000a]

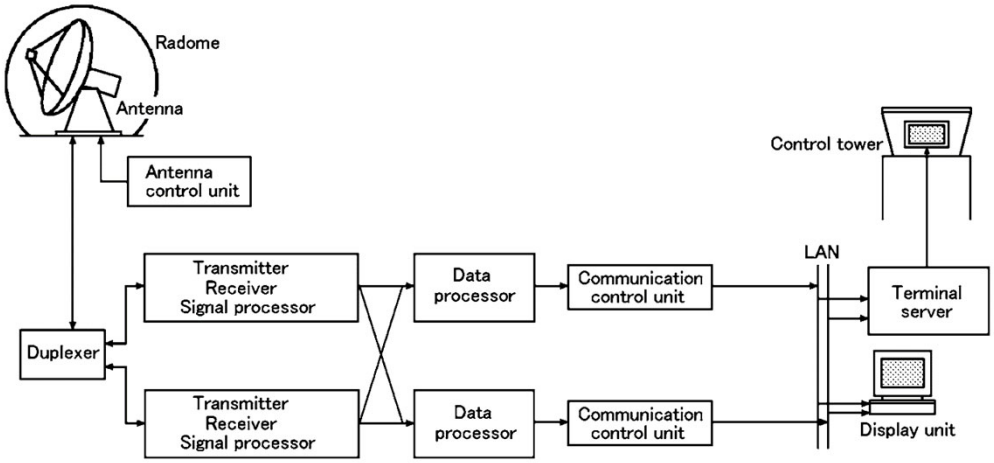

Fig. 9.6 The system configuration of the DRAW. Main equipment except for the antenna and related units of the radar are dualized

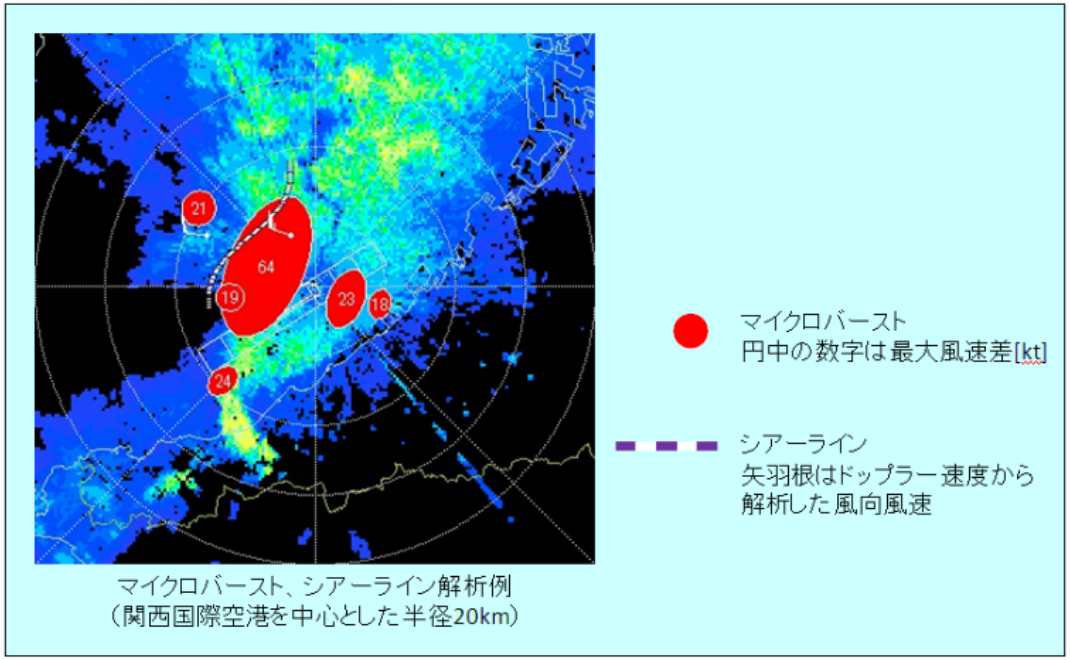

JMA network (C-band, 2000s-)

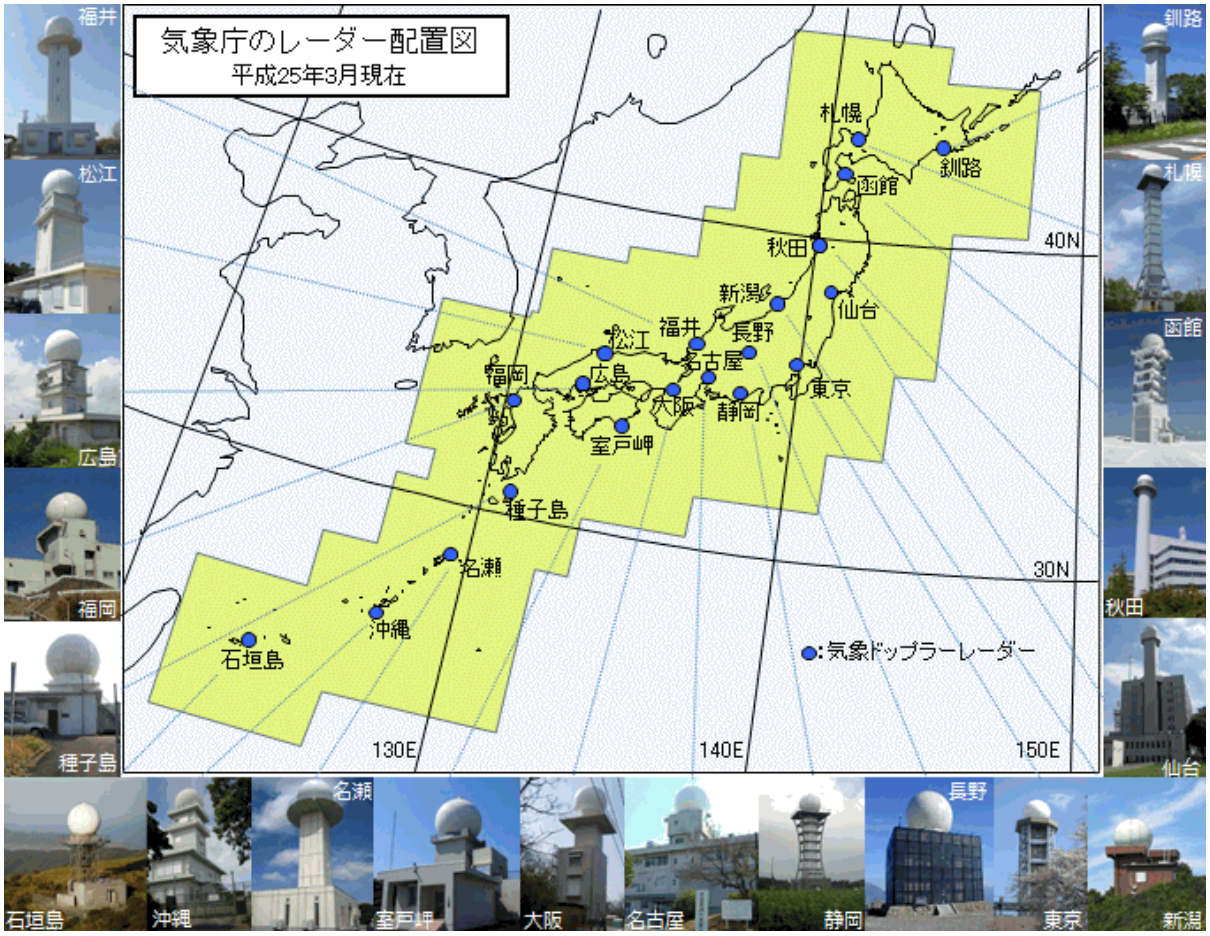

Table 9.5 Basic specifications of the operational meteorological radar of the Japan Meteorological Agency

Radar range	Reflectivity 400 km, Doppler velocity 150 km
Transmitted frequency	5.25–5.37 GHz
Antenna type	Parabolic dish, diameter 4 m
Antenna gain	42 dB
Beam width	1.0° (half power width)
Polarization	Linear horizontal
Antenna scan speed	Azimuth 36° s^{-1} maximum, elevation 15° s^{-1} maximun
Pulse repetition frequency	1,500 Hz maximum
Transmitter	Klystron
Peak transmitted power	250 kW
Pulse width	1 µs (short), 2.5 µs (long)
Minimum receive power	−110 dBm
Noise figure	3 dB
Receiver dynamic range	80 dB
Data digitization	14 bits
Range bin spacing	1.67 µs (250 m)

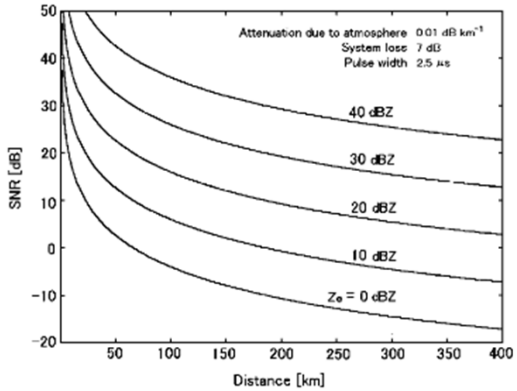

Fig. 9.8 The SNR of the operational meteorological radar, where the received signal power is calculated based on Table 9.5. The SNR is given for various magnitude of the equivalent radar reflectivity factor. Here, the system loss of 7.0 dB, the transmission loss of 2.5 dB and the reception loss of 4.5 dB, and the loss due to the atmosphere of 0.01 dB km^{-1} per one way are assumed. It is also assumed there is no precipitation between the radar and the scatterers

Radar network for typhoon observations

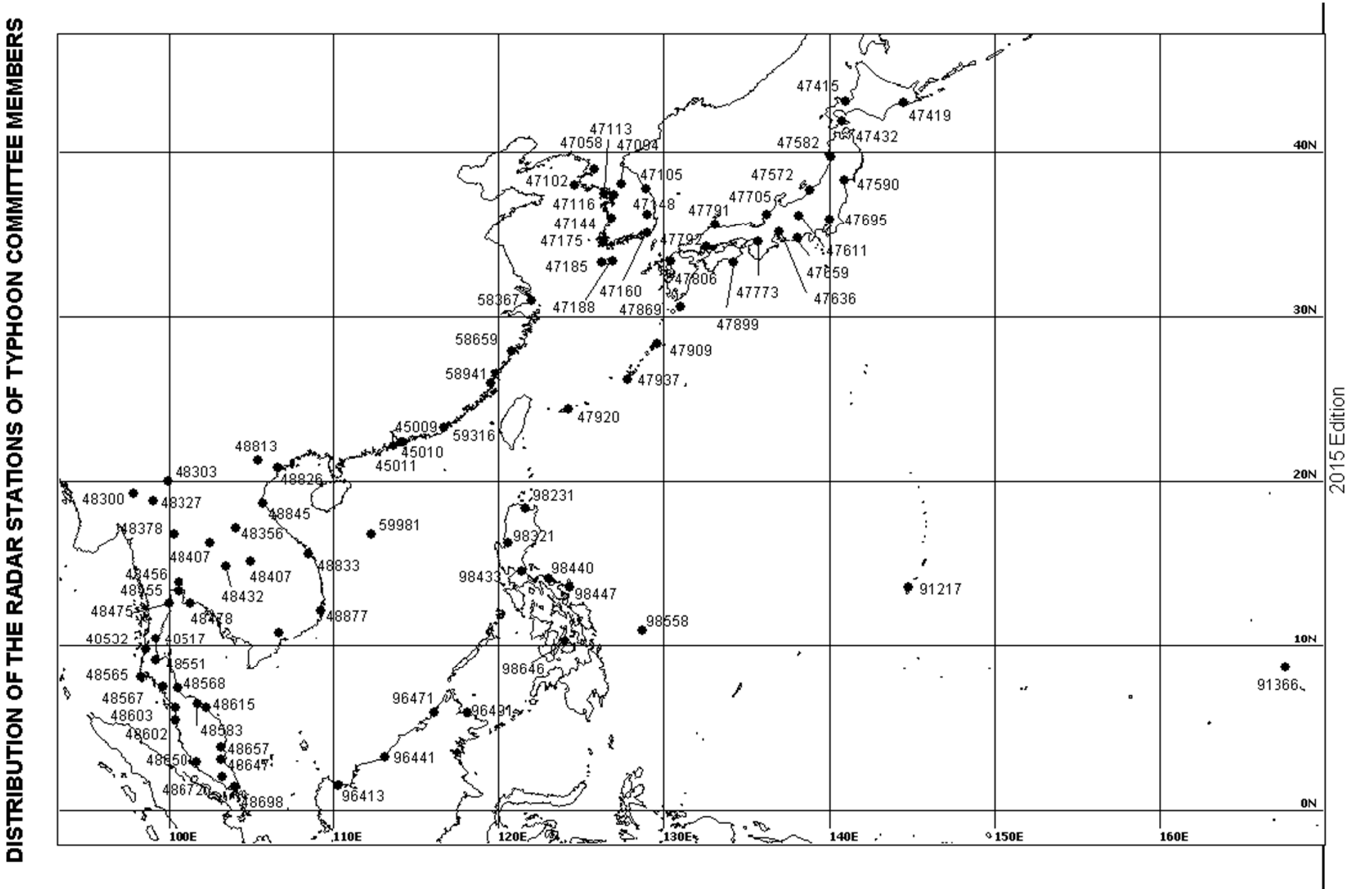

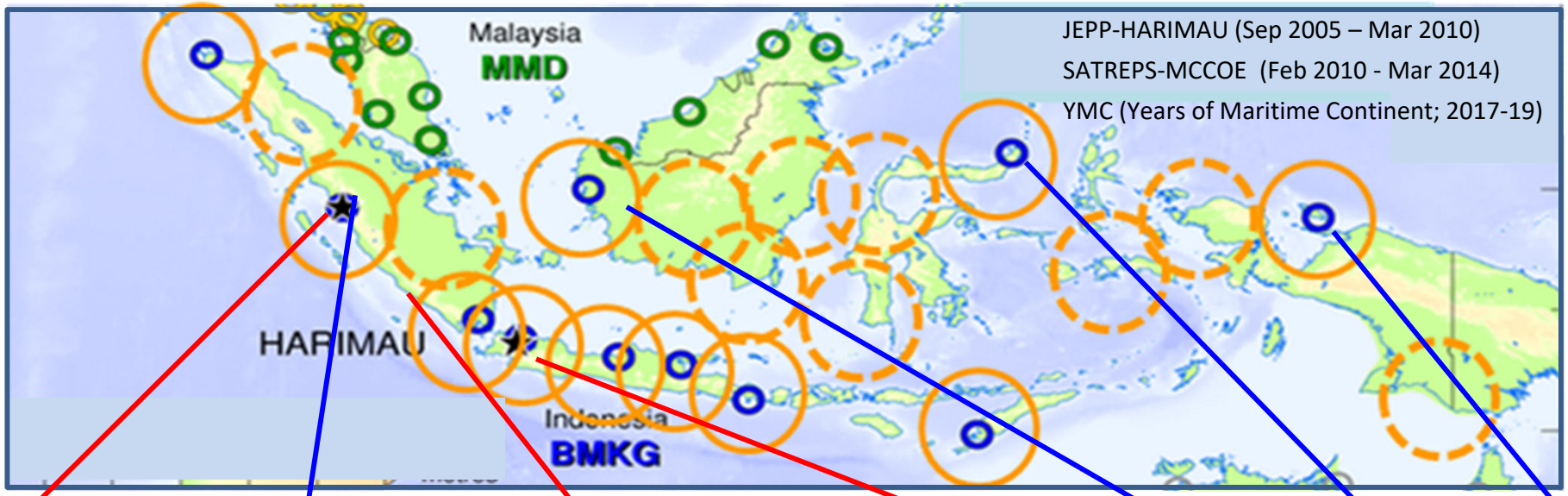

XDR (2006-14, JAMSTEC-BPPT)

VHF-EAR (2001-, KU-LAPAN)

Transportable X-MPR (2012-, JAMSTEC-BPPT)

CDR (2007-14, JAMSTEC-BPPT)

UHF-WPRs, 2007- JAMSTEC,KU-BPPT,BMKG,LAPAN, 2008-)

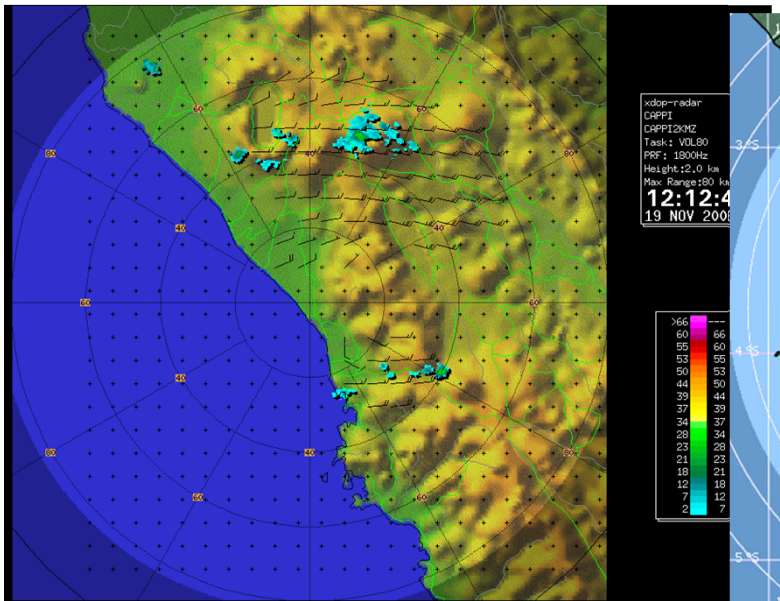

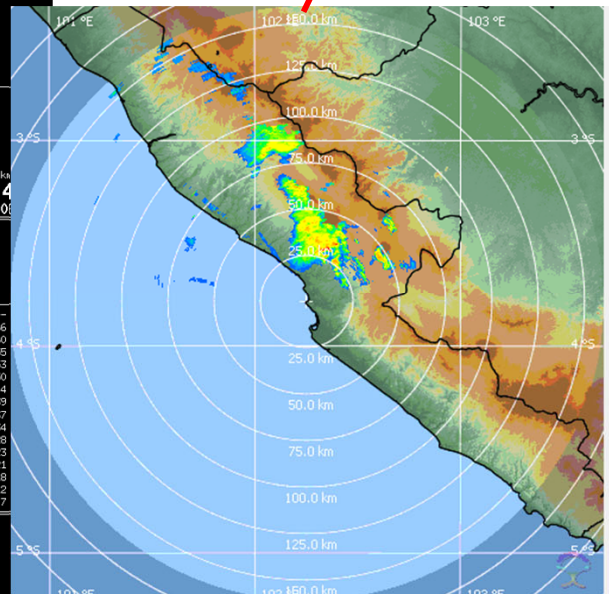

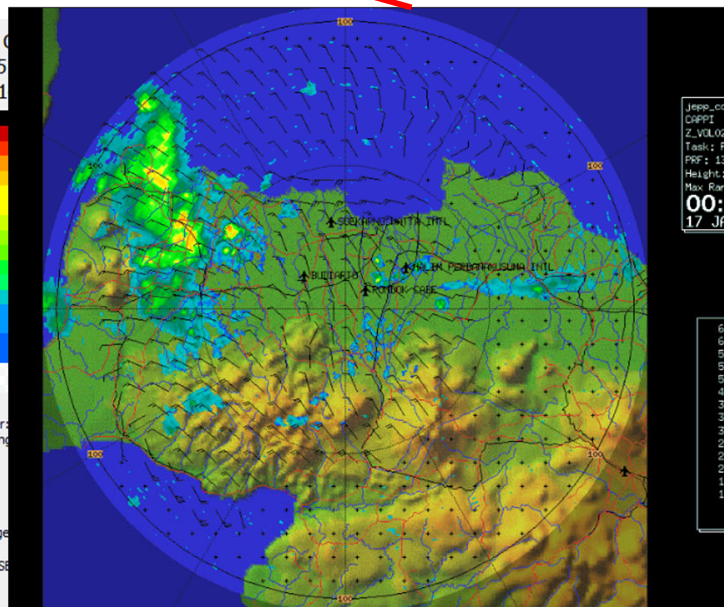

BMKG observation networks

(as of March 2017)

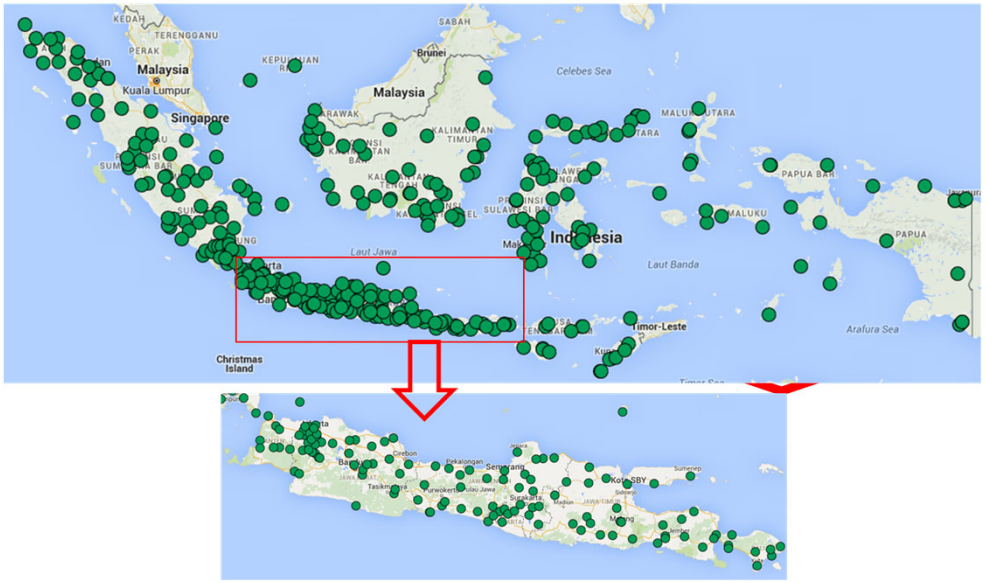

Automatic weather stations（361）

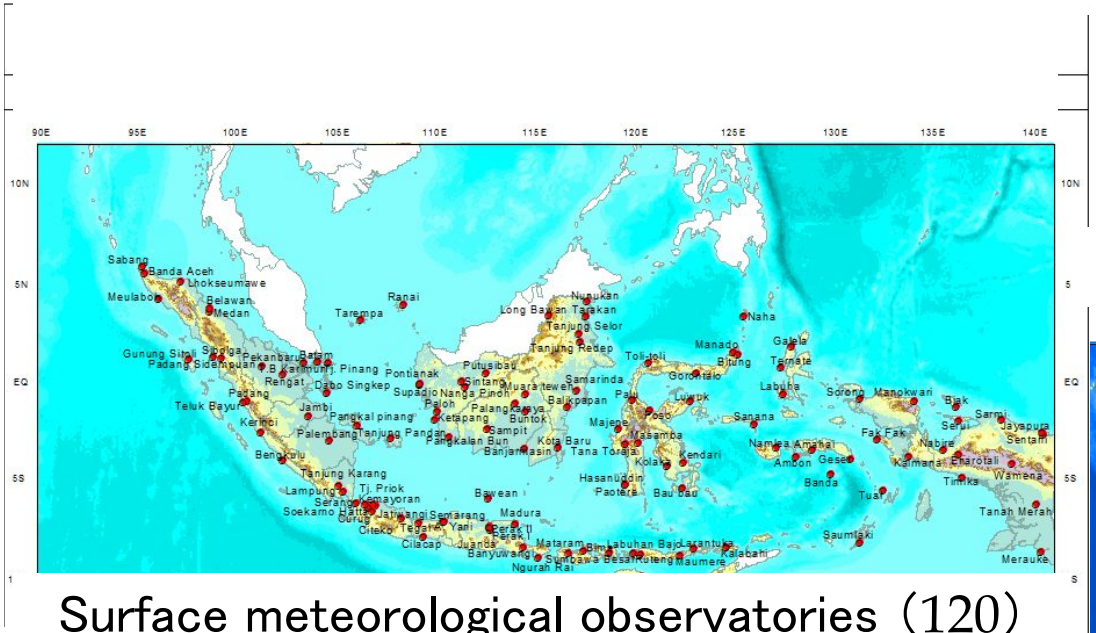

Surface meteorological observatories（120）

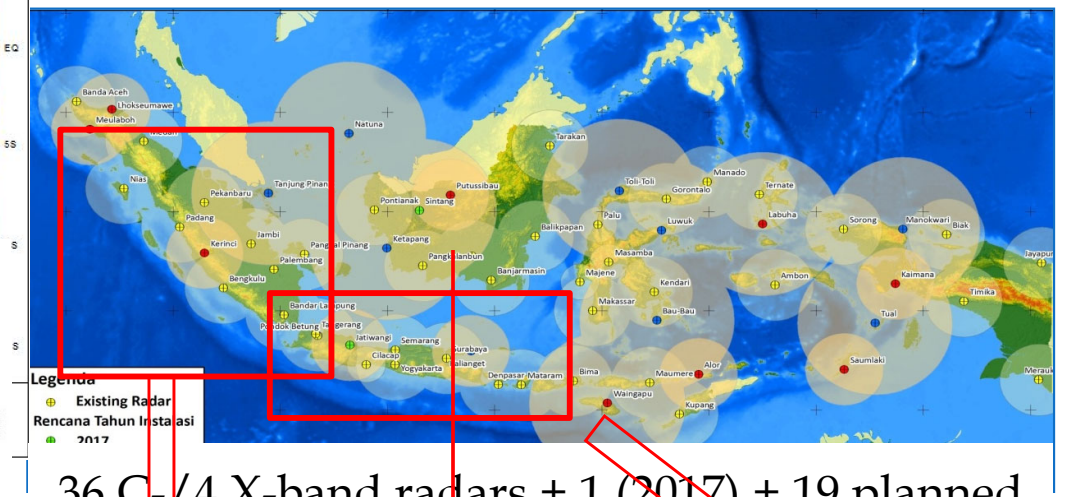

36 C-/4 X-band radars + 1 (2017) + 19 planned

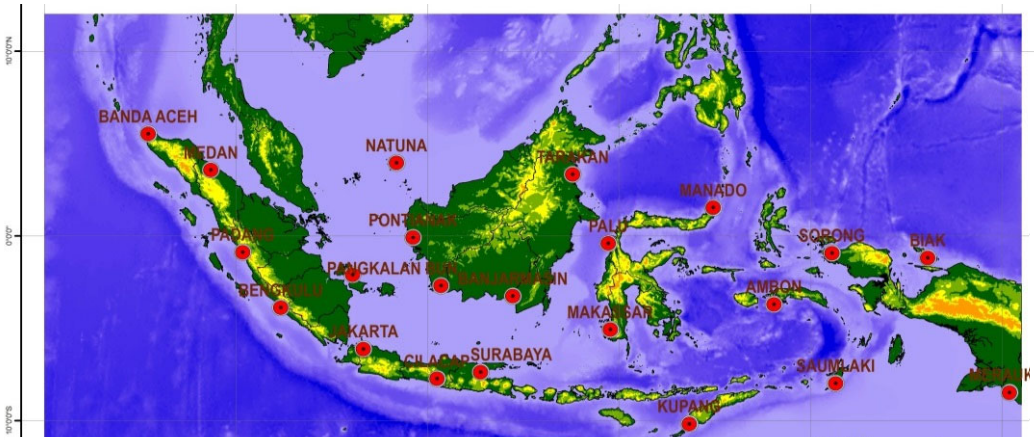

Radiosonde stations（22）

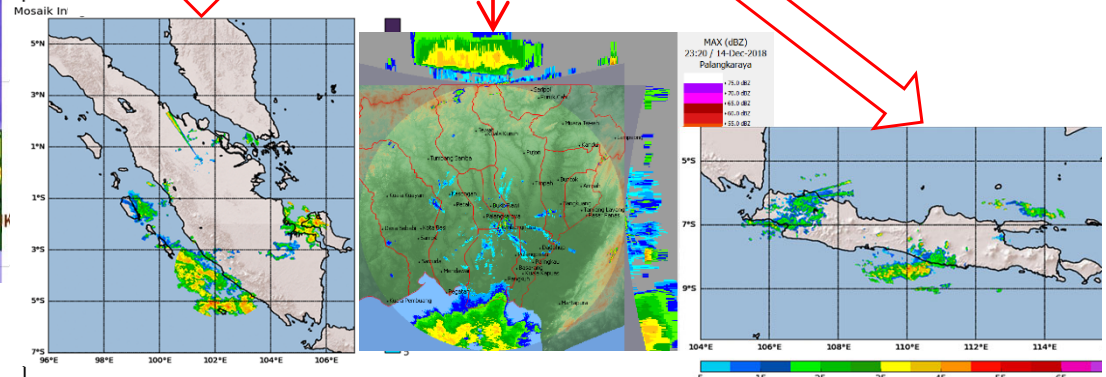

6.3. Conditional instability of second kind (CISK) and tropical cyclone

Typhoon as a "mini-earth" with different heating distribution

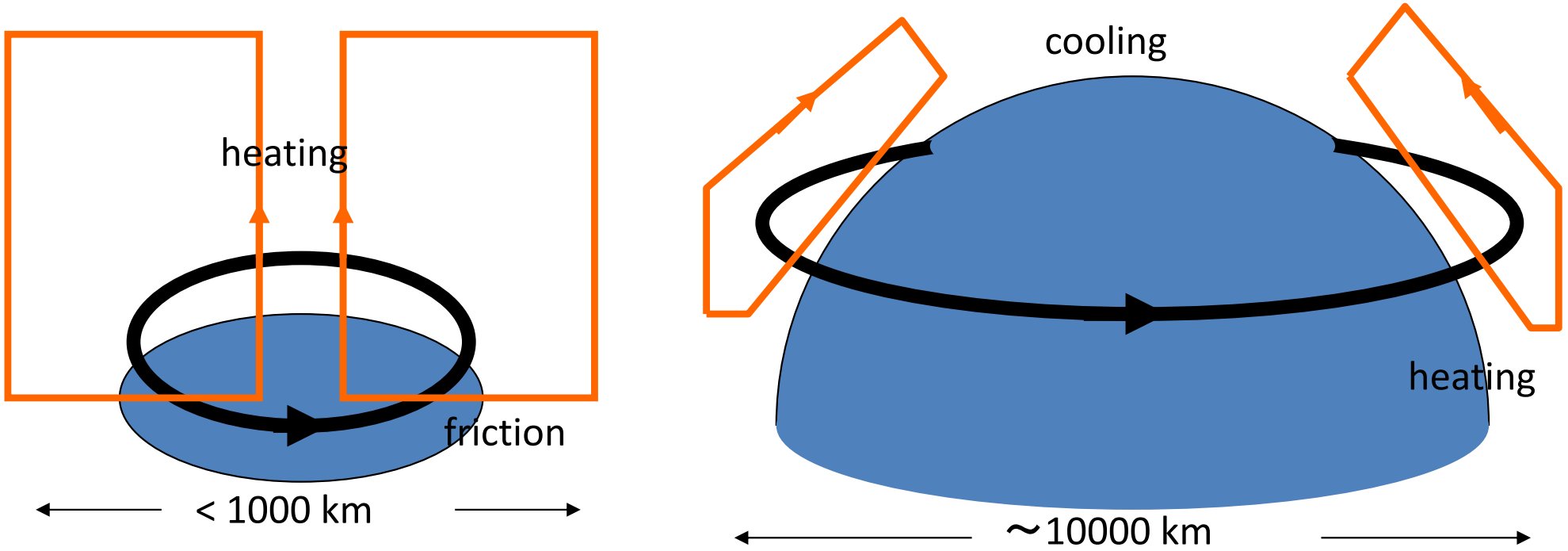

Tangential wind ⇔ Pressure gradient

Radial wind ⇔ Surface friction, turbulence /drag

Vertical velocity ⇔ Latent heat by cloud/precipitation

Himawari 8 (July 2015-)

Temporal/horizontal resolution: 2.5-10 min, 0.5-1 km

A supertyphoon T1513 Soudelor

Cloud distribution variations
relative to the typhoon center →

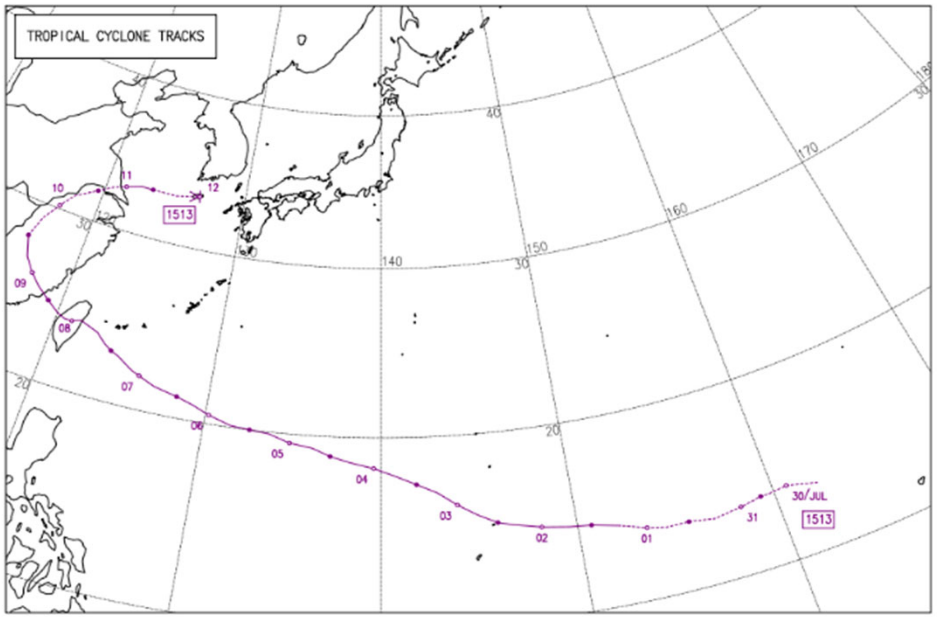

http://www.data.jma.go.jp/fcd/yoho/typhoon/route_map/bstv2015.html
http://www.data.jma.go.jp/fcd/yoho/data/typhoon/T1513.pdf

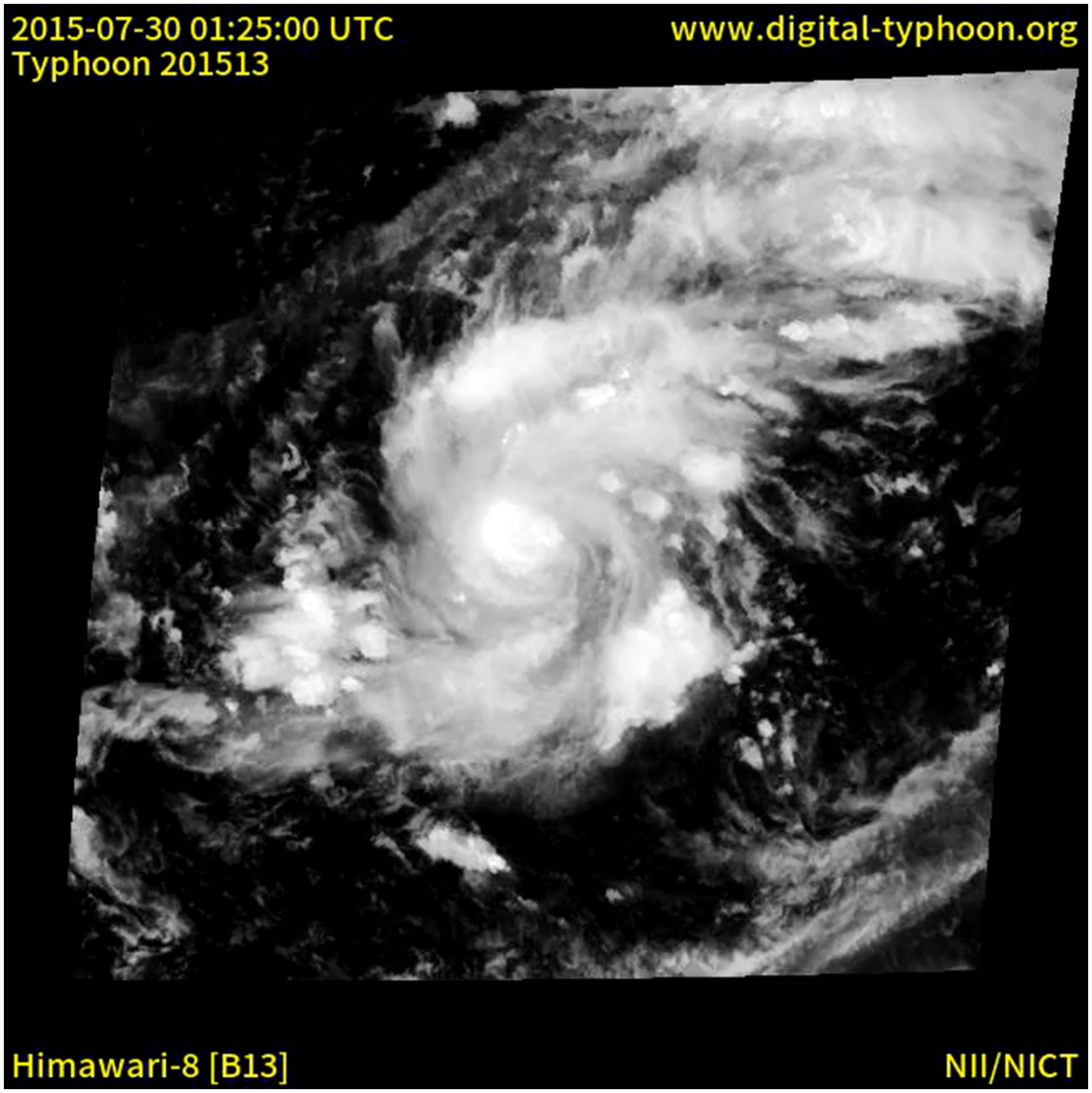

http://agora.ex.nii.ac.jp/digital-typhoon/animation/wnp/r3/B13/mp4/201513.mp4

However, still radar observations of rainfall in much higher resolutions are necessary.

Geographical Distribution of Tropical Cyclones

(Max. Wind ≧ 17 m/s

1979-88

(Neumann, 1993)

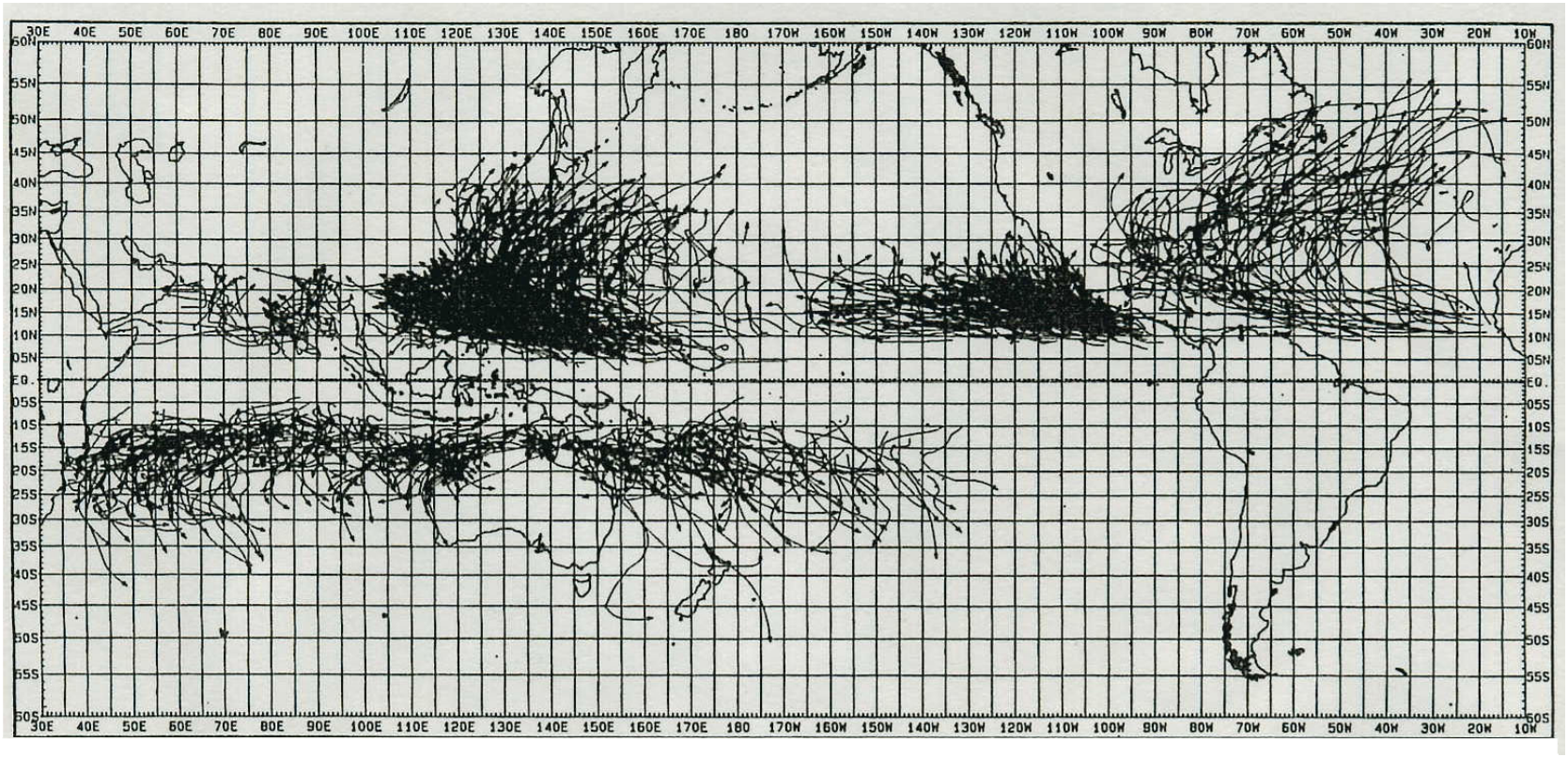

1995-2004

(Liu, 2007; original by Neumann)

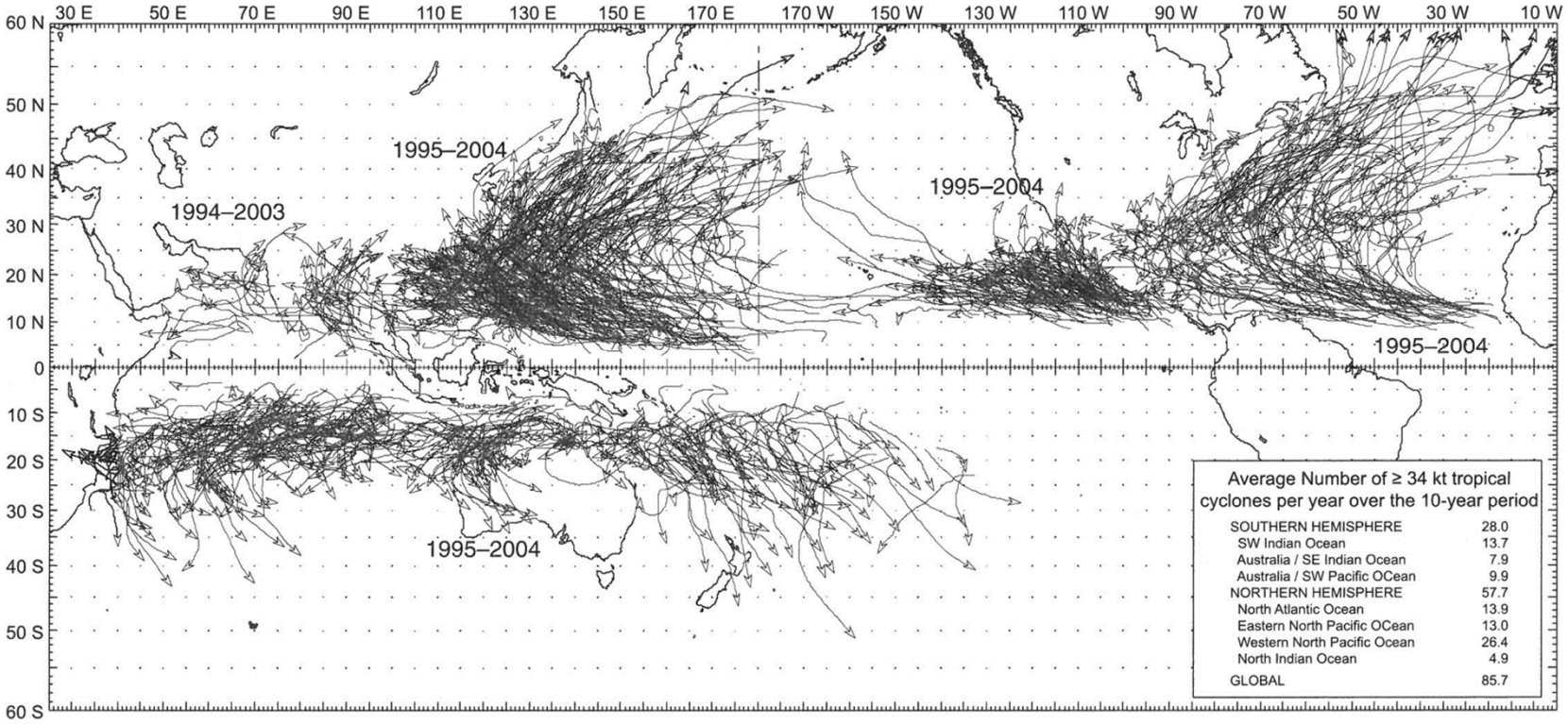

"Borneo vortex"

(Not tropical storm, but related to torrential rainfalls)

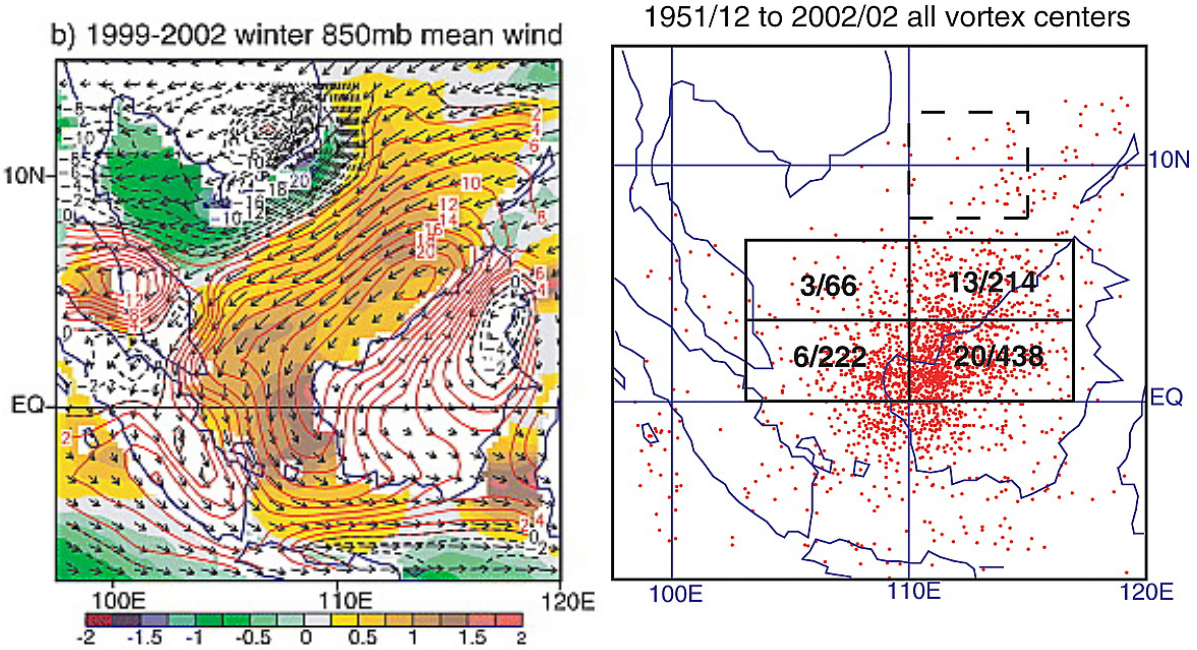

(Chang et al., 2003, *GRL*)

Badai Tropis "Vamei"

(Dec 2001; 1st case <1,5º lat)

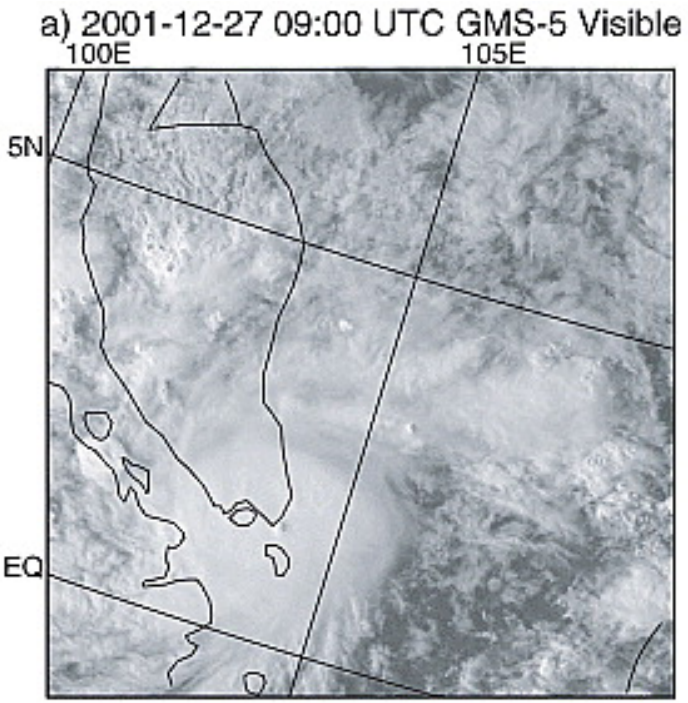

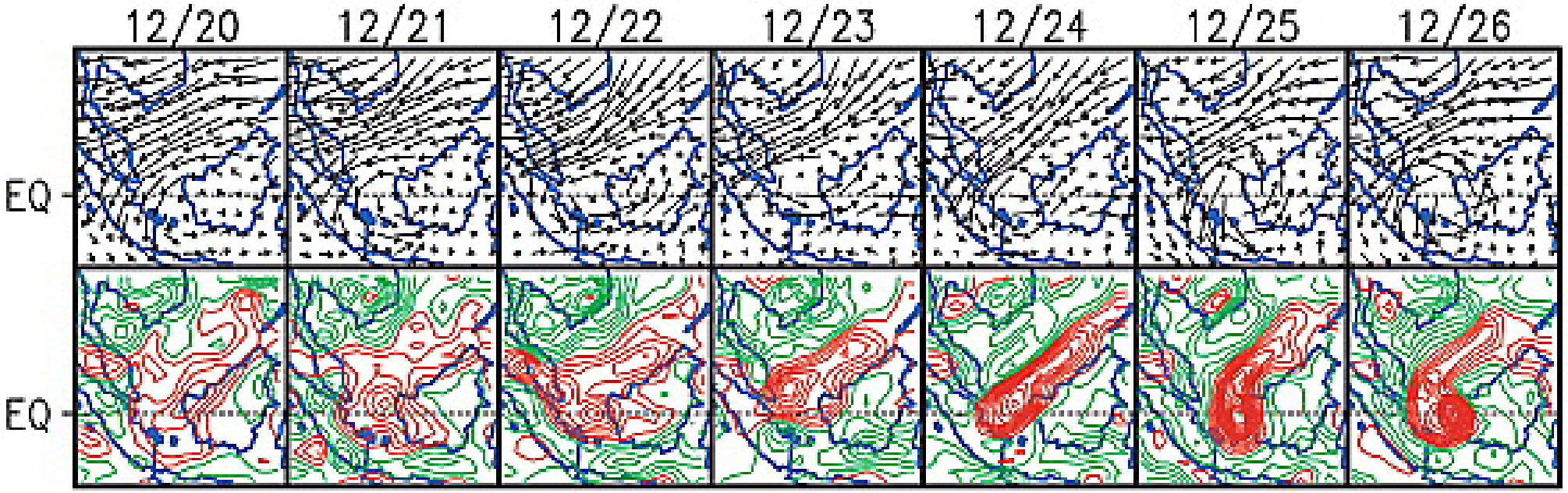

Badai Tropis “Isobel”

(Dec 2006-Jan 2007)

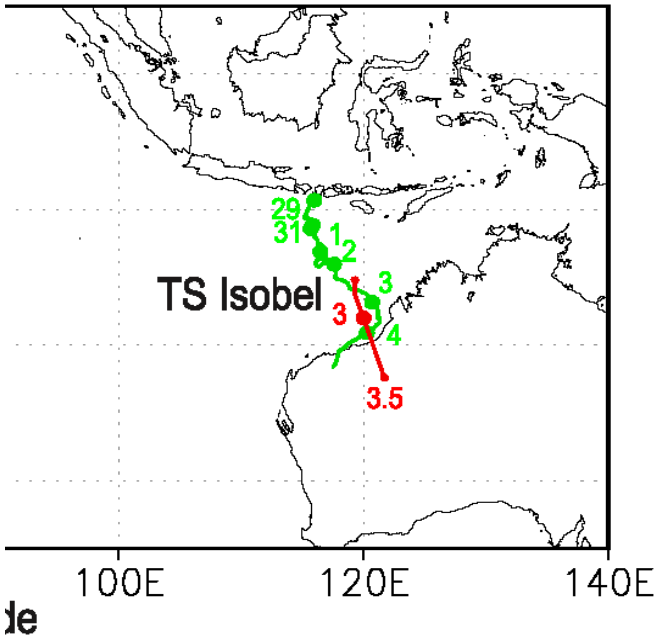

(Fudeyasu et al., 2008, *GRL*)

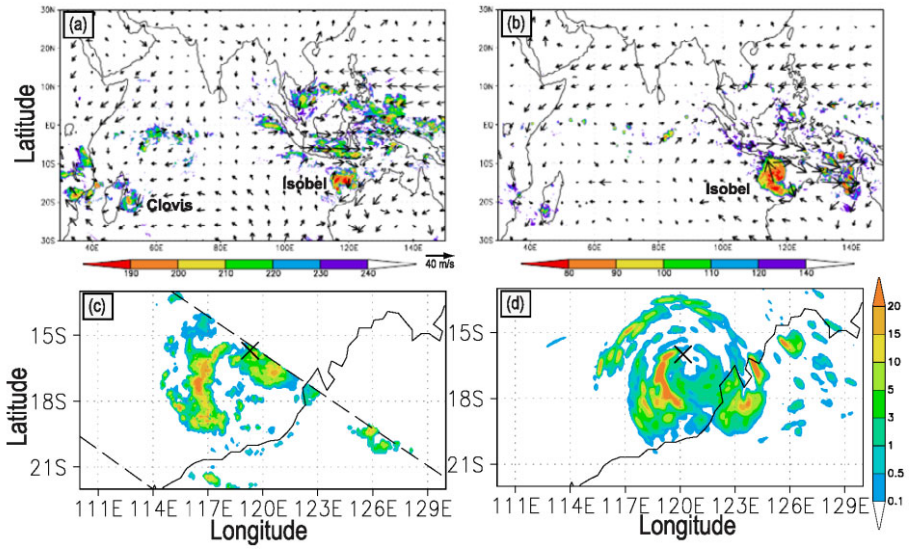

Figure 3. Same as Figure 2 except for cross sections. The time is (a) and (b) 0000 UTC, (c) 0920 UTC, and (d) 2230 UTC 2 January 2007. Crosses represent the position of the storm center.

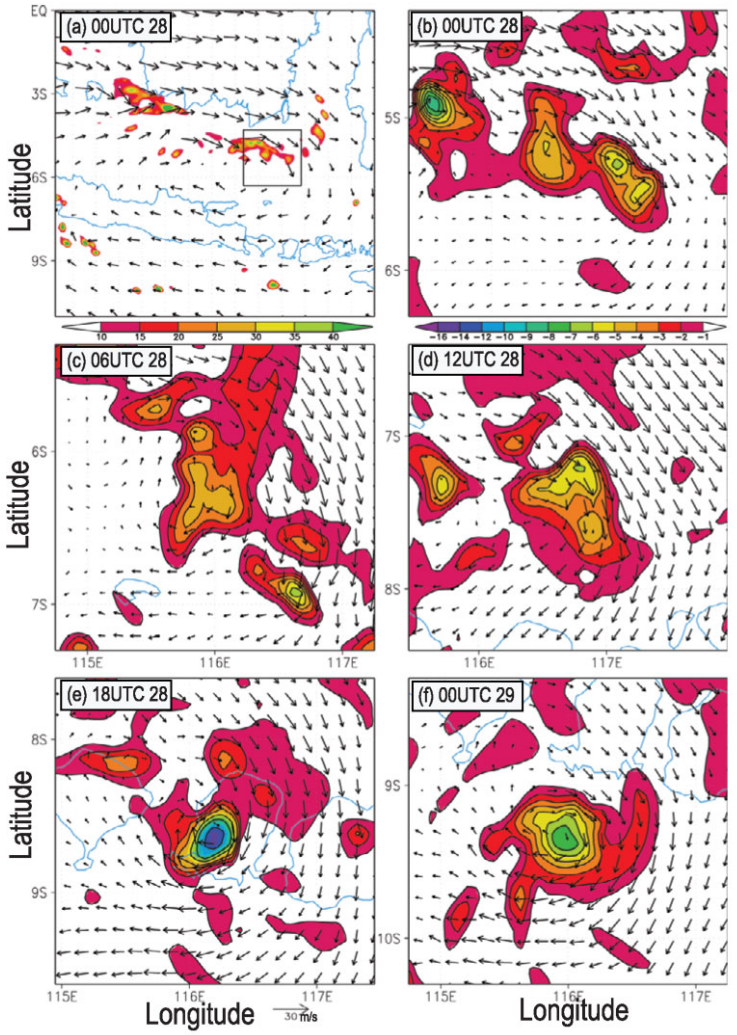

Figure 4. (a) Precipitation rate (shading, mm h^{-1}) and horizontal winds at 310-K level at 0000 UTC 28 December 2006 showing the WWB associated with the MJO. The evolution of cyclonic potential vorticity (shading and contour, PVU) and horizontal winds at 310-K level in a 2.5° × 2.0° box are shown at (b) 0000 UTC, (c) 0600 UTC, (d) 1200 UTC, (e) 1800 UTC 28, and (f) 0000 UTC 29 December 2006. Rectangle in Figure 4a represents the domain in Figure 4b.

6.4. Wave CISK and intraseasonal (Madden Julian) oscillations

http://dx.doi.org/10.1175/1520-0469(1971)028<0702:DOADOI>2.0.CO;2

Detection of a 40–50 Day Oscillation in the Zonal Wind in the Tropical Pacific

ROLAND A. MADDEN AND PAUL R. JULIAN

National Center for Atmospheric Research,[1] Boulder, Colo.

(Manuscript received 21 December 1970, in revised form 29 March 1971)

ABSTRACT

Nearly ten years of daily rawinsonde data for Canton Island (3S, 172W) have been subjected to spectrum and cross-spectrum analysis. In the course of this analysis a very pronounced maximum was noted in the co-spectrum of the 850- and 150-mb zonal wind components in the frequency range 0.0245–0.0190 day^{-1} (41–53 days period). Application of *a posteriori* sampling theory resulted in a significance level of ~6% (0.1% prior confidence level). This type of significance test is appropriate because no prior evidence or reason existed for expecting such a spectral feature. Subsequent analysis revealed the following structure of the oscillation. Peaks in the variance spectra of the zonal wind are strong in the low troposphere, are weak or non-existent in the 700-400 mb layer, and are strong again in the upper troposphere. No evidence of this feature could be found above 80 mb, or in any of the spectra of the meridional component. The spectrum of station pressure possesses a peak in this frequency range and the oscillation is in phase with the low tropospheric zonal wind oscillation, and out of phase with that in the upper troposphere. The tropospheric temperatures exhibit a similar peak and are highly coherent with the station pressure oscillation; positive station pressure anomalies are associated with negative temperature anomalies throughout the troposphere. Thus, the lower-middle troposphere appears to be a nodal surface with u and P oscillating in phase but 180° out of phase above and below this surface. Evidence for this phenomenon was found in shorter records at Kwajalein (9N, 168E) but not at Singapore (1N, 104E) or Balboa, Canal Zone (9N, 79W). We speculate that the oscillation is a large circulation cell oriented in zonal planes and centered in the mid-Pacific.

Intra-Seasonal Variation (Madden-Julian Oscillation) and its hierarchical structure

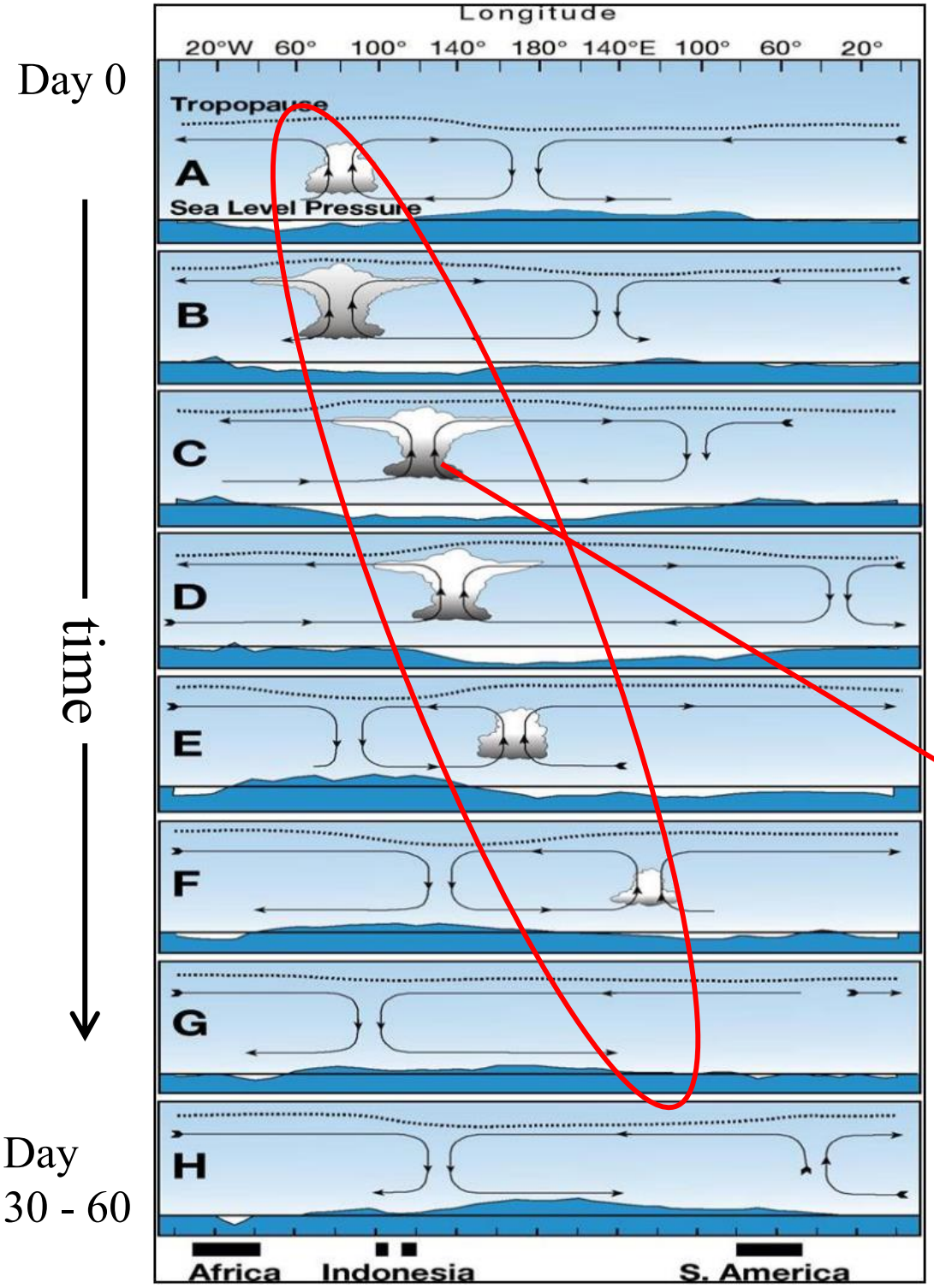

(Madden and Julian, 1972; Madden, 2003)

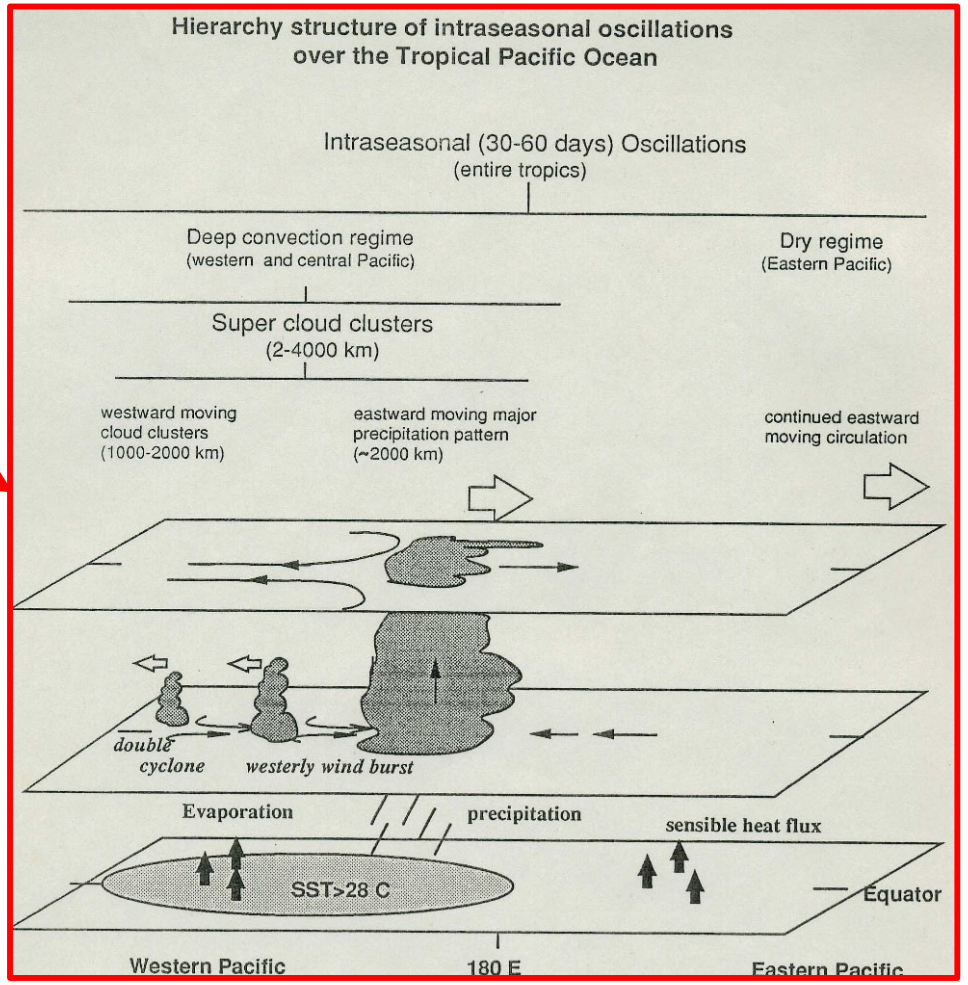

(Nakazawa, 1985; Lau et al., 1987)

Localized convection (Super cloud cluster / ISV)

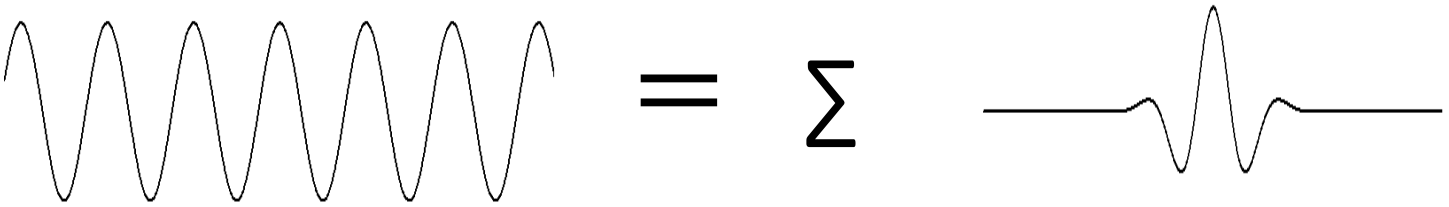

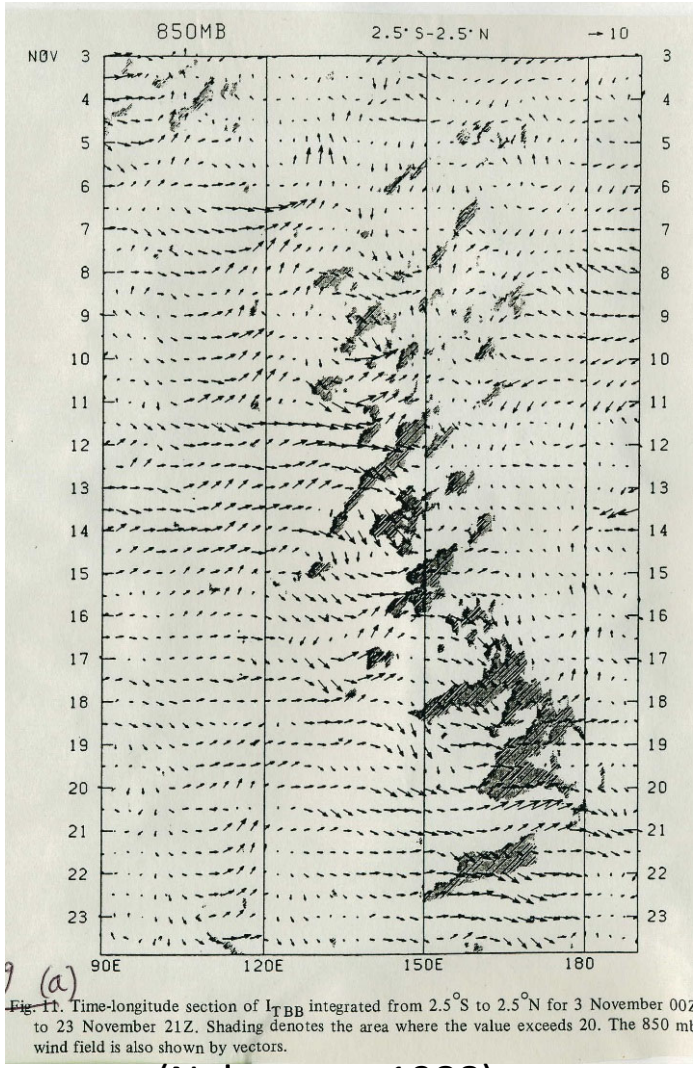

Fig. 11. Time-longitude section of I_{TBB} integrated from 2.5°S to 2.5°N for 3 November 00Z to 23 November 21Z. Shading denotes the area where the value exceeds 20. The 850 mb wind field is also shown by vectors.

(Nakazawa, 1988)

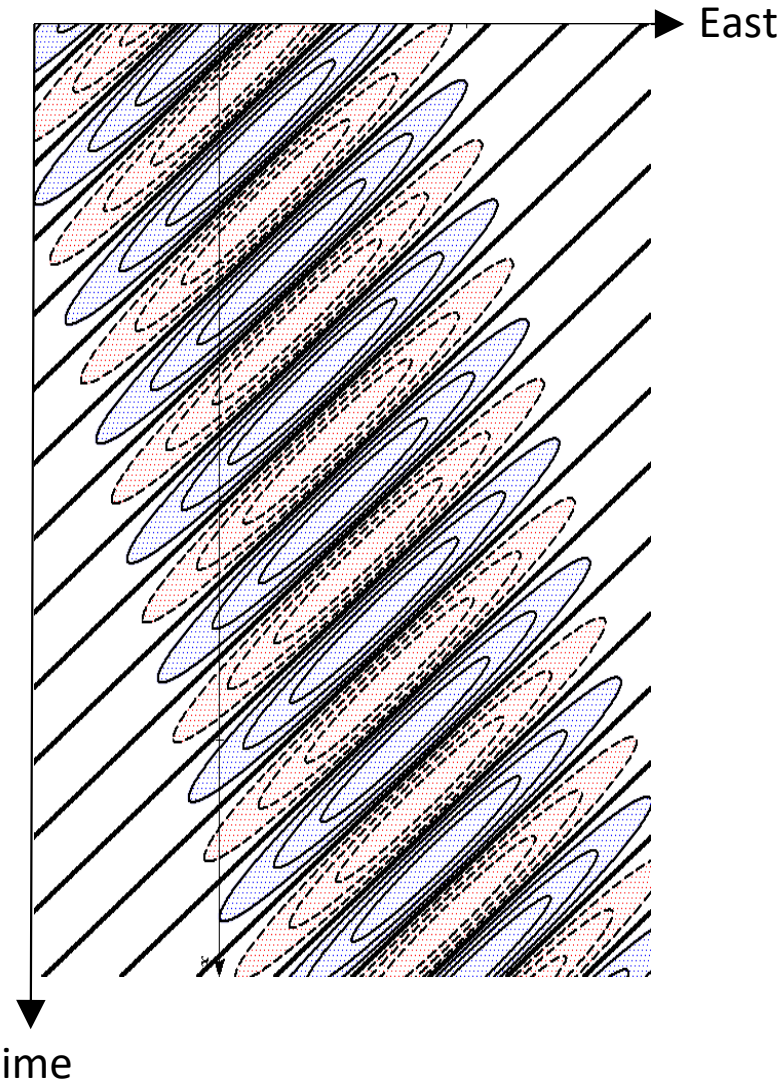

Intraseasonal / diurnal variations of convection (Hamada et al., 2008)

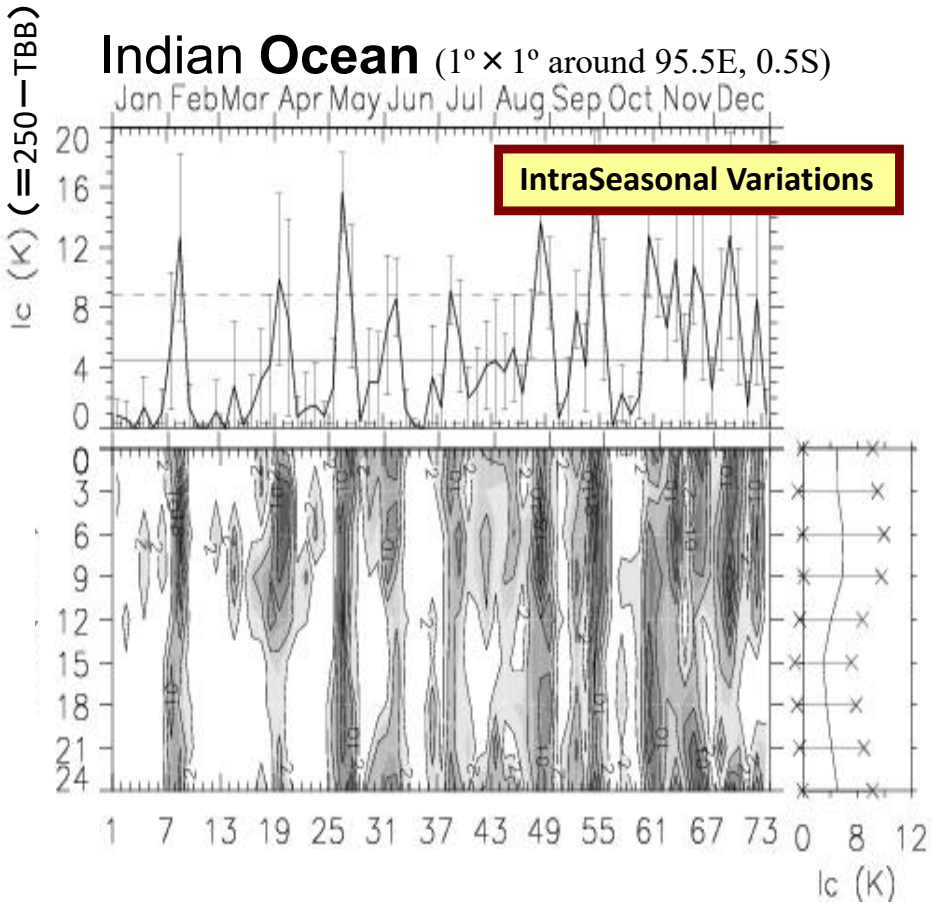

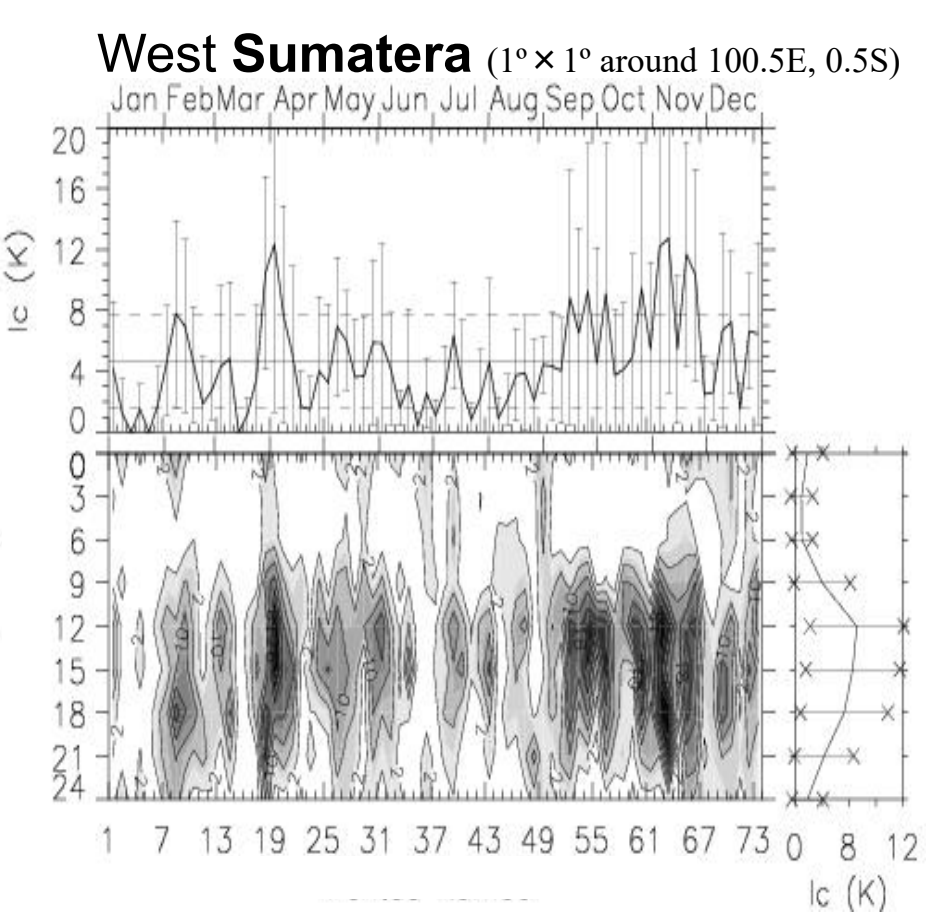

Rainfall in **Coastal** region

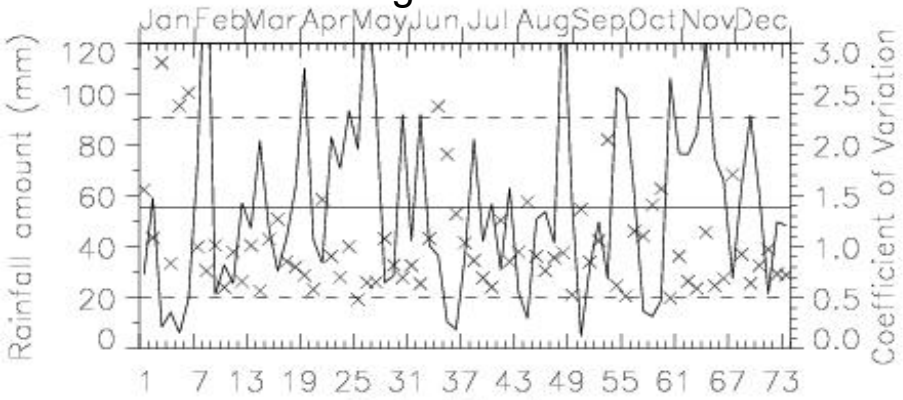

Rainfall in **Inland** region

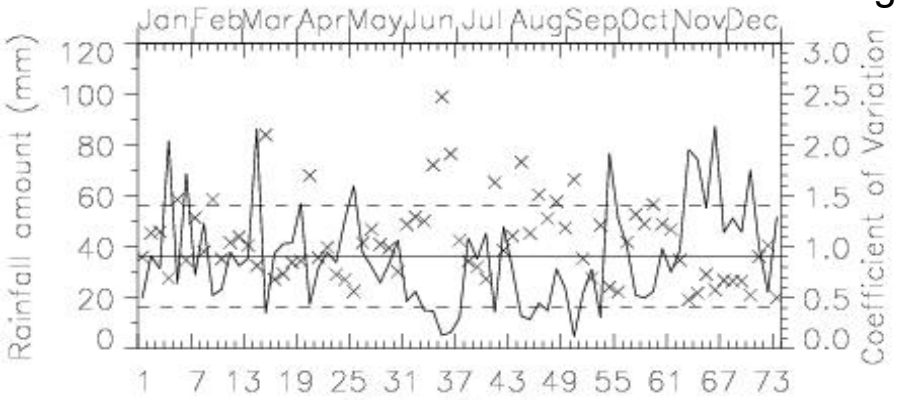

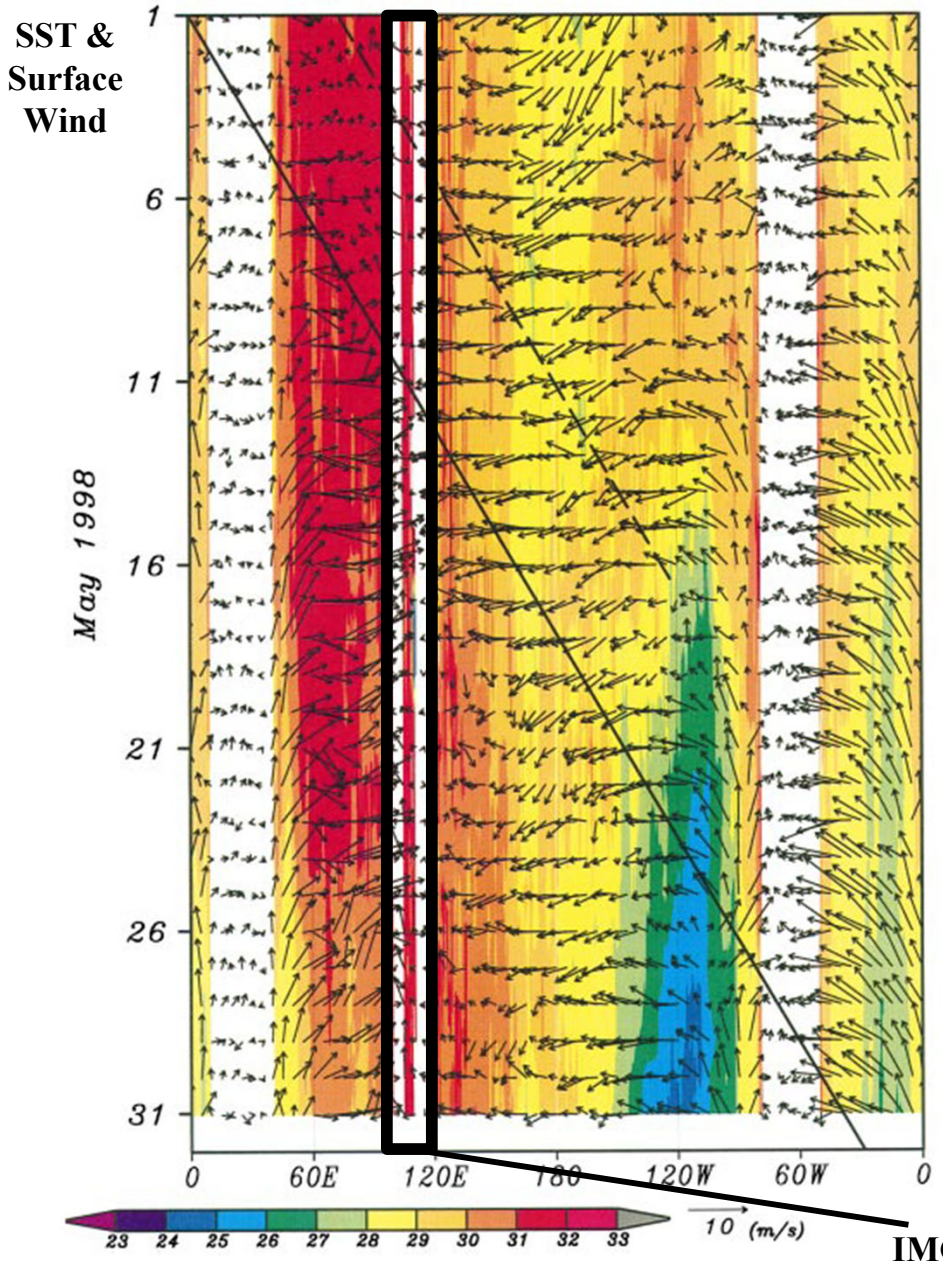

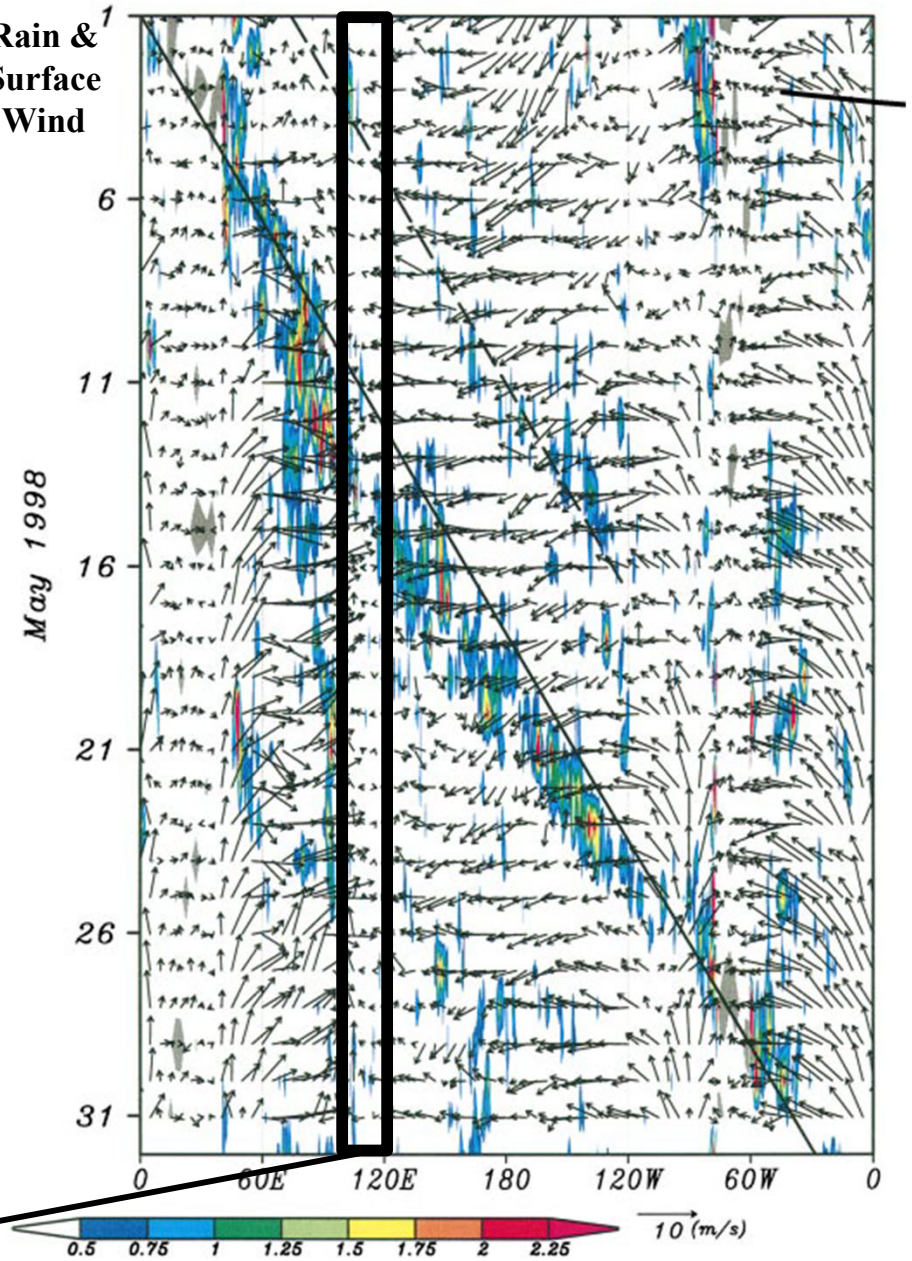

IMC

IMC "barrier effect" > 75% (Zhang & Ling, 2017)

Figure 2 Time–longitude sections of SST and the surface winds. Colours indicate the SST derived from the TMI data and averaged from 3° N to 3° S. Units on the colour scale are °C. The vectors are the ECMWF surface winds on the Equator. The abscissa is the longitude starting from the Greenwich meridian, and the ordinate is for the period of 1 May–1 June 1998. The solid line corresponds to the propagation of the major rain system found in Fig. 3, and the dashed line shows that of the preceding rain system (see text for details).

Figure 3 Time–longitude sections of the rain rate and the surface winds. Colours show the rain rate obtained from the SSM/I retrievals (see text), and the grey shades show that obtained from the TRMM precipitation radar with the PR2a25 algorithm (T.I., manuscript in preparation) for values >0.5 mm h $^{-1}$, and averaged from 10° N to 10° S. Units on the colour scale are mm h $^{-1}$. The vectors are the ECMWF surface winds on the Equator.

(Takayabu et al., 1999, *Nature*)

WPR tracing of ISV (compared with Aqua-Planet)

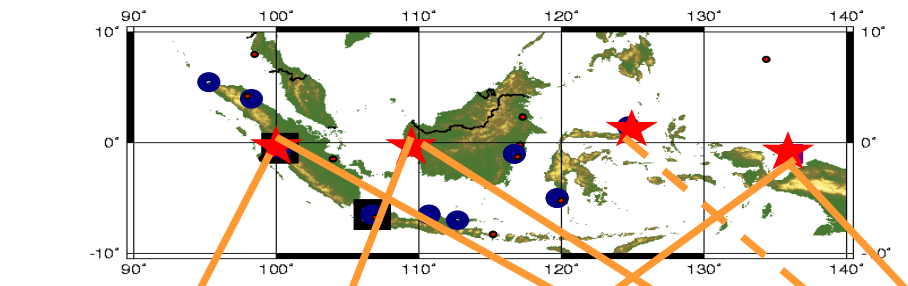

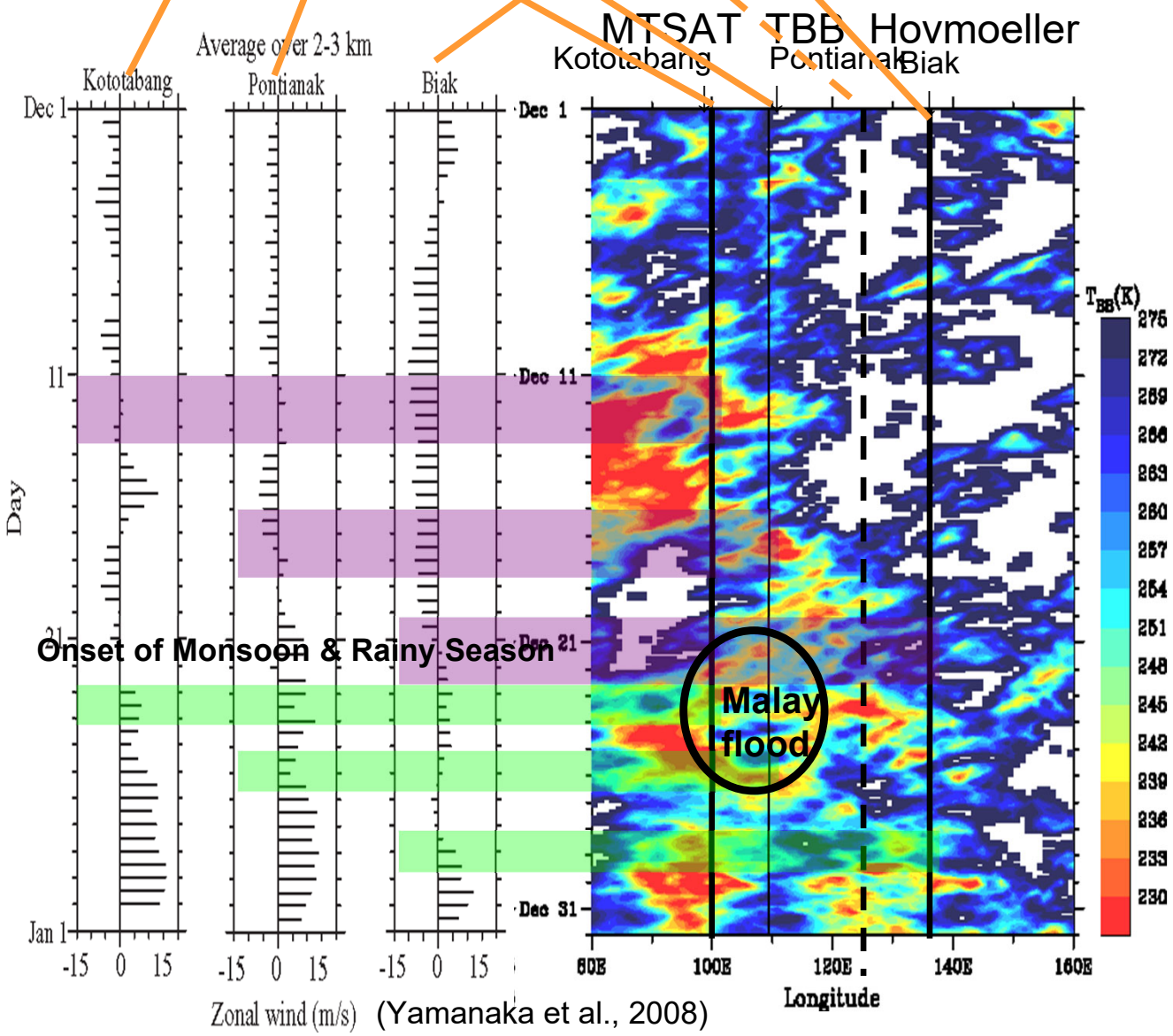

(Yamanaka et al., 2008)

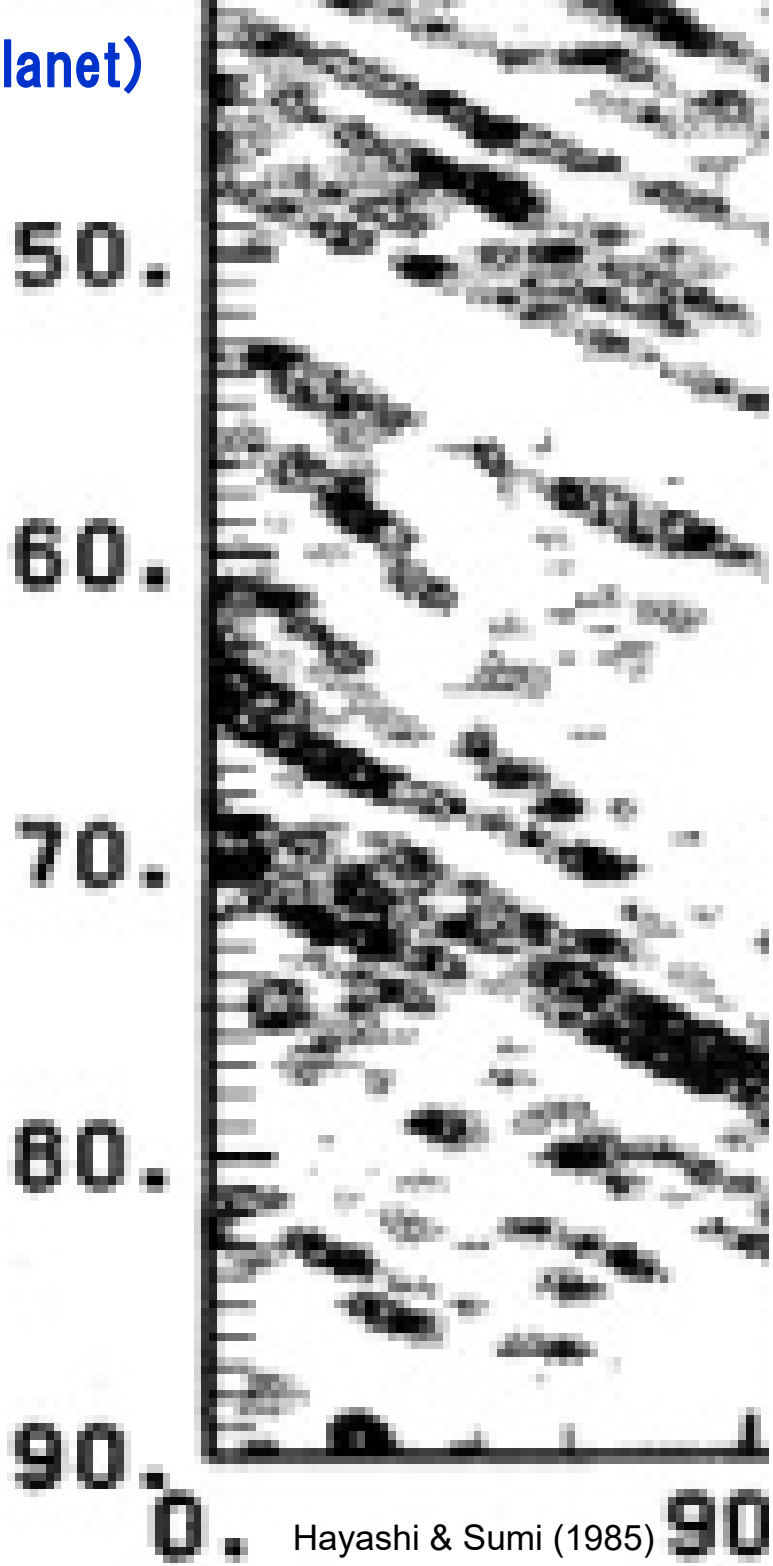

Hayashi & Sumi (1985)

Jakarta flood by "cross-equatorial" cold surge

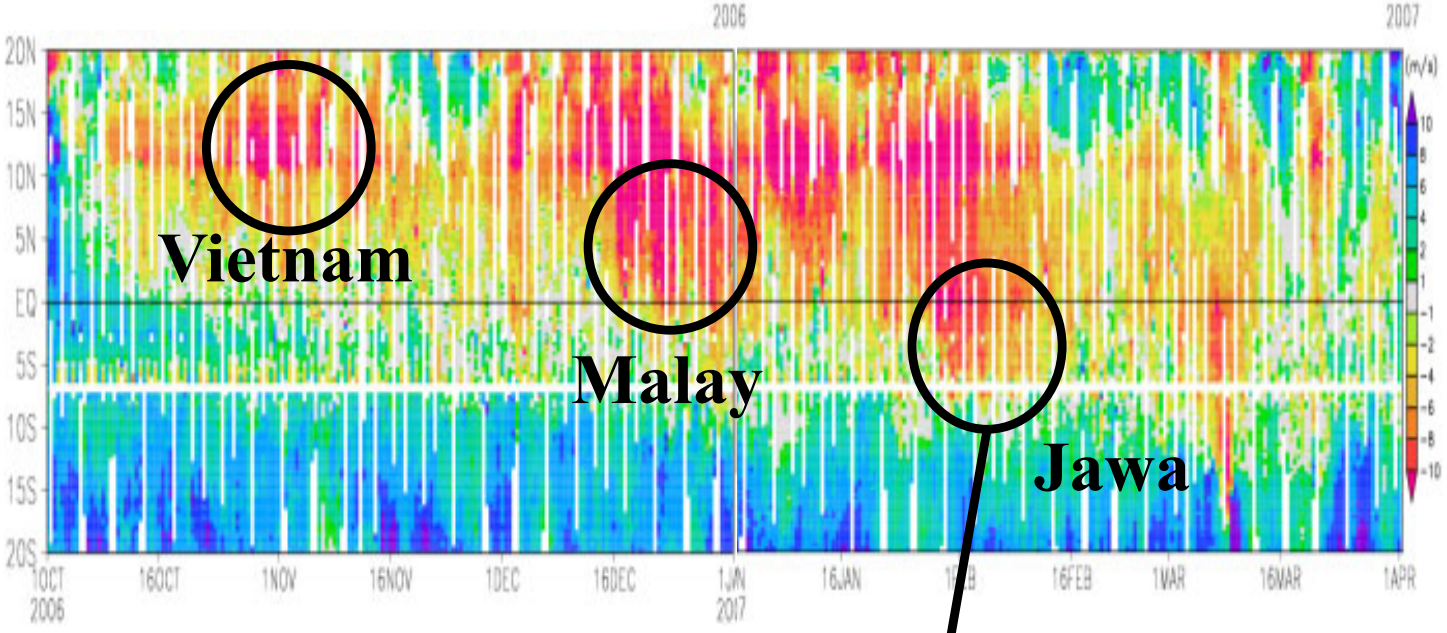

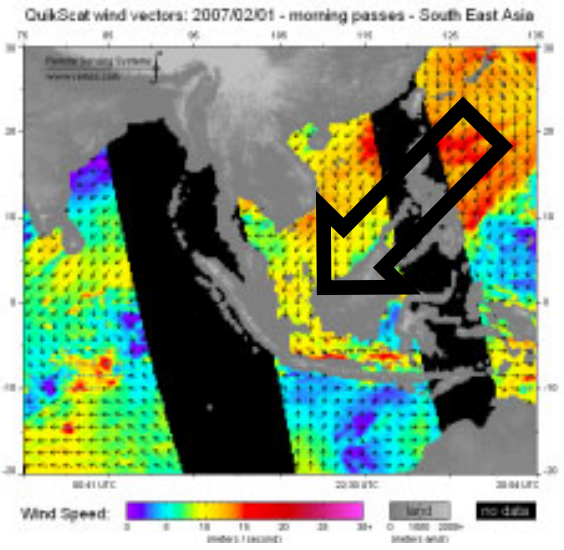

Jakarta Flood (Jan-Feb 2007)

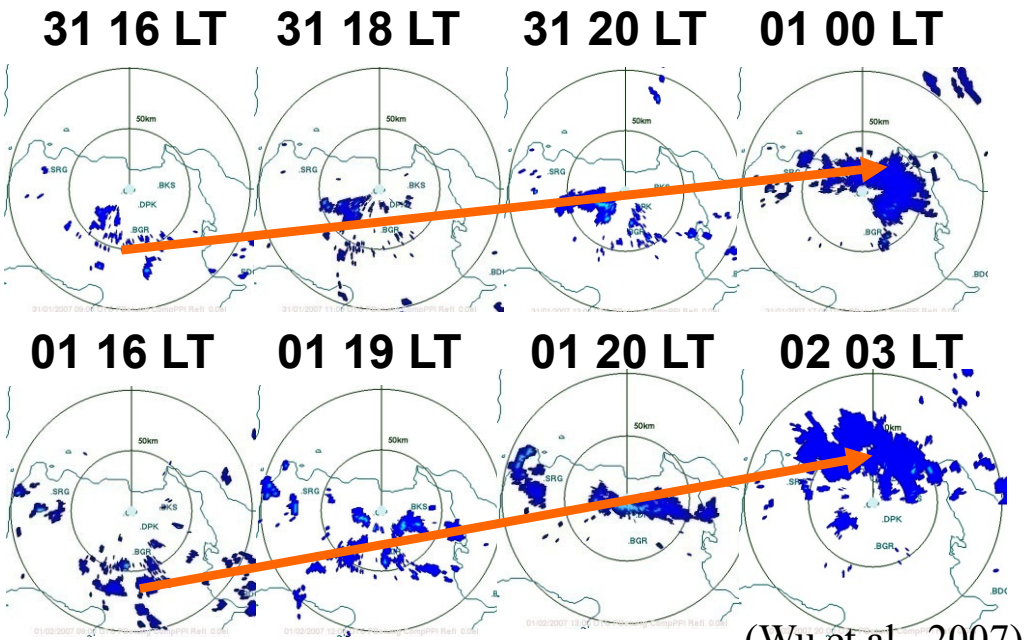

(Wu et al., 2007)

Matsuno-Gill pattern associated with an ISV (MJO) observed during HARIMAU2011 IOP

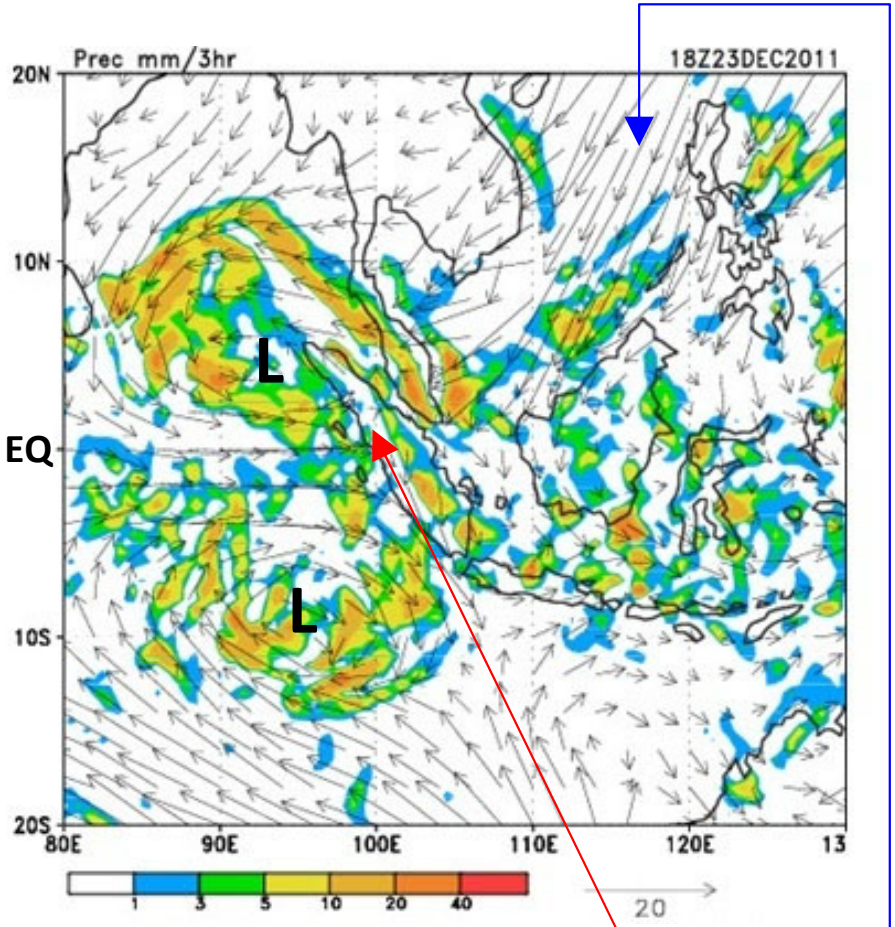

Diurnal cycle (clear land after midnight)

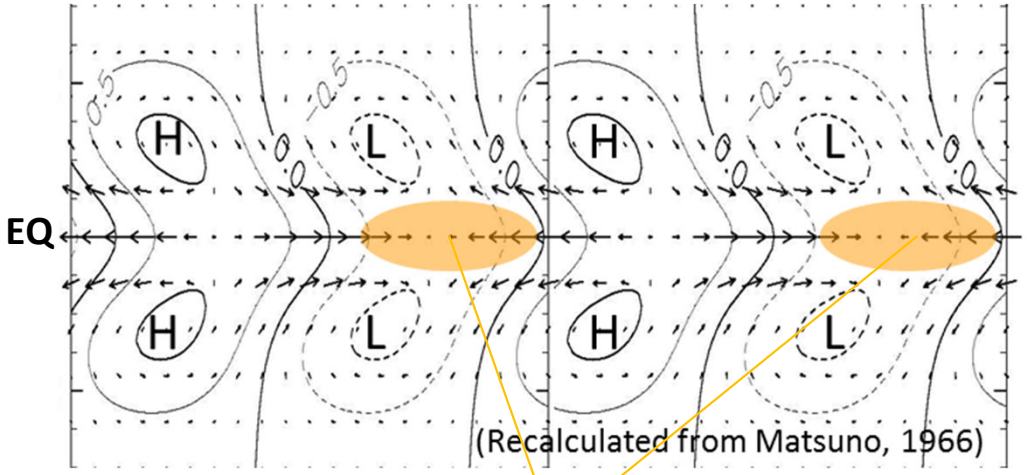

"Hot spot" (aligned or isolated)

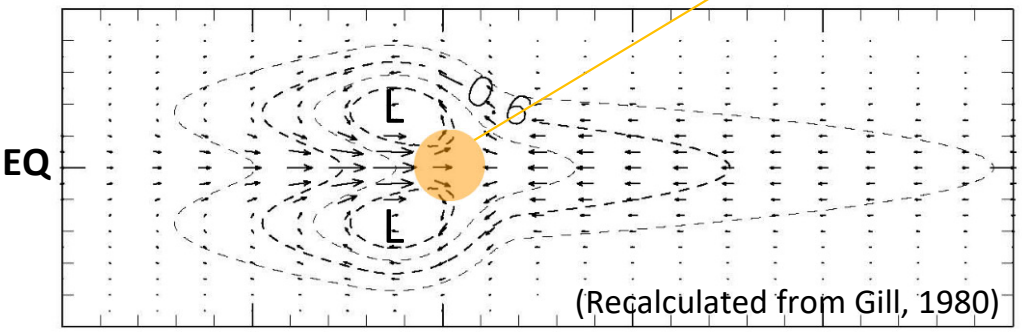

Boreal winter monsoon (so-called *cold surge*)

MJO index

http://dx.doi.org/10.1175/1520-0493(2004)132<1917:AARMMI>2.0.CO;2

An All-Season Real-Time Multivariate MJO Index: Development of an Index for Monitoring and Prediction

MATTHEW C. WHEELER AND HARRY H. HENDON

Bureau of Meteorology Research Centre, Melbourne, Australia

(Manuscript received 11 September 2003, in final form 10 February 2004)

ABSTRACT

A seasonally independent index for monitoring the Madden–Julian oscillation (MJO) is described. It is based on a pair of empirical orthogonal functions (EOFs) of the combined fields of near-equatorially averaged 850-hPa zonal wind, 200-hPa zonal wind, and satellite-observed outgoing longwave radiation (OLR) data. Projection of the daily observed data onto the multiple-variable EOFs, with the annual cycle and components of interannual variability removed, yields principal component (PC) time series that vary mostly on the intraseasonal time scale of the MJO only. This projection thus serves as an effective filter for the MJO without the need for conventional time filtering, making the PC time series an effective index for real-time use.

The pair of PC time series that form the index are called the Real-time Multivariate MJO series 1 (RMM1) and 2 (RMM2). The properties of the RMM series and the spatial patterns of atmospheric variability they capture are explored. Despite the fact that RMM1 and RMM2 describe evolution of the MJO along the equator that is independent of season, the coherent off-equatorial behavior exhibits strong seasonality. In particular, the northward, propagating behavior in the Indian monsoon and the southward extreme of convection into the Australian monsoon are captured by monitoring the seasonally independent eastward propagation in the equatorial belt. The previously described interannual modulation of the global variance of the MJO is also well captured.

Applications of the RMM series are investigated. One application is through their relationship with the onset dates of the monsoons in Australia and India; while the onsets can occur at any time during the convectively enhanced half of the MJO cycle, they rarely occur during the suppressed half. Another application is the modulation of the probability of extreme weekly rainfall; in the "Top End" region around Darwin, Australia, the swings in probability represent more than a tripling in the likelihood of an upper-quintile weekly rainfall event from the dry to wet MJO phase.

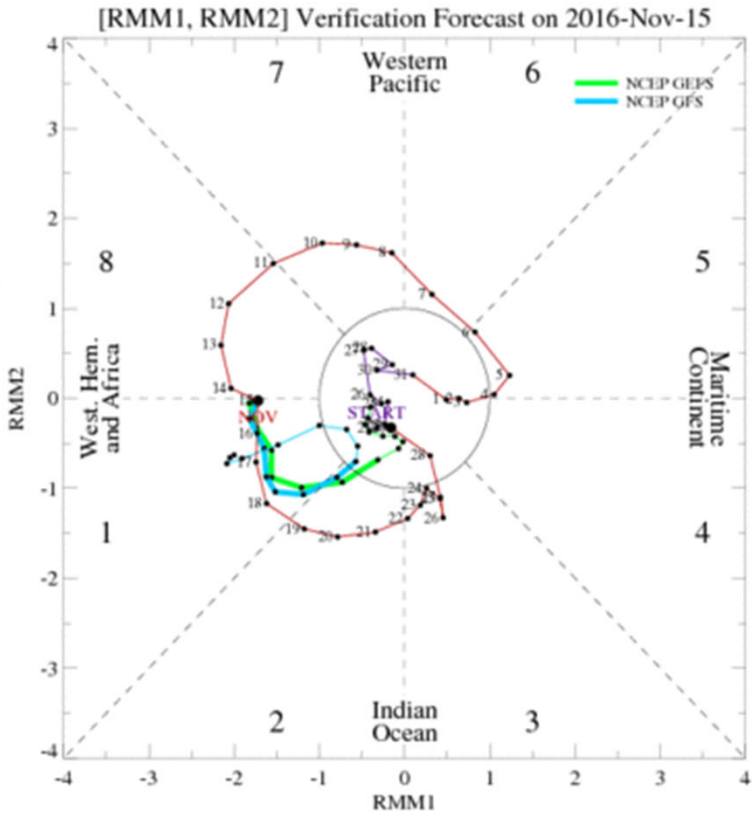

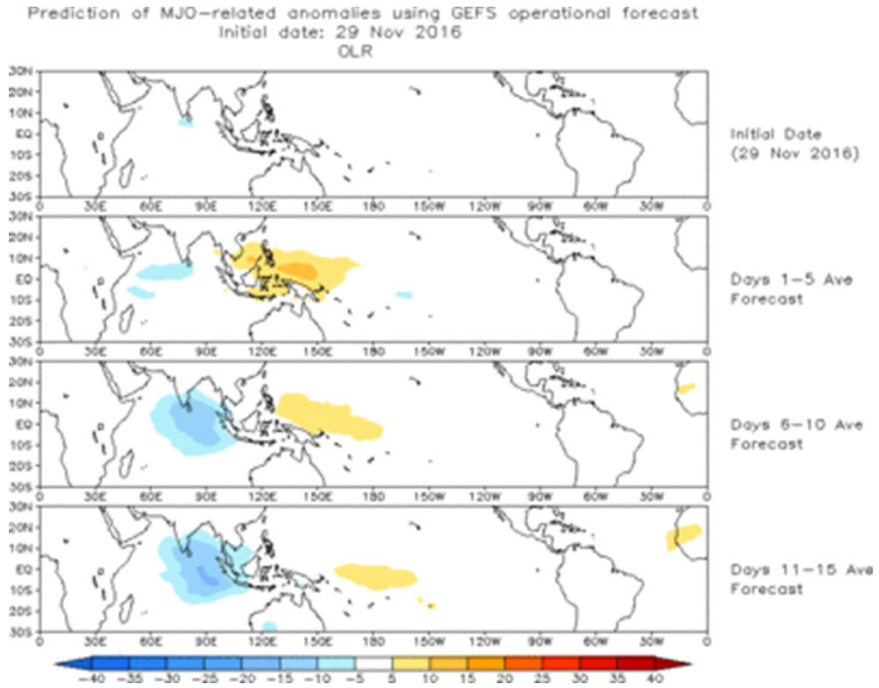

http://www.cpc.ncep.noaa.gov/products/precip/CWlink/MJO/mjo.shtml

MJO index:
Phase 4-5 at the Indonesian maritime continent

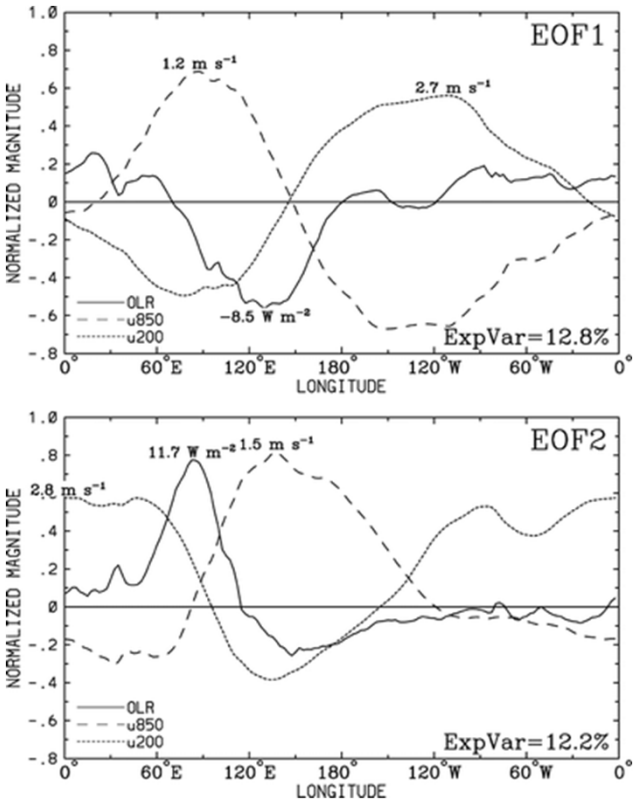

The first two empirical orthogonal functions (EOFs)

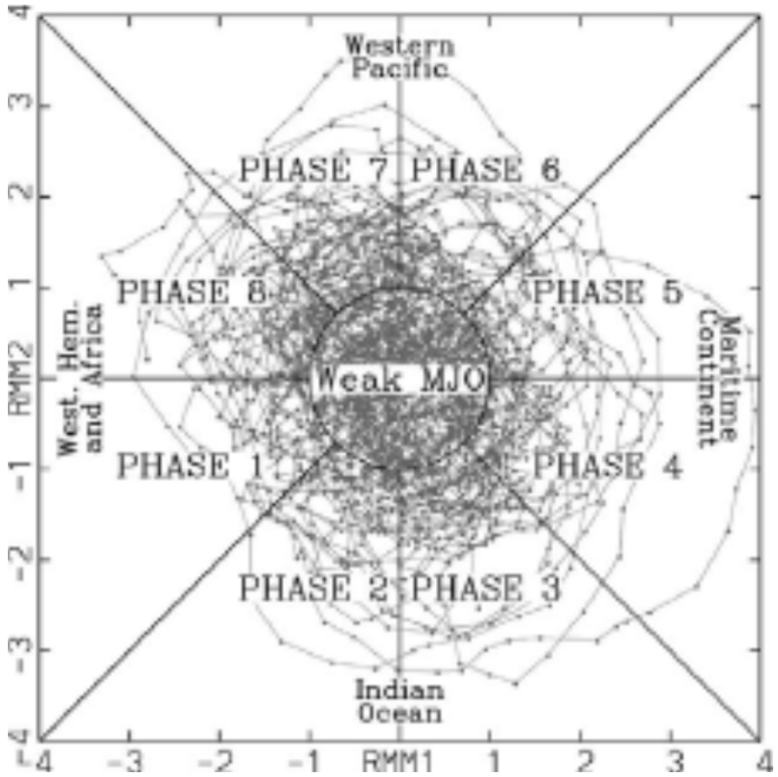

The real-time multivariate MJO (RMM) index space indicating eastward propagation of MJO

(Wheeler & Hendon, 2004)

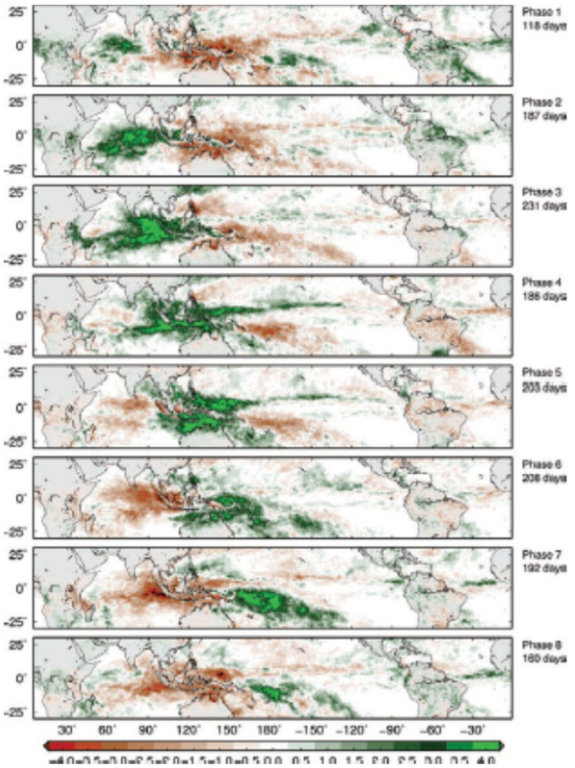

Composites of IS (30-90 d) anomalies in TRMM rain (mm/d) in Nov-Dec 1998-2012 based on the RMM index

(Zhang, 2013)

Six essentials of tropical climatology/meteorology

Radiative "imbalance" compensated by water cycle

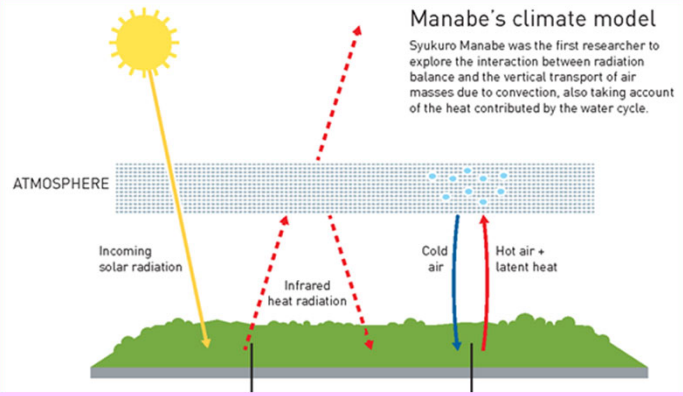

Insolation, greenhouse effect and condensation = infrared cooling, parasol effect

Strong wind - rotation/vortex balance

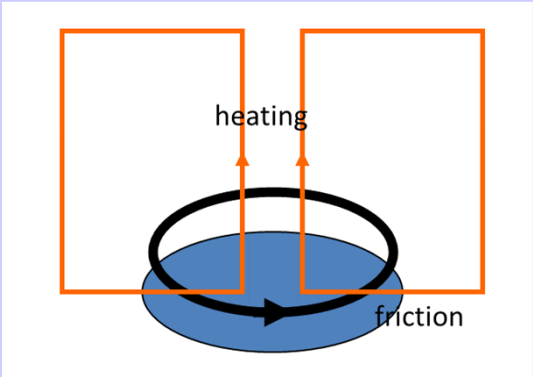

Typhoon is developed only over "sub"tropical warm ocean..

Wind makes cloud in the mid-latitudes, whereas cloud makes wind in the tropics

Air (momentum) - sea (energy) interaction

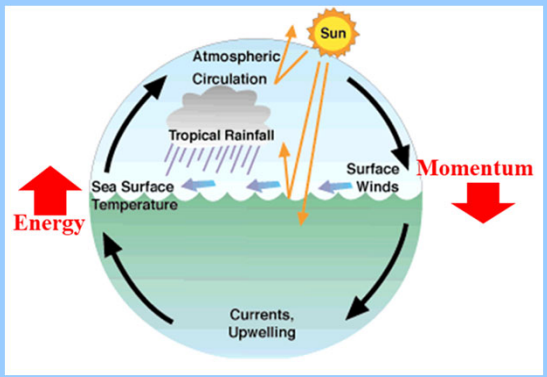

Interannual (ENSO/IOD) and intraseasonal (MJO) variability

Land (solid) - sea (liquid) heat contrast

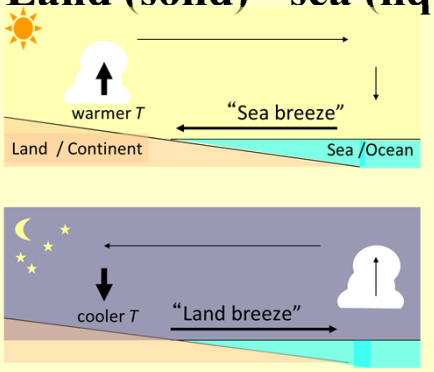

Diurnal cycle is basic in the tropics, whereas annual cycle is basic in the extratropics.

No tropical night in the tropics.

Sea wind -river balance

"Conditional instability" (convection-cloud) paradox

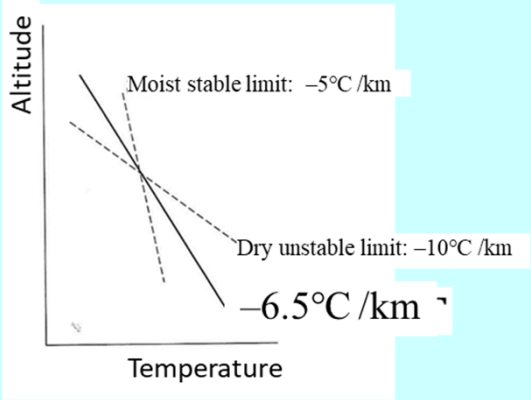

Convection needs condensation, whereas condensation needs convection

Water cycle accelerated by warming

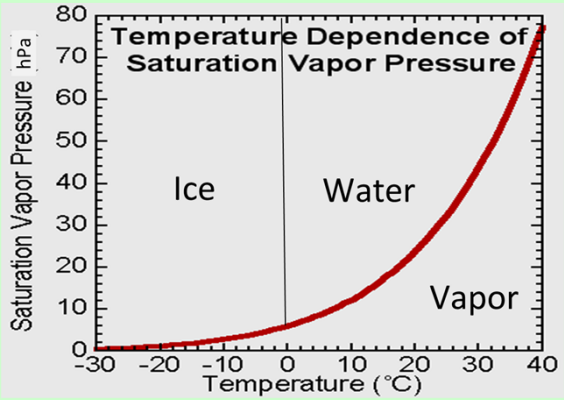

Precipitable water is increased with temperature.

For future: The Earth Bio-Anthroposphere system

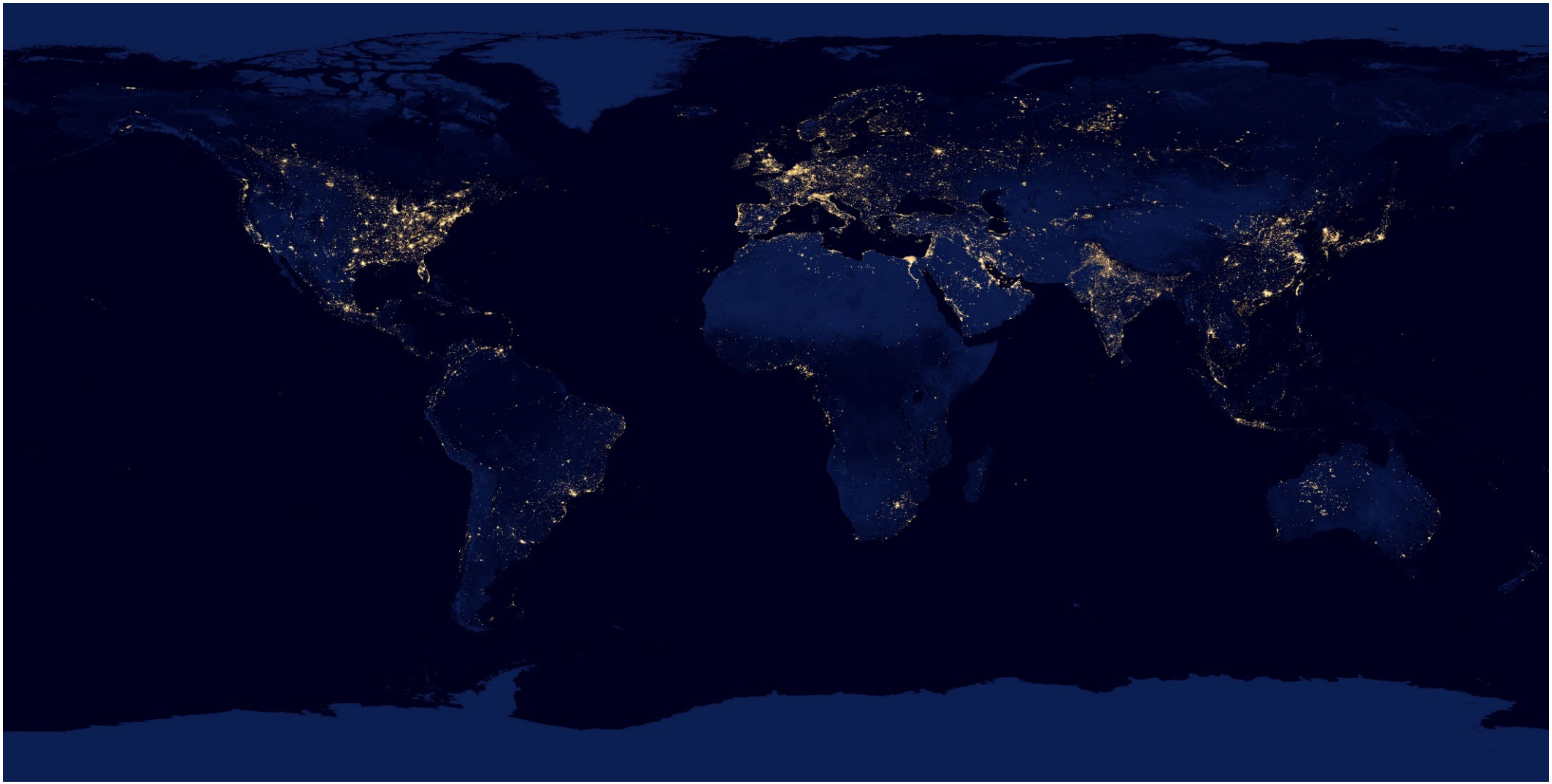

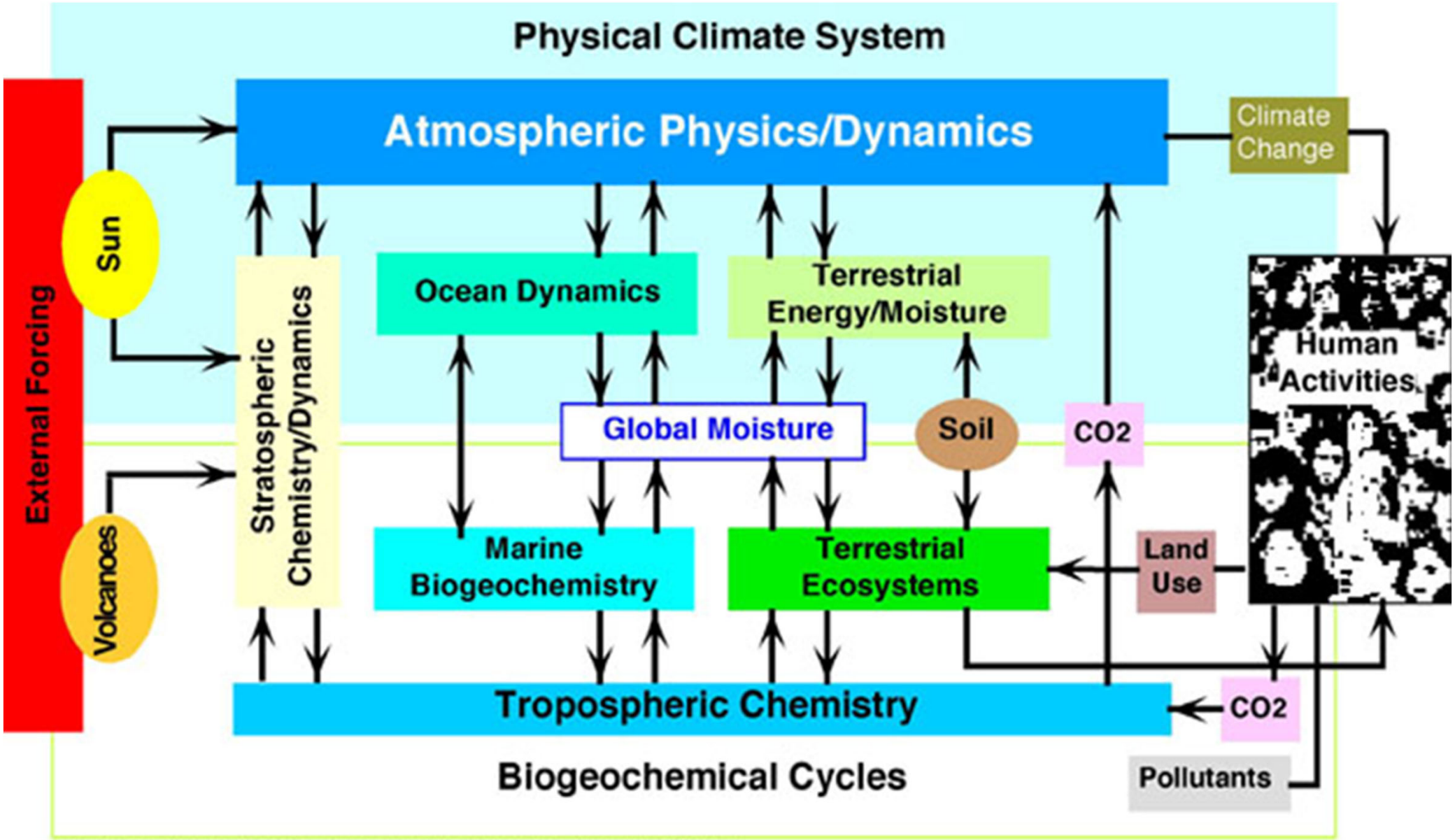

(from Earth System Science: An Overview, NASA, 1988)

Independence of Anthroposphere from Biosphere

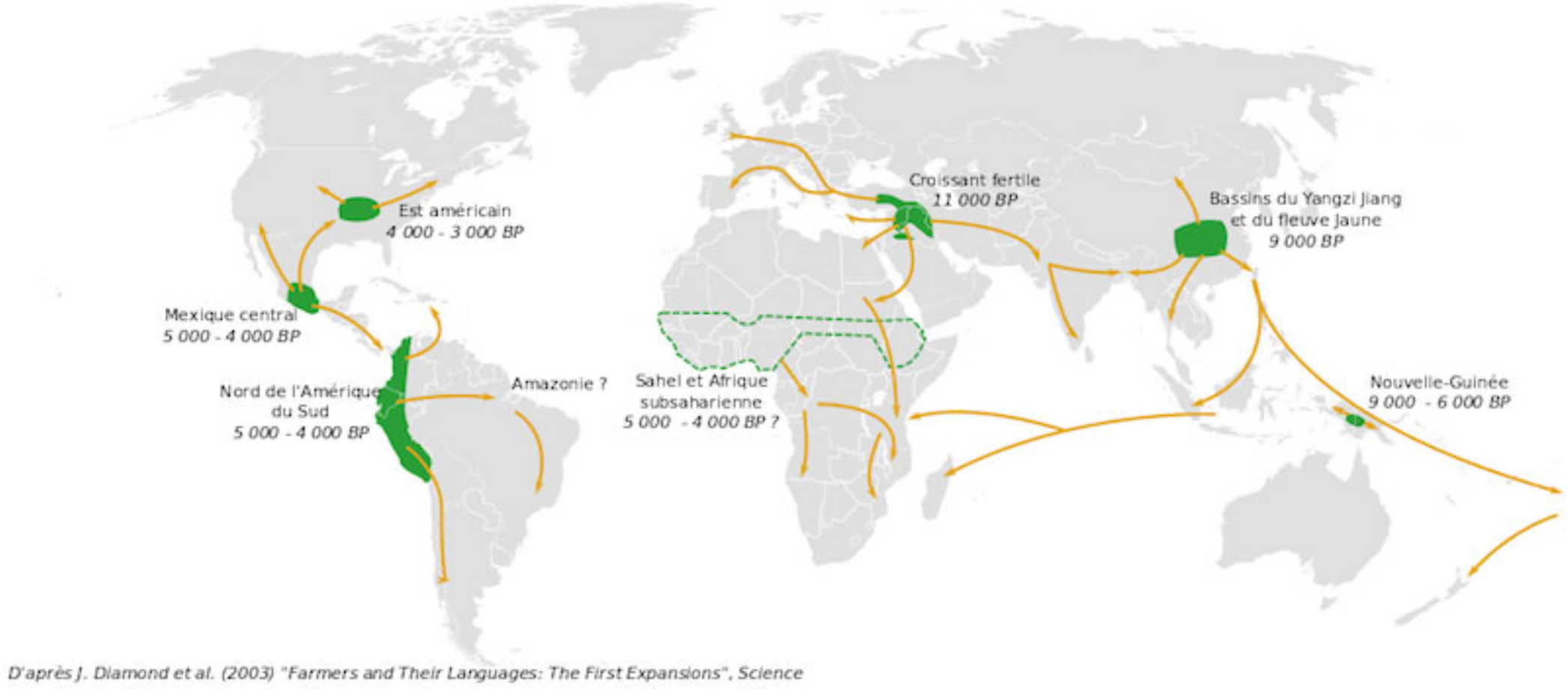

D'après J. Diamond et al. (2003) "Farmers and Their Languages: The First Expansions", Science

- **However, seafoods are difficult to be separated from natural ocean.**
- **Now 55 % of humans live in cities with homogeneous closed indoor environment.**

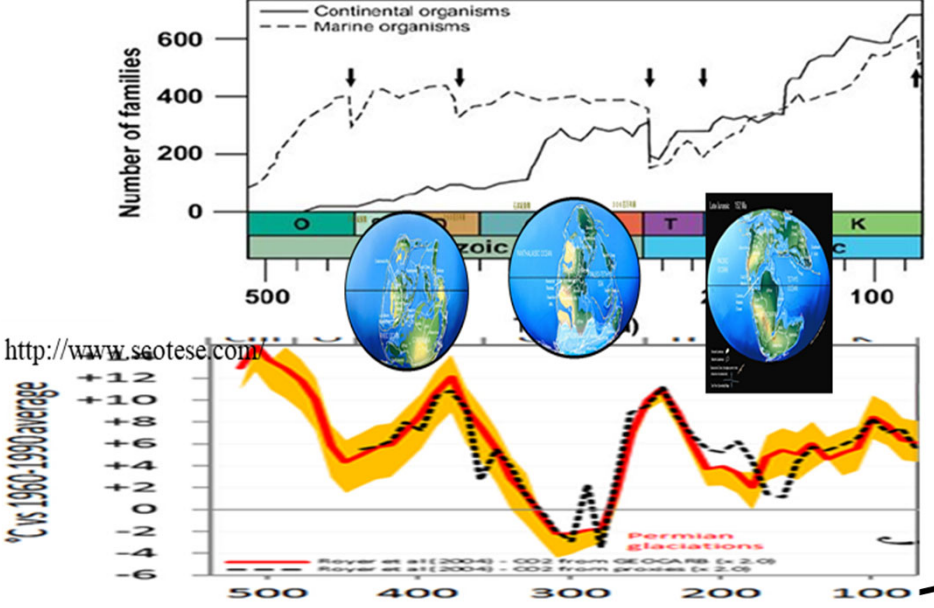

(Benton, 1995; Raup and Sepkoski, 192; Muñoz-Bertomeu et al., 2016)

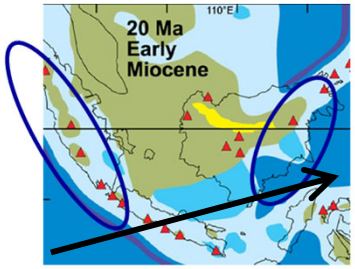

(Hall, 2009; Sheldon, 2016)

Coastal peatland 20 Myrs ago

(JCOAL, 2011)

Coalfield at present

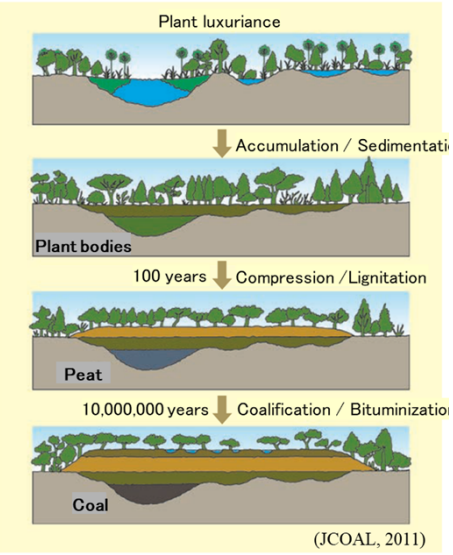

(JCOAL, 2011)

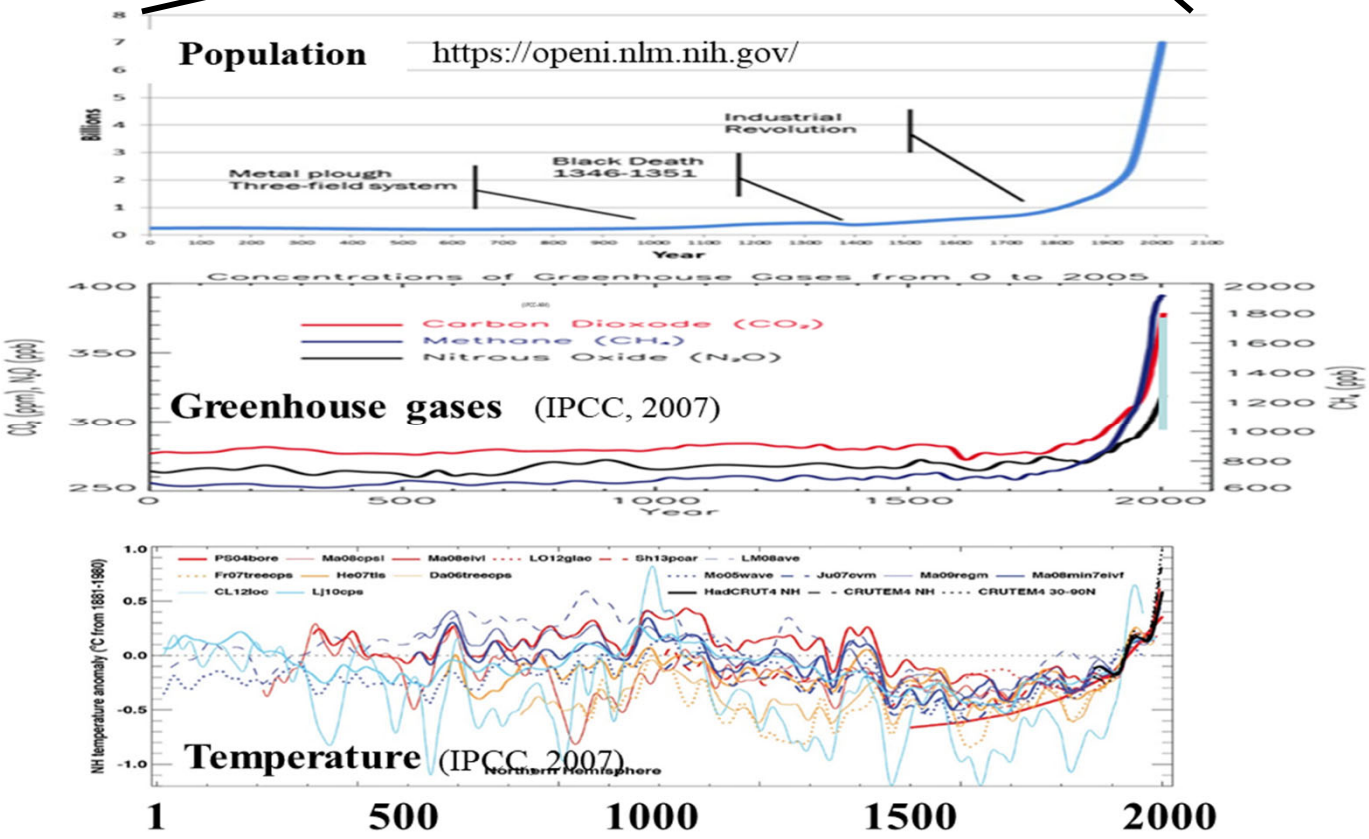

“Great Journey” (since 100 kyrs ago）

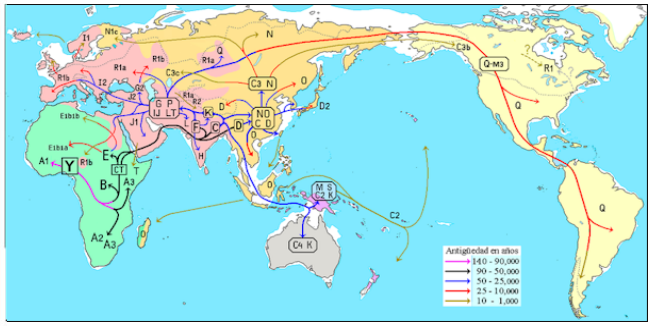

(Hayes, 2009)

“Great Voyages” (15 – 17 C)

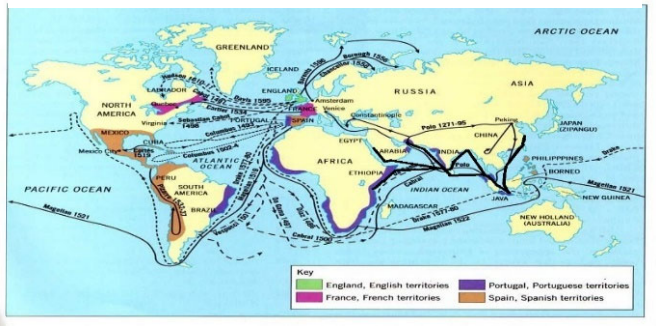

(mrfreebird.webs.com)

Landform classification and coastal lowlands

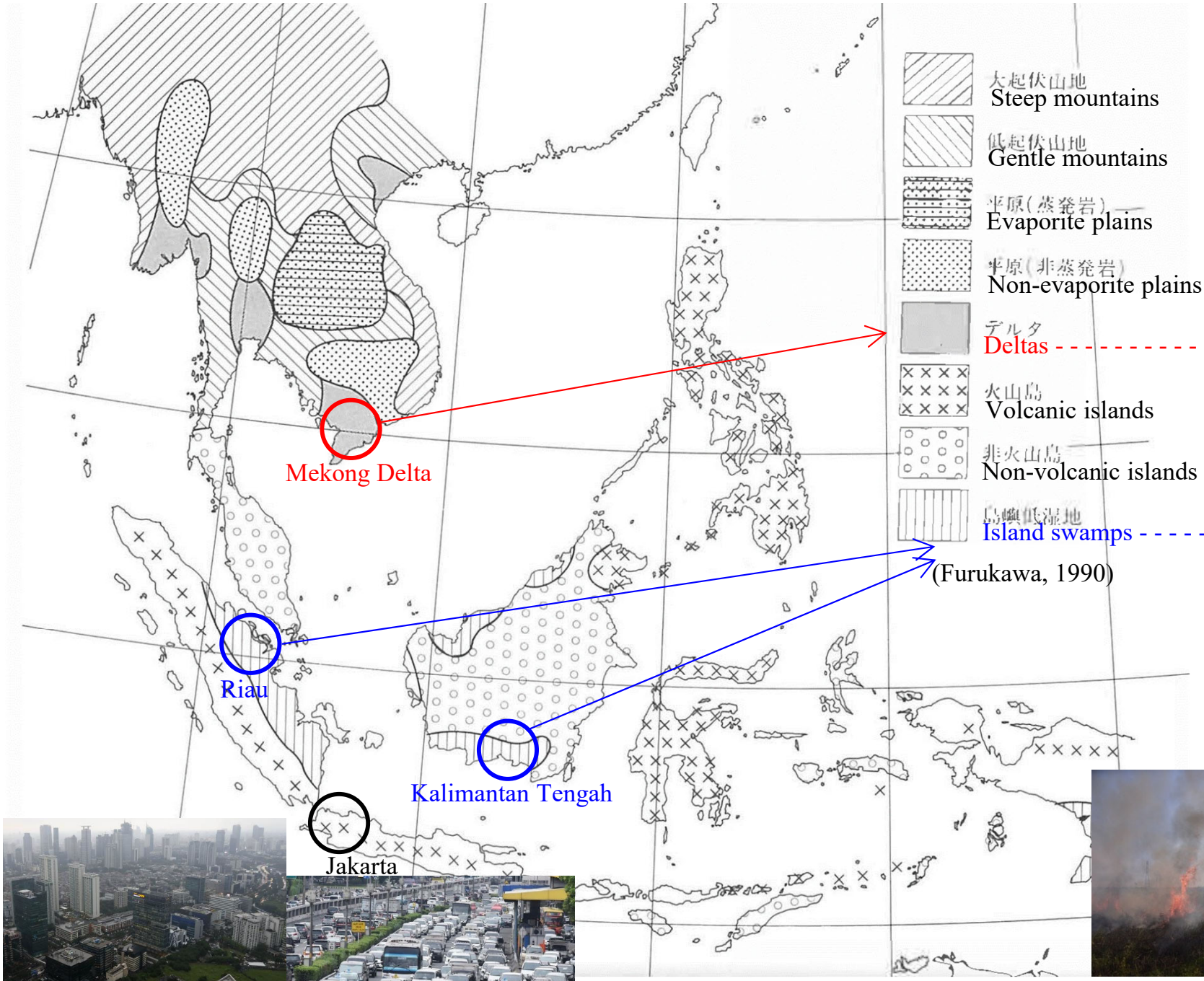

Deltas - - - - - - - - - - River sediment, Sands
Urbanization, Pollution

Island swamps - - - - - - Offlap mudflat, Peatlands
Plantation, Aridification

(Furukawa, 1990)

Megacity/Air pollution

Carbon/heat/water budget changes with peatland forest to plantation

(S. Shiodera, personal comm.)

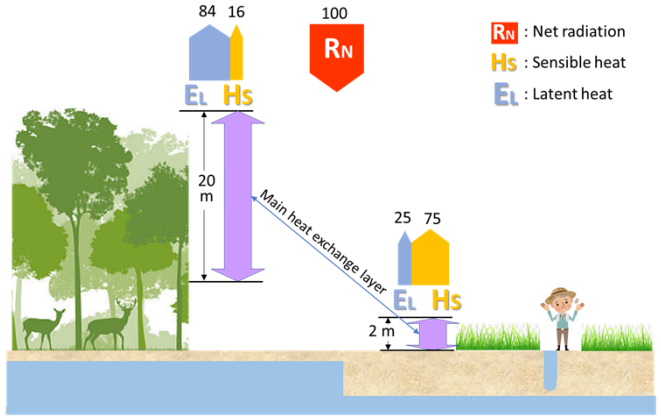

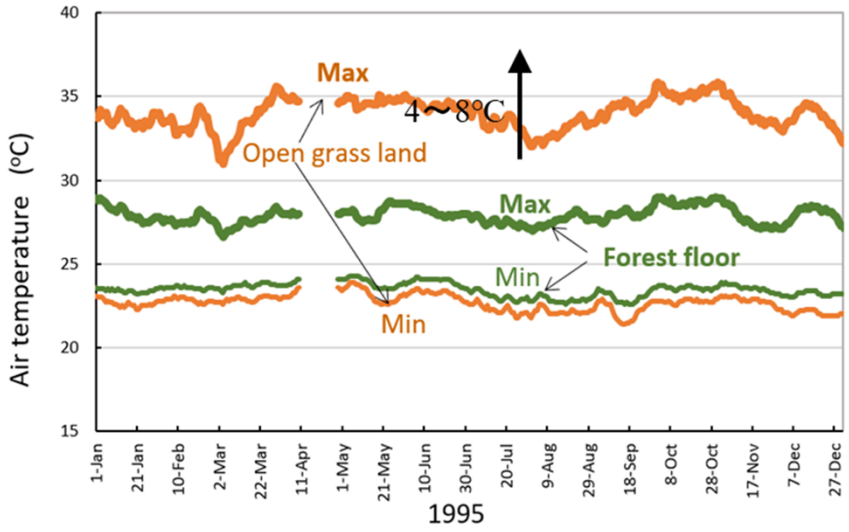

Max- & Min- air temperature in the forest floor of tropical peat swamp forest & thr open grassland in drained peatland, Central Kalimantan

(H. Takahashi & M. Osaki, personal comm.)

BMKG radar detection of smoke layer top

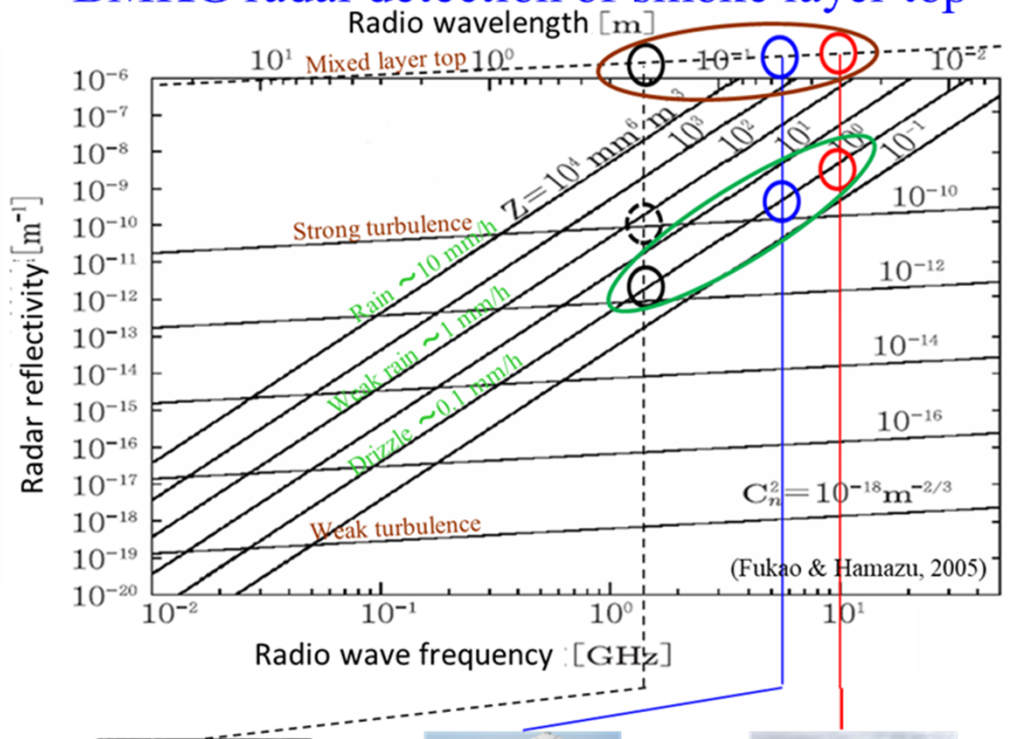

L-band (1.3 GHz, Mitsubishi)
Serpong/Kyoto U (1992~2009)
(Hashiguchi et al, 1995, *JMSJ*)

C-band (5.6 GHz, SELEX)
Palangkaraya/BMKG
(2009/2010~)

X-band (9 GHz, Furuno)
Bengkalis/RIHN-Kyoto U
(Feb 2020~)

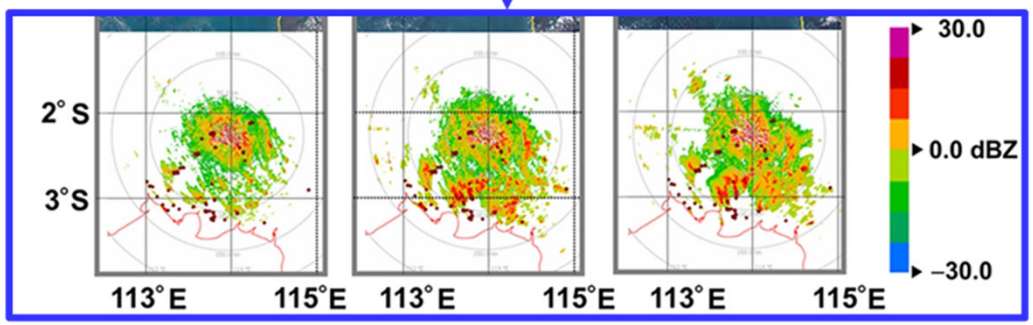

(Rahman et al, 2021, *Sci. Rep.*)

Batavia/Jakarta growing rapidly as a megacity

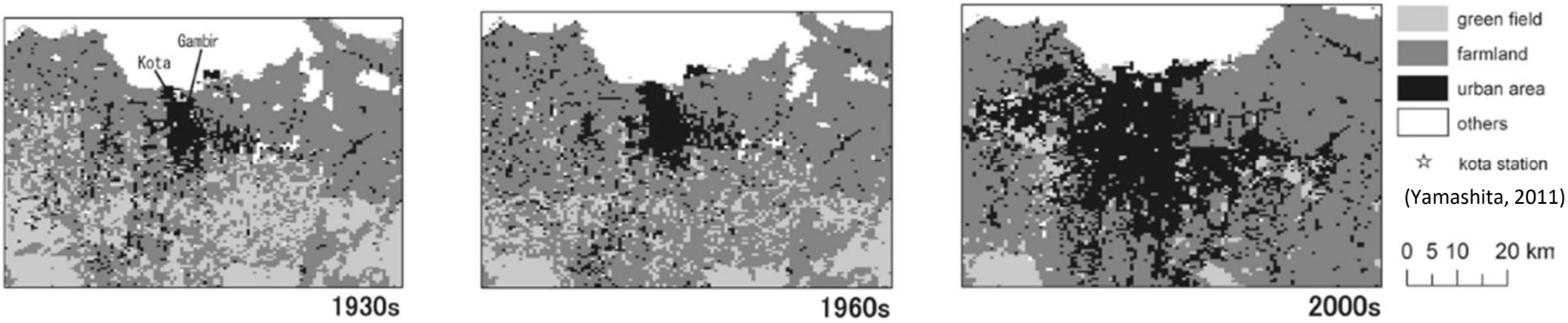

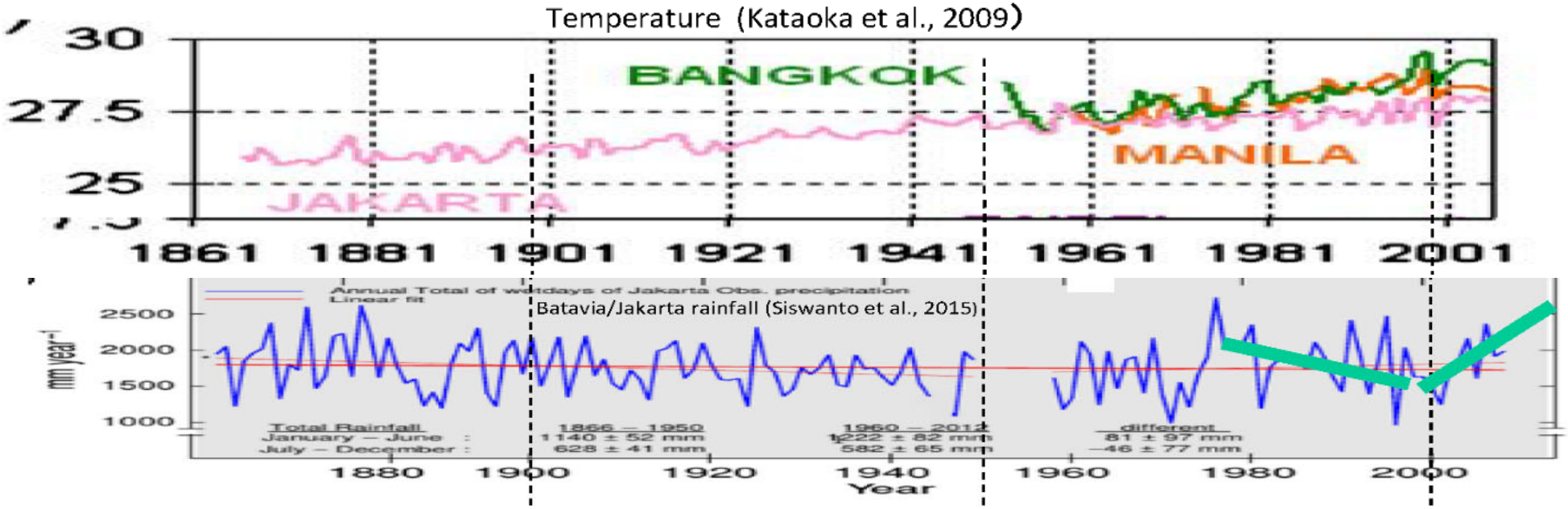

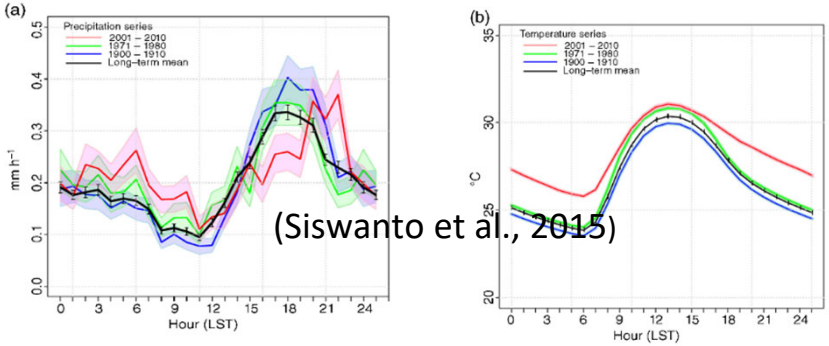

(Siswanto et al., 2015)

Human influence has warmed the climate at a rate that is unprecedented in at least the last 2000 years

Intergovernmental Panel for Climate Change (IPCC) Sixth Assessment Report (AR6) (August 2021)
https://www.ipcc.ch/report/sixth-assessment-report-working-group-i/

Changes in global surface temperature relative to 1850–1900

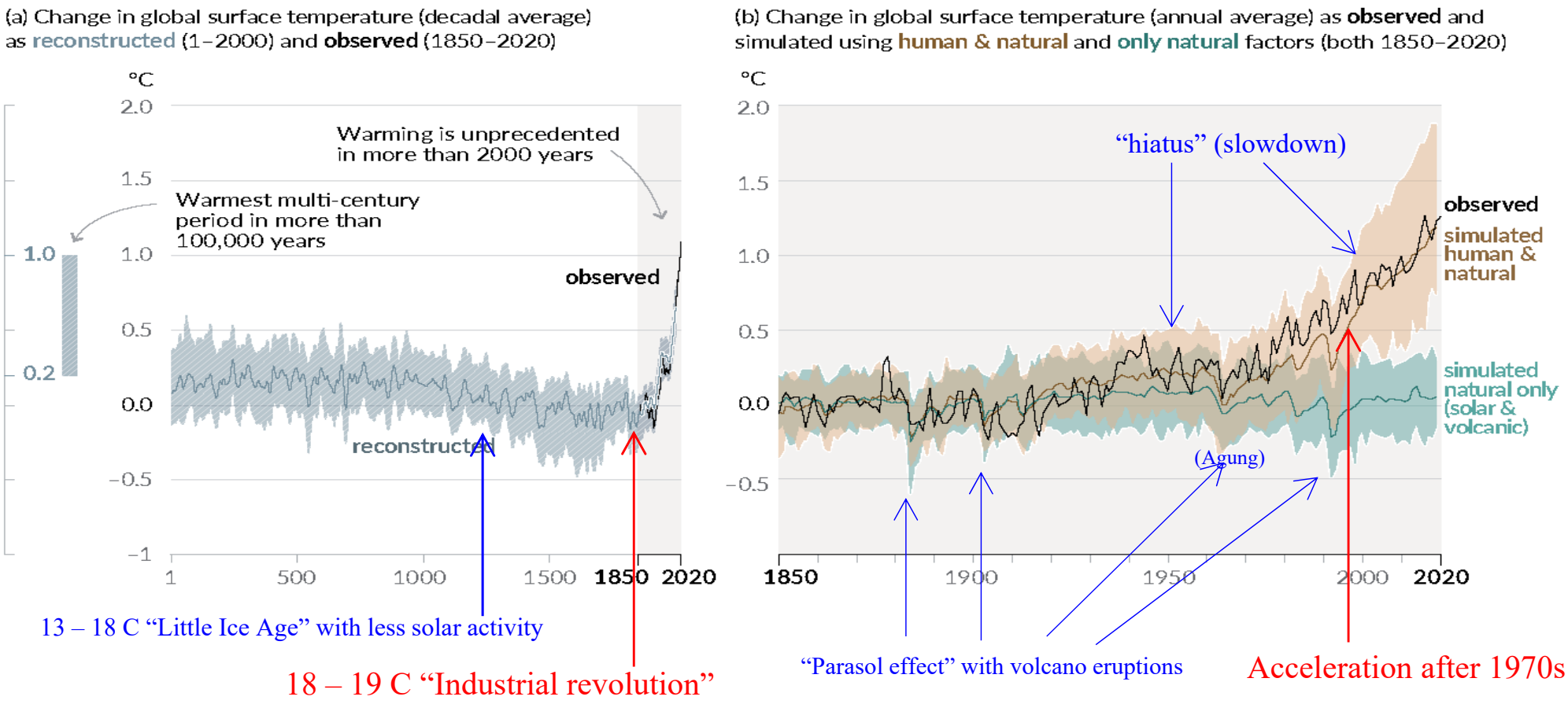

Figure SPM.1 | History of global temperature change and causes of recent warming

Panel (a) Changes in global surface temperature reconstructed from paleoclimate archives (solid grey line, years 1–2000) **and from direct observations** (solid black line, 1850–2020), both relative to 1850–1900 and decadally averaged. The vertical bar on the left shows the estimated temperature (*very likely* range) during the warmest multi-century period in at least the last 100,000 years, which occurred around 6500 years ago during the current interglacial period (Holocene). The Last Interglacial, around 125,000 years ago, is the next most recent candidate for a period of higher temperature. These past warm periods were caused by slow (multi-millennial) orbital variations. The grey shading with white diagonal lines shows the *very likely* ranges for the temperature reconstructions.

Panel (b) Changes in global surface temperature over the past 170 years (black line) relative to 1850–1900 and annually averaged, compared to Coupled Model Intercomparison Project Phase 6 (CMIP6) climate model simulations (see Box SPM.1) of the temperature response to both human and natural drivers (brown) and to only natural drivers (solar and volcanic activity, green). Solid coloured lines show the multi-model average, and coloured shades show the *very likely* range of simulations. (See Figure SPM.2 for the assessed contributions to warming).

{2.3.1; Cross-Chapter Box 2.3; 3.3; TS.2.2; Cross-Section Box TS.1, Figure 1a}

Clausius-Clapeyron relation:
Warming increases atmospheric water vapor and precipitation

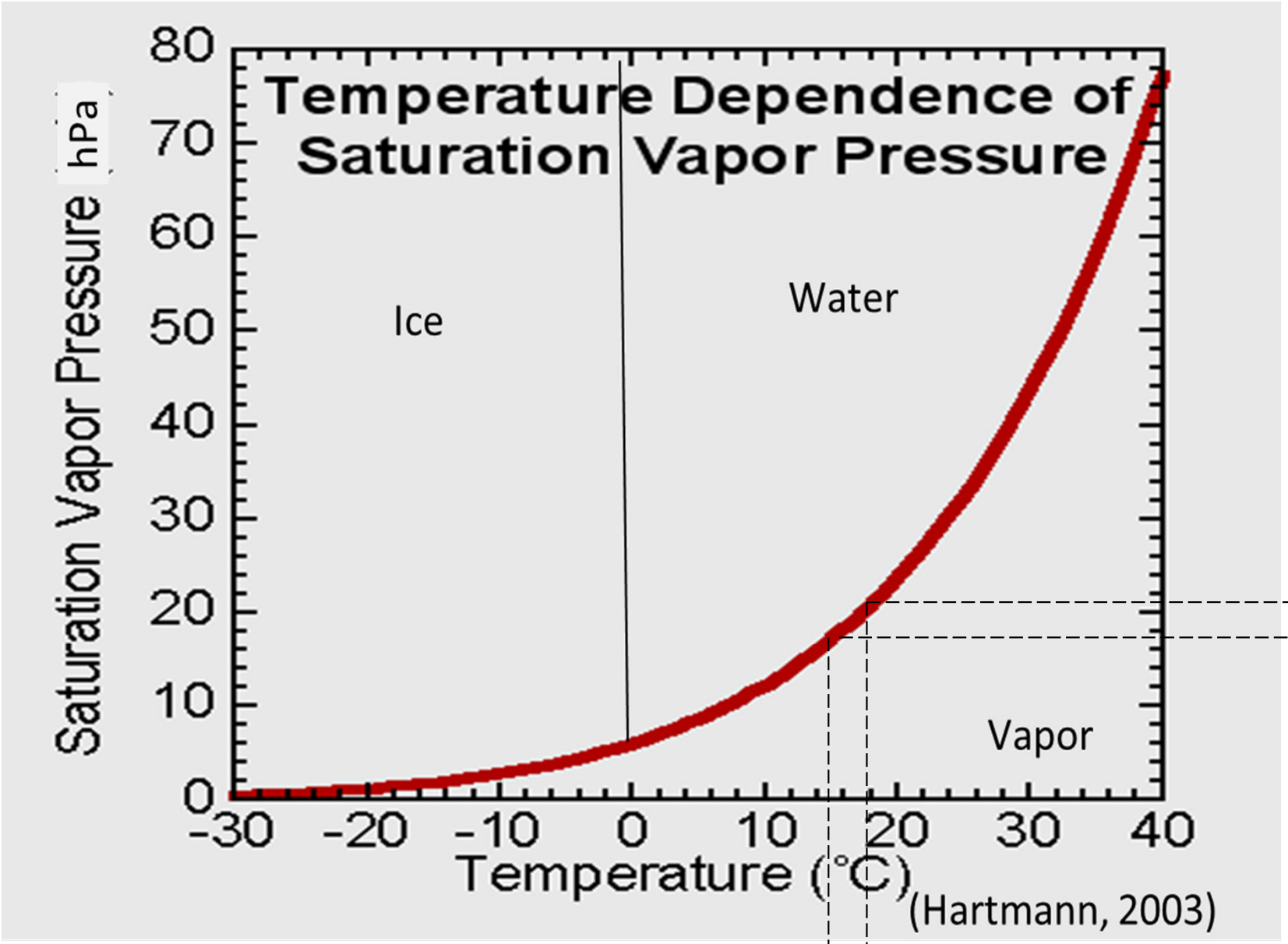

20% increase of maximum of atmospheric water vapor

20% increase of maximum of rainfall

Human activities affect all the major climate system components, with some responding over decades and others over centuries

Intergovernmental Panel for Climate Change (IPCC) Sixth Assessment Report (AR6) (August 2021)
https://www.ipcc.ch/report/sixth-assessment-report-working-group-i/

Figure SPM.8 | Selected indicators of global climate change under the five illustrative scenarios used in this Report

The projections for each of the five scenarios are shown in colour. Shades represent uncertainty ranges – more detail is provided for each panel below. The black curves represent the historical simulations (panels a, b, c) or the observations (panel d). Historical values are included in all graphs to provide context for the projected future changes.

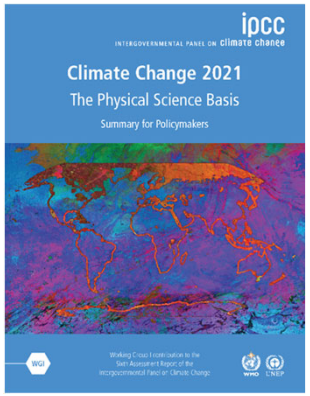

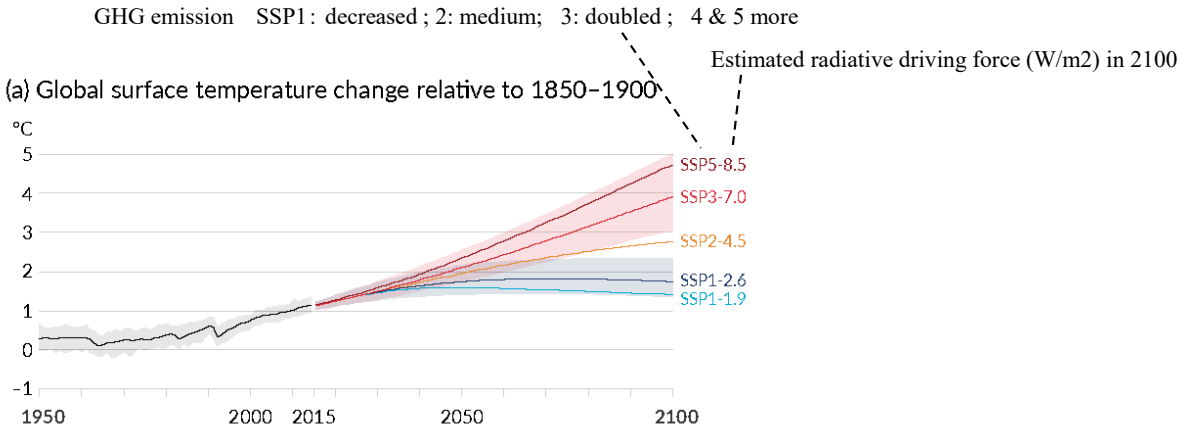

- **GHG increase ⇒ warming ⇒ water vapor increase ⇒ more warming**
- **Warming ⇒ Sea water expansion (+ ice melting) ⇒ Sea level arising**

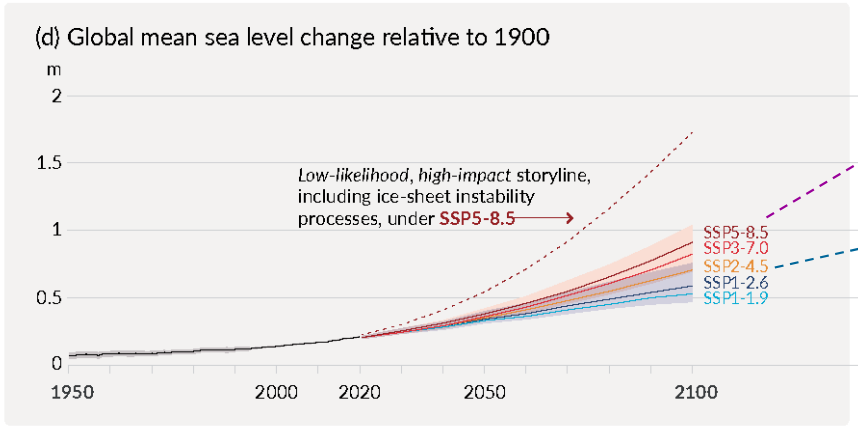

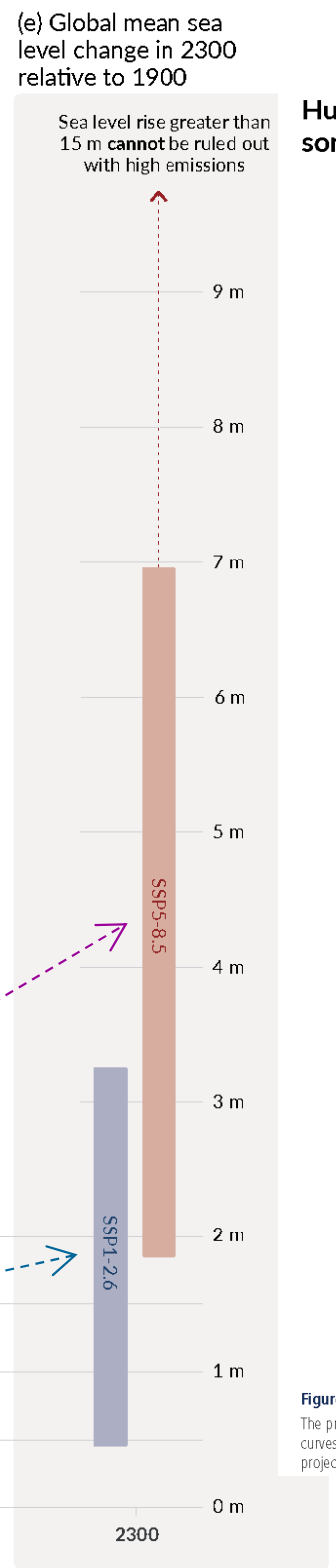

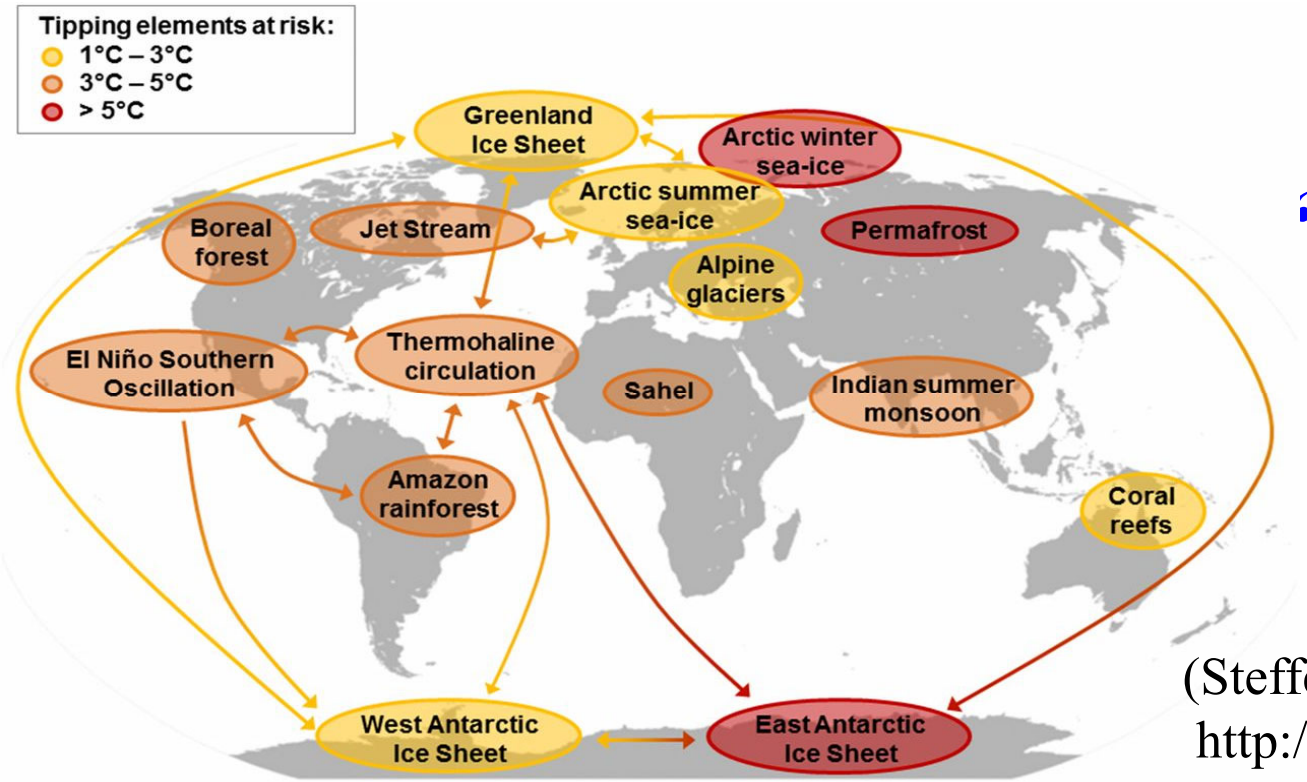

Risk for 'Hothouse Earth"

Too large changes must be unreversible.

(Steffen et al., 2018, *PNAS*)
http://www.pnas.org/content/115/33/8252